HUMAN STEM CELL DELIVERY AND PROGRAMMING FOR FUNCTIONAL REGENERATION OF LARGE SEGMENTAL BONE DEFECTS

A Dissertation
Presented to
The Academic Faculty

By

Kenneth Michael Dupont

In Partial Fulfillment
Of the Requirements for the Degree
Doctor of Philosophy in Mechanical Engineering

Georgia Institute of Technology
May 2010

HUMAN STEM CELL DELIVERY AND PROGRAMMING FOR FUNCTIONAL REGENERATION OF LARGE SEGMENTAL BONE DEFECTS

Approved by:

Dr. Robert E. Guldberg, Advisor
School of Mechanical Engineering
Georgia Institute of Technology

Dr. Andrés J. García
School of Mechanical Engineering
Georgia Institute of Technology

Dr. Evan A. Zamir
School of Mechanical Engineering
Georgia Institute of Technology

Dr. Johnna S. Temenoff
School of Biomedical Engineering
Georgia Institute of Technology

Dr. Alexandra Peister
School of Biology
Morehouse College

Date Approved: December 18, 2009

ACKNOWLEDGEMENTS

I would like to acknowledge Dr. Robert Guldberg for bringing me into the lab. It has been a pleasure working with him these past few years, and I am extremely grateful for his guidance and support throughout this challenging process. I can only say that it was with his expert surgical training that I was able to match his segmental defect surgery time of 34 minutes. I am proud to be a Guldberg lab alum and I know the IBB is in good hands for the future with him as its director.

I would like to thank my other committee members for their guidance and support as well. Andres, thanks for being there to serve as the voice of the reviewer; you always act to make our work stronger. Alex, thanks for being there to help teach me about cell culture and biology; I'm sure there aren't a whole lot of mechanical engineers who can claim a skill set like mine now. Johnna and Evan, thank you both for your input and advice which have helped me to produce a stronger thesis.

I would next like to thank all of my fellow Guldbergers, the labmates without whose help the studies performed in my thesis would never have been possible. I truly believe that the team atmosphere of the lab is one of its greatest strengths. First I would like to thank all of the labmates that came before me, with a special thanks to Dr. Megan Oest for the training that she provided me in all things segmental defect model. She put in the groundwork in developing the model that all of us that have followed have built upon, and we all owe her a debt of gratitude. I would next like to thank Angela Lin for all of the many things that she does in the lab; she is truly a Jill-of-all-trades. I am grateful for her help with my first mechanical testing experiments as well as countless

answers to Micro-CT questions, as well as for co-introducing me to the Rusan's sushi buffet along with Alex. Next I would like to thank Dr. Yash Kolambkar, my fellow Fall 2004 lab inductee. He is a diligent worker always ready to offer help and his unexpected yet hilarious comments were always welcome. Next I would like to thank Mela Johnson, whose happy demeanor and bright scrubs always helped to wake everyone up during early surgery mornings. Thanks to Joel Boerckel for his long hours in surgery (29 minute record!) and his continued optimism and enthusiasm for our work. It is truly a gift and a credit to him as a person that makes him a true asset of a labmate. Chris Dosier I would like to thank for his help with my *in vitro* studies and for sticking up for me when a Vegas poker dealer cheated me out of my bet. Eric Deutsch I would like to thank for help with some of my *in vitro* scaffold preparation steps. Jessica O'Neal I would like to thank for help in surgery, and I charge you with keeping the music selection a bit more diverse than just classic/80's rock and Dave Matthews Band (not that there's anything wrong with them). Dr. Liqin Xie I would like to thank for Micro-CT and surgery help; you are truly a data generating machine. Jason Wang I also thank for surgery help. I would like to thank Dr. Tamim Diab for all of his help in surgery and with cell culture. Thank you to Kapil Sharma, my mentee who helped me a great deal during the preliminary *in vitro* quantum dot studies. Brent Uhrig, I thank you for surgery and late night injection help, and I charge you to keep the Guldberg IBB intramural basketball tradition alive. Tanu Thote, Alice Li, and Ashley Allen, I entrust you to keep the high quality of work (and play) alive and well in the lab in the years to come, and I especially encourage Ashley to give Chapter 6 of this thesis a read if she needs some ideas for what to do for her project. I would also like to thank lab manager and office mate Hazel

Stevens. She was always there to help out, whether it was histology, surgery, ten month IACUC protocol application processes, or whatever else I might need help with. She is truly an integral part of the lab and it is lucky to have her. Finally, I would like to thank Vivian Johnson for all of her help with placing orders, preparing with logistics for trips and conferences, and all of the many other ways that she has made life easier.

A group thank you goes out to our partners in crime in the Garcia lab. In particular, Kellie Templeman, officemate extraordinaire, I thank for her wisdom in all things GA Tech and for the conversations on all random non-GA Tech issues. I thank Dr. Abbey Wojtowicz for her segmental defect surgery help and for providing me with a steady supply of GFOGER. Dr. Tim Petrie, thanks for all the GFOGER and for serving as the longterm IBB intramural bball captain.

I would like to thank the staff of the IBB's Physiological Research Laboratory, without whose help and animal care no one would be able to complete their *in vivo* studies. Thanks to Dr. Laura O'Farrell for all of her expertise and knowledge on proper animal care and procedures as well as for helping with scheduling of equipment. Thanks to Kim Benjamin for her help with animal orders and with the logistics of my studies. Thank you to O'Dell, Autumn, and Andrea for all of the animal care and observation that have provided that made my studies possible.

I would like to thank other members of the IBB, starting with Steve Woodard, who has been very helpful with imaging techniques, biosafety issues, and day to day concerns within the IBB. I would like to thank Johnafel Crowe for his help with confocal microscope imaging. Thank you to Allen Echols for his help with packages and presentation setups. I would like to recognize Sha'Aqua Asberry for her help with

histological techniques. I would like to thank James Godard, Alyceson Andrews, and Floyd Wood in the IBB office for all of their help with a variety of administrative and building issues.

I would like to thank members of the George W. Woodruff School of Mechanical Engineering, including the staff of the office of student services and especially Glenda Johnson for her patience in answering my many questions regarding ME procedures and requirements. Thank you to Dr. Wayne Whiteman for his help during my initial search for a lab, Dr. Jeffrey Donnell for his help with fellowship applications and technical writing advice, and Rekha Patel with her help moving money where it needed to go to place orders.

I would also like to thank collaborators at the University of Rochester who helped me with the AAV studies described in Chapter 5. In particular, I would like to thank Dr. Edward Schwarz, Dr. Hani Awad, Tulin Dadali, David Reynolds, Cemal Yazici, and Masahiko Takahata.

Additionally, I would like to acknowledge the funding sources which helped to make my graduate studies more bearable. I would like to thank the National Science Foundation for a Graduate Research Fellowship, the National Institutes of Health for a Biotechnology Training Grant, Medtronic for a fellowship, and the Georgia Institute of Technology for a President's Fellowship. Additionally, funding was provided by a GTEC Critical Models Seed Project fund.

Finally, I would like to send my largest thank you to my family, without whose support I could not have made it through these past five and a half years. To my sister Lisa Townsend, I admire you for your courage to stick hard to what you believe in even if

it made your life more difficult at times. To my dad, Steve Dupont, I cannot thank you enough for the limitless amount of support you have given me throughout my life. No matter what, I've always known that you were there to have my back and I cannot tell you the comfort that that has brought me during difficult times. I can only hope to one day be half the father that you have been. To my fiancée Ashley Davis, I know it has been a looooooooooooonger road than what either of us might have originally expected, and I thank you for hanging on with me. Thanks for the love and support you have given me and for helping me to be sure to focus on life outside of the lab. I'm excited about moving on to the next stage of our life together. Hutch P. Nelson, thank you for introducing me to the world of dogs and the happiness that comes with it. I've got a cheeseburger waiting for you. Lane and Rory, the terrible two, you've provided a welcome distraction during the long hours of work and writing during the past couple of years. Finally, I would like to send a special thank you to my mom, Joan Jackewicz Dupont. While you haven't physically been here throughout my time at GA Tech, I have still felt your support and love and I know that a large part of the strength and heart that it took to make it through came from you. I thank you and dad for instilling in me a love of science and biology which likely led me to choose the specific research area for my thesis, and I hope that this work is something that would make you proud.

TABLE OF CONTENTS

LIST OF FIGURES

LIST OF SYMBOLS AND ABBREVIATIONS

2-D	two-dimensional
3-D	three-dimensional
AAV	adeno-associated virus
AFS Cell	amniotic fluid-derived stem cell
α-MEM	α-modified eagle's medium
ALP	alkaline phosphatase
BMP	bone morphogenetic protein
BV	bone volume
caALK2	constitutively active ALK2
CPC	calcium phosphate cement
DNA	deoxyribonucleic acid
ESC	embryonic stem cell
FDA	food and drug administration
HA	hydroxyapatite
HEK	human embryonic kidney cells
Luc	luciferase
micro-CT	micro-computed tomography
MOI	multiplicity of infection
MSC	marrow-derived stem cell
MV	mineral volume
PCL	polycaprolactone

PEG	polyethylene glycol
PLDL	poly(L-lactide-co-D,L-lactide)
QD	quantum dot
TCP	tricalcium phosphate
VEGF	vascular endothelial growth factor
VOI	volume of interest

SUMMARY

Large bone defects pose a significant clinical challenge, affecting large numbers of patients at high costs. The current clinical standard for treating these defects is implantation of bone grafts. While autograft bone is the gold standard for graft material, there is generally an insufficient amount available for treating large bone defects. Devitalized allograft bone from cadavers is more readily available; however this material displays limited integration with host bone resulting in as many as 1/3 of these grafts failing within 2-3 years after implantation. Bone tissue engineering strategies aim to replace bone grafting procedures with treatment by a combination of a structural scaffold, biochemical cues, and / or cells capable of enhancing healing. Cellular therapies may be of particular importance when treating large bone defects because many patients lack an adequate endogenous supply of osteogenic cells or osteoprogenitor cells.

The goal of this thesis was to quantitatively compare stem-cell based strategies for treating large bone defects. First, we developed a challenging large bone defect model in immunocompromised rats for use as a reproducible test bed to quantitatively compare human stem cell-based therapies, and then we evaluated the abilities of adult and fetal stem cells to enhance defect healing when delivered on porous polymer scaffolds. Our results showed that stem cell-seeded porous polymer scaffold therapy enhanced defect healing compared to treatment with acellular scaffolds alone in the absence of added osteogenic signals, but was insufficient to fully regenerate limb function. Second, we sought to label stem cells with an *in vivo* tracking agent, the quantum dot, to determine biodistribution of delivered cells during the bone healing process. We showed that while

quantum dots effectively label human stem cells *in vitro* and have negligible effects on cell viability and osteogenic differentiation *in vitro*, their use as a long term *in vivo* tracking agent was inconclusive due to uptake by host macrophages. Post mortem immunohistochemistry analysis confirmed that at least a small population of human cells remained at defect sites four weeks post implantation. Finally, we treated defects with both *in vitro* and *in vivo* osteogenic gene therapy approaches, using scaffolds coated with an adeno-associated viral (AAV) vector to encode the gene for the osteogenic signal bone morphogenetic protein 2 (BMP2) in human stem cells prior to implantation or in host defect cells after scaffold implantation. Effective BMP2 gene transfer to stem cells and induction of osteogenic differentiation was first verified *in vitro*. However, treatment of segmental defects with scaffolds containing BMP2-transduced stem cells (*in vitro* gene therapy) produced less robust healing than the *in vivo* gene therapy approach with scaffolds delivering the BMP2 gene to host cells.

In conclusion, this work has produced a challenging and reproducible model of large bone defects that can be used to gain new insights into the cell-mediated defect repair process through quantitative comparison of human stem cell-based bone tissue engineering therapies. This work has confirmed the therapeutic benefit of stem cell-seeded construct delivery over acellular construct delivery for enhancement of defect healing in the absence of added osteogenic stimuli and suggested the therapeutic potential of fetal amniotic-fluid derived stem cells as an alternative to adult marrow-derived stem cells for treatment of large bone defects. This work has refuted the ability of the fluorescent quantum dot to serve as an effective long term *in vivo* cell tracking agent, which will impact the choice of cell tracking agents used in future studies of cell-

mediated tissue repair therapies. Finally, this work is the first to present proof of concept results of a true off-the-shelf, donor bone graft-free orthotopic large bone defect repair therapy in which pre-sized thermostable porous polymer scaffolds lyophilized with scAAV2.5-BMP2 could be frozen at length until needed for clinical implantation in large bone defect sites.

Chapter 1

INTRODUCTION

Motivation and Introduction

Bone related injuries are a common problem faced by large numbers of patients at significant costs. There are 150,000 wrist, hip, and vertebral fractures each year in the UK due to osteoporosis with an estimated cost of 17 billion pounds (Dawson and Oreffo 2008). As the aging population grows, worldwide the number of annual hip fractures alone is expected to rise from 1.7 million in 1990 to 6.3 million by 2050 (Dawson and Oreffo 2008). In addition to bone injuries related to systemic conditions, local problems such as fracture nonunions and large bone defects present a challenging problem facing orthopaedic surgeons as well. The normal healing response to bone damage consists of initial inflammation, followed by soft then hard fracture callus formation, and finally bone remodeling (Khan, Yaszemski et al. 2008). In fracture nonunions and large bone defects this healing does not occur or does so only to a limited extent, due to a variety of factors such as soft tissue damage, loss of vascularity, distraction of fracture fragments, soft-tissue interposition, malnutrition, infection, instability, periosteal stripping, and systemic disease such as rheumatoid arthritis (Tseng, Lee et al. 2008), (Kalfas 2001). Lack of healing creates a need for surgical intervention, and thus out of the approximately 1.5 million bone-grafting operations performed annually in the United States (Einhorn 2003), 500,000 are for patients with nonunions or large defects (Bucholz 2002).

There is currently no optimal clinical treatment for the repair of large bone defects. Autograft bone is only available in limited volumes while allograft bone fails to integrate with host bone, creating a high rate of failure within a short period after implantation. Bone tissue engineers aim to create a graft substitute possessing the benefits of both autograft and allograft without their drawbacks (Guldberg, Oest et al. 2004) that could be used as a large bone defect treatment for restoration of bone structure and function. The general bone tissue engineering therapy consists of some combination of structural scaffold, bone forming cells, and biochemical signaling cues to increase bone formation. Therapies delivering signaling cues through bolus delivery of osteogenic proteins have shown some therapeutic potential for healing large bone defects, but there are growing concerns over negative side effects such as inflammation and ectopic bone formation that are associated with the large doses of delivered protein needed for improved repair (Cahill, Chi et al. 2009). In light of these concerns, cell-based bone tissue engineering treatments present an attractive alternative that may be especially important for treating large bone defects in patients lacking sufficient endogenous cell populations (Bruder 1999). Stem cells are an attractive cell choice for bone tissue engineering therapies because they can proliferate to a large number of cells as well as differentiate into bone forming cells.

While multiple systemic and local site-specific stem cell delivery methods have been investigated, the optimal delivery strategy is unclear and much about the relationship between delivery method and the stem cell-enhanced healing process remains unknown (Chamberlain, Fox et al. 2007). Although a variety of stem cell sources have been investigated for bone repair in *in vitro* and ectopic *in vivo* models

(Zhang, Teoh et al. 2009), few comparative *in vivo* studies have been performed in orthotopic *in vivo* models which better represent clinical bone defects. Furthermore, limited cell survival following implantation remains a key issue (Waese, Kandel et al. 2008).

The *overall objective* of this thesis was to establish a critically-sized rat femoral defect model in immunocompromised rats and then to effectively treat defects with human fetal and adult stem cell-based bone tissue engineering therapies, with the *goal* of restoring bone structure and function. The *central hypothesis* was that stem cell-based tissue engineering therapies would enhance defect bone regeneration over comparable acellular therapies in a developmental stage-dependent manner, both in the absence and presence of osteogenic cues. The research objectives of this thesis have been divided into three specific aims:

Specific Aim I

Establish a challenging large bone defect model in immunocompromised nude rats for evaluation of the abilities of human adult and fetal stem cell-based therapies to enhance defect healing.

The objectives of this aim were to establish a model of critically-sized large bone defects suitable for evaluation of human stem cell-based therapies and to quantitatively compare therapeutic potentials of tissue engineered constructs containing either adult bone marrow-derived or fetal amniotic fluid-derived stem cells. Our *working hypothesis* was that treatment of large bone defects with stem cell-seeded scaffolds would enhance defect healing over treatment with acellular scaffolds alone, and that stem cells would affect healing in a developmental stage-dependent manner. To accomplish this aim, we

first verified the critical size of 8 mm femoral defects in nude rats that would serve as a challenging test bed for xenogeneic, human stem cell-based therapies. Next, we verified the *in vitro* osteogenic potential of human marrow-derived stem cells (hMSCs) and human amniotic fluid-derived stem cells (hAFS Cells) seeded on 3D porous polymer scaffolds when cultured in the presence of osteogenic stimuli. Finally, we evaluated the *in vivo* therapeutic potentials of the two stem cell sources for treating large bone defects. The outcomes of this Aim are discussed in Chapter 3.

Specific Aim II

Determine stem cell biodistribution and viability throughout the large bone defect healing process by labeling them with an *in vivo* tracking agent.

The objectives of this aim were to first effectively label stem cells with a tracking agent compliant with long term *in vivo* imaging modalities and then to track stem cells delivered to segmental defects throughout the bone repair process. Our *working hypothesis* was that a population of delivered labeled stem cells would remain viable at the segmental defect site to contribute to the bone healing response. We first performed *in vitro* analyses of a novel cell tracking agent, the fluorescent quantum dot, to assess its internalization into both human adult and fetal stem cells as well as any potential negative effects on cell viability and osteogenic differentiation. We then implanted quantum dot-labeled stem cells seeded on porous polymer scaffolds into segmental defects and tracked fluorescent signals both through *in vivo* scans and post mortem histological analysis. Finally we assessed *in vivo* quantum dot fate after stem cell death by delivering devitalized stem cells to defects, evaluated quantum dot effects on defect healing, and

confirmed the long term associations of quantum dots with defect cell types. The outcomes of this Aim are described in Chapter 4.

Specific Aim III

Evaluate the effects of added stimulatory cues to program stem cells to differentiate towards an osteogenic lineage capable of enhancing segmental defect bone formation.

The main objective of this aim was to develop and test a novel viral delivery system for introducing osteogenic signals to human stem cells, thereby enhancing stem cell differentiation and promoting large bone defect repair. Our *working hypothesis* was that delivery of osteogenic signals to segmental defect sites would enhance healing, and that delivery of signals through genetically modified stem cells programmed towards osteogenic differentiation would further enhance healing. To accomplish this aim, we first tested the ability of porous polymer scaffolds coated with an adeno-associated viral (AAV) vector to deliver a reporter gene to cells surrounding the segmental defect site. Next we assessed the ability of AAV encoding the gene for the osteogenic protein bone morphogenetic protein 2 (BMP2) to transduce human stem cells and enhance osteogenic differentiation in both 2D and 3D *in vitro* systems. Finally, we evaluated the segmental defect healing response when treated with either scAAV2.5-BMP2 coated constructs or scAAV2.5-BMP2 coated constructs pre-seeded with hMSCs. Control defects were treated with AAV-Luciferase coated constructs or AAV-Luciferase coated constructs pre-seeded with hMSCs.

Significance

Large bone defects pose a common clinical challenge currently lacking an optimal solution. Bone tissue engineering strategies aim to best current therapies, and strategies that include cellular components may be particularly important in treating severe defects lacking adequate endogenous cell populations. This work is *significant* because it established a challenging orthotopic bone defect model for human cell-based therapeutics and quantitatively compared a variety of stem cell-based treatments. It evaluated efficacy of both adult and fetal stem cell-based tissue engineering constructs and assessed the effects of added osteogenic stimulatory cues on defect healing. This work produced the following outcomes: 1) Established a rigorous and reproducible small animal large bone defect model for allogeneic or xenogeneic cell-based therapies with quantitatively comparable outcome measures, 2) Displayed the therapeutic benefits of stem cell-seeded constructs over acellular constructs, 3) Revealed limitations in use of quantum dots as a long term *in vivo* cell tracking agent, 4) Displayed the therapeutic potential of a novel method for gene therapy-based osteogenic bioactivation of scaffolds for use in both *in vivo* and *in vitro* gene therapy applications.

Chapter 2

LITERATURE REVIEW

Bone Introduction

Bone Function

Bone serves a variety of physiological functions. Bones participate in mineral level homeostasis, including storage and release of calcium, phosphate, sodium, and magnesium to regulate ion concentrations in body fluids. The marrow cavity in bone is the site of hematopoiesis, which is the formation and development of red and white blood cells, and it also contains a population of mesenchymal progenitor cells that can differentiate down a variety of cell lineages. Bone also serves a variety of mechanical functions, including protecting vital organs such as the brain, spinal cord, and heart, supporting soft tissues attached to bone, and serving as a structural framework of levers on which muscles can act to cause motion (Baron 1993). Finally, the small bones of the ear play an important role in hearing.

Bone Structure

Bone structure can be evaluated on a variety of size scales, from entire whole bones at the largest level down to micron-sized structural features at the ultrastructural level (Weiner 1998). A bottom-up analysis of the multiple scales from smallest to largest presents a clear picture of the overall structure of bone.

Ultrastructural Level: Woven and Lamellar Bone / Bone Matrix

The ultrastructural bone level exists at a length scale of 1-10 microns and can be divided into woven and lamellar bone. Woven bone is composed of randomly aligned collagen fibers and irregularly shaped vasculature lined with osteoblasts (Kalfas 2001). It

is found primarily during embryonic development, wound repair processes, and in some disease states. Woven bone remodels into mature lamellar bone, which features uniformly aligned collagen fibrils that form sheets called lamellae. Lamellar bone is found within healthy mature bone and is stronger than woven bone due to its organized collagen fiber network and thicker individual fibers. Fibers in adjacent lamellae are aligned at differing angles and additional fibers bridge between them, providing strength under a number of loading directions.

The bone extracellular matrix can be described as a composite material consisting of three phases (Recker 1992). The mineral phase of bone is comprised mostly of calcium phosphate and calcium carbonate which form crystals known as hydroxyapatite and makes up approximately 65% of bone dry weight, contributing to bone strength and stiffness. The organic phase of bone is comprised primarily of type I collagen fibers and makes up approximately 35% of bone dry weight, contributing to bone toughness and ductility. The third phase of bone is water, which makes up approximately 20% of bone total weight, also contributing to bone ductility.

Apparent Bone Level: Cortical and Trabecular Bone

The apparent bone level exists at a length scale of 5-10 millimeters, and the bone structures making up whole bone can be divided into cortical and trabecular bone. Dense cortical (also called compact) bone forms the internal and external tables of flat bones and the outer surfaces of long bone shafts. The primary cortical bone substructures are osteons, which are concentric cylindrical bone formations of lamellae surrounding vascular channels called Haversian canals oriented along the longitudinal axes of bones. Transverse channels called Volkmann's canals connect adjacent osteons, providing a

space for vascular connections and allowing fluid flow and mass transport to the bone's outer surface (Currey 1984). Osteocytes are bone cells that are embedded within osteons in small cavities called lacunae, and these cells form connections with each other by extending cytoplasmic cellular processes through canaliculi and forming gap junctions. It is through these connections that transfer of ions and nutrients can occur as well as transmission of signals that are vital to bone remodeling. The networks of osteons in long bones are contained between an inner membrane known as the endosteum that is adjacent to the bone's central marrow cavity and an outer membrane known as the periosteum which covers the outer surface of the bone. Both membranes provide a vascular supply and are hosts to osteoprogenitor cells. Cortical bone makes up approximately 80% of the human body's bone mass (Buckwalter, Glimcher et al. 1996).

Trabecular (also called cancellous) bone exists between cortical bone surfaces and can typically be found at the ends of long bones and within vertebral bodies. Trabecular bone consists of a network of rods and plates known as trabeculae that are joined together in a sponge-like network resulting in a higher surface area per unit weight than cortical bone. The network of trabecular struts or trusses acts like a shock absorber and its orientation can vary as the bone adapts to local changes in mechanical loads. Marrow and cells occupy the pore spaces of the trabecular bone. Trabecular bone makes up approximately 20% of the body's bone mass.

Whole Bone Level: Long, Short, Flat, and Irregular Bones

The whole bone level exists at a length scale of one centimeter or longer and can be divided by general shape into long, short, flat, and irregular classes (Gray 1918). Long bones are characterized by a central shaft known as the diaphysis bordered by

expanded ends known as the epiphyses. The epiphyseal ends are covered with articular cartilage to facilitate motion within joints. Between the two regions lie cartilaginous growth plates in long bone sections called the metaphyses. Long bones have high length to width ratios. The majority of bones in the limbs are long bones except for the wrist, ankle, and patella. While large bones like the femur and tibia are long bones, so are small bones such as the metacarpals and metatarsals. Short bones are approximately cube-shaped, being as wide as they are long, and include the bones of the wrist and ankle, such as the carpals and tarsals. A subset of the short bones are the sesamoid bones, which are bones embedded in tendons that serve as spacers, moving the tendon away from the adjacent bone surface and providing muscles with increased leverage for motion. Examples are the patella and pisiform. Flat bones are generally thin and curved. These bones serve to protect the internal organs, and include most bones in the skull, the sternum, the scapula, and the pelvic girdle. Irregular bones have odd shapes that do not fit into the other three shape categories. The vertebrae of the spine and some facial bones such as the mandible are irregular.

Key Cell Types Found In Bone:

Osteoblasts

Osteoblasts are mature mesenchyme-derived bone cells that contribute to the bone formation process through secretion of osteoid, the unmineralized organic matrix that subsequently becomes mineralized after 24-74 hours. Osteoid mineralization occurs through nucleation of calcium phosphate crystals followed by crystal growth and finally hydroxyapatite formation (Robey 1989). Osteoblasts and osteoprogenitor cells are present on all nonresorptive bone surfaces, including the deep layer of the periosteum on

the outer bone surface and the inner endosteal surface within the medullary canal space (Kalfas 2001). Osteoprogenitor differentiation to mature osteoblasts is dependent on expression of a number of factors, with runt-related transcription factor-2 (Runx2) and Osterix being two of the most important (Robling, Castillo et al. 2006), (Harada and Rodan 2003). Markers of mature osteoblasts include the matrix proteins type I collagen and osteocalcin as well as the enzyme alkaline phosphatase.

Osteocytes

Osteocytes are mature osteoblasts that become trapped within secreted bone matrix. Osteocytes represent the majority of bone cells. Osteocytes maintain cytoplasmic connections with each other and other cells through a network of cylindrical canaliculi (Baron 1993). Osteocytes help to control extracellular concentrations of calcium and phosphorus, and they also play a role in bone remodeling under certain stimuli (Kalfas 2001). Genetic markers of osteocytes include dentin matrix protein-1 and matrix extracellular phosphoglycoprotein (Robling, Castillo et al. 2006).

Osteoclasts

Osteoclasts are multinucleated cells of hematopoietic origin (mostly from the liver and spleen) that form through differentiation of monocyte/macrophage precursors at or near bone surfaces. Osteoclasts are responsible for bone resorption through acid hydrolysis. Osteoclast differentiation and function are both highly regulated by receptor activator of nuclear factor κB ligand (RANKL), which is itself expressed by osteoblasts (Karsenty 2003). Markers of mature osteoclasts include tartrate-resistant acid phosphatase and calcitonin receptor.

Osteoprogenitors

Bone marrow, the endosteum, and the periosteum contain a population of osteoprogenitor cells with the potential to differentiate into a variety of mesenchymal tissues such as bone, cartilage, muscle, and fat (Patterson, Kumagai et al. 2008). These cells differentiate into osteoblast precursors and then into mature osteoblasts when directed by specific signaling stimuli such as Runx2, Osterix, or other growth factors.

Key Biochemical Factors Influencing Bone Formation

Bone metabolism and development are affected by a multitude of molecules, both found within and attached to bone matrix and as soluble factors (Sikavitsas, Temenoff et al. 2001), (Allori, Sailon et al. 2008), (Wozney, Rosen et al. 1988). Some of the more important matrix molecules, along with their presumed roles, include osteocalcin (mineralization inhibitor / bone resorber), osteonectin (nucleator for matrix mineralization), alkaline phosphatase (ALP – promoter of matrix crystal formation), fibronectin (promoter of cell attachment), thrombospondin (organizer of extracellular matrix components / growth factor), proteoglycans I and II (collagen fiber growth modulator), osteopontin (cell attachment promoter), and bone sialoprotein (cell attachment promoter).

Some of the more important soluble factors include vitamin D (stimulator of both bone resorption and matrix mineralization), growth factors such as bone morphogenetic proteins (BMPs – stimulator of chondrocyte and osteoblast proliferation / osteoprogenitor differentiator), fibroblast growth factors (FGFs – stimulator of osteoprogenitor, osteoblast, and chondrocyte proliferation), insulin-like growth factors (IGFs – stimulator of osteoblast and chondrocyte proliferation and matrix secretion), platelet-derived growth factor (PDGF – stimulator of chondrocyte and osteoblast proliferation), transforming

growth factor-β (TGF- β – differentiator of osteoprogenitors to chondrocytes, stimulator of chondrocyte and osteoblast proliferation), epidermal growth factor (EGF – stimulator of chondrocyte proliferation), and vascular endothelial growth factor (VEGF – stimulator of angiogenesis through enhanced proliferation and migration of endothelial cells) (Carano and Filvaroff 2003), hormones such as parathyroid hormone (PTH – differentiator of osteoprogenitors to osteoclasts, liberator of calcium from bone matrix), estrogen (reducer of bone resorption by osteoclasts), dexamethasone (promoter of osteoprogenitors to chondrocytes and osteoblasts), thyroxine (stimulator of osteoclastic bone resorption), and calcitonin (inhibitor of osteoclast function), and cytokines such as prostaglandins (stimulator of osteoclast proliferation and osteoprogenitor differentiation to osteoclasts) and interleukin-1 (stimulator of proliferation of osteoclast precursors).

Bone Development

Bone development occurs by three processes: endochondral ossification, intramembraneous ossification, and appositional bone formation (Sikavitsas, Temenoff et al. 2001), (Kronenberg 2003). Endochondral ossification, as occurs in long and short bone development and fracture healing, begins when osteoprogenitors condense, differentiate into chondrocytes, and secrete a cartilaginous matrix in the general pattern of the bone to be formed. Chondrocytes proliferate and a periosteal layer forms in the diaphyseal region of the developing bone which then begins to mineralize, forming a primary ossification center known as a bone collar. Chondrocytes then become hypertrophic, enabling them to produce proteins to enhance matrix mineralization. Next chondroclasts degrade some of the matrix of the periosteum of the diaphysis and a vascular network begins to form along with a marrow cavity. Osteoprogenitors invade

the cartilage and then differentiate into osteoblasts. The osteoblasts proliferate and contribute to bone growth that increases longitudinally from the central primary ossification center, followed by formation of secondary ossification centers at the ends of the forming bone. The bone ends grows radially rather than longitudinally and cartilage formed in the region develops into growth plates. The calcified cartilage becomes mineralized by the osteoblasts, eventually forming woven bone which later becomes lamellar bone. The long bones continue to grow longitudinally as epiphyseal cartilage is replaced by mineralized bone on the diaphyseal bone ends (Buckwalter, Glimcher et al. 1996).

Flat bone formation occurs through intramembraneous ossification. The process begins as groups of mesenchymal osteoprogenitors form layers and produce a matrix containing blood vessels and more osteoprogenitors. Eventually osteoprogenitors differentiate into osteoblasts and secrete bone matrix, fusing the layers without the initial presence of a cartilaginous layer.

Radial long bone growth in the diaphysis occurs through a process called appositional bone formation. In this process osteoblasts form new bone on older bone surfaces rather than on cartilaginous tissue. Appositional bone formation also occurs during bone remodeling. All three bone formation processes can occur simultaneously.

Bone Homeostasis, Modeling, and Remodeling

Bone is a dynamic tissue that must adapt to biochemical and mechanical environmental changes in order to adequately perform its key functions described previously. In the 19th century Julius Wolff was one of the first suggest that bone structure adapts to changes in functional need. In the 20th century Harold Frost expanded

upon this idea, suggesting that mechanical strain levels were responsible for changes in bone structure (Frost 1963). Frost's mechanostat theory suggests that in developed bones there is a homeostatic physiological strain level between approximately 200 and 1500 microstrain, and that strain levels below this threshold (such as caused by extensive bedrest or spaceflight) will cause bone loss, while strain levels above this threshold (such as caused by vigorous exercise or weight lifting) will result in additional bone formation (although extremely high strains will result in bone damage and fracture). The processes of either enhanced bone formation or resorption are known as modeling, while the homeostatic process of coupled bone formation and resorption is known as bone remodeling (Robling, Castillo et al. 2006).

The effectors of bone modeling are either osteoblasts which form new bone or osteoclasts which resorb bone, while remodeling uses a coupled combination of the two cell types. In the remodeling process, hormonal or physical stimuli cause osteoclasts to form groups called cutting cones that attach to bone surfaces through cytoskeletal rearrangement (Parfitt 1984). Next osteoclasts form tight junctions with bone surfaces, creating a compartment into which they secrete hydrolytic enzymes that dissolve both the organic and inorganic components of bone matrix, resulting in shallow pits in the bone called Howship's lacunae (Dee 1988). Osteoblasts then deposit layers of osteoid in the pit, which are later mineralized.

Bone modeling and remodeling are controlled by a wide variety of signaling cues. RANKL upregulation by signals from stromal-derived cells induces osteoclast activity by binding to RANK on osteoclasts. Osteoclast activity is blocked by downregulation of

RANKL or by expression of osteoprotegerin, a decoy receptor that binds RANKL, thus preventing osteoclast activity and leading to osteoclast apoptosis.

Bone Pathophysiology, Defects, and Repair

Bone Pathophysiology and Defects

Bone defects include both chronic and acute conditions. Many chronic skeletal diseases are linked to imbalances in bone remodeling. Osteoporosis, periodontal disease, rheumatoid arthritis, multiple myeloma, and metastatic cancer are linked to excessive osteoclast activity leading to excessive bone resorption (Boyle, Simonet et al. 2003), while other diseases such as osteopetrosis are caused by excessive osteoblast activity with limited resorption. Acute conditions can be caused by tumor resection or traumatic injury. Trauma can cause transverse or spiral fractures in bone, while extreme cases can cause more severe bone shattering. Large bone defects caused by severe trauma or osteotomy of large sections of bone are particularly challenging to repair (Werntz, Lane et al. 1996), as are cases of osteomyelitis, which is acute or chronic bone infection.

Fracture Healing

The normal long bone healing response to damage in the form of fracture consists of initial inflammation, followed by soft then hard fracture callus formation, and finally late bone remodeling (Khan, Yaszemski et al. 2008). In the inflammatory stage, a hematoma develops within hours to days after injury followed by fibroblast and inflammatory cell invasion. Early vascular invasion accompanies formation of granulation tissue along with migration of osteogenic precursors. During the second stage lasting from a few weeks to months a collagen matrix is formed along with osteoid secretion from osteoblasts, forming a soft callus around the fracture site. If the fracture

site is immobilized through fixation, such as by attachment of metal plates and screws, the osteoid becomes increasingly mineralized forming a hard callus between bone ends primarily made up of woven bone. The last repair stage occurs during a period of months to years as bone remodels with woven bone being gradually replaced by organized lamellar bone and bone structure and strength returning to pre-damage levels (Kalfas 2001).

Clinical Need For Large Bone Defect Repair

As mentioned previously, in fracture nonunions and large bone defects the normal fracture healing response does not occur or does so only to a limited extent, due to a variety of factors such as soft-tissue damage, loss of vasculature, distraction of fracture fragments, soft-tissue interposition, malnutrition, infection, instability, periosteal stripping, and systemic disease such as rheumatoid arthritis (Tseng, Lee et al. 2008). The lack of a healing response creates a need for surgical interventions, such that approximately one third of bone grafting procedures performed in the United States are for patients with nonunions or large defects (Bucholz 2002).

Current Clinical Techniques For Treatment Of Large Bone Defects

The current gold standard for treating large bone defects is the autograft. Autografts possess all of the key features contributing to bone repair: the bone donor and patient are the same person so there are no risks of immune rejection, they contain live osteogenic cells capable of responding to signals to generate bone, they contain blood vessels to deliver nutrients and remove waste, and they have the properties of both osteoconduction (supporting bone growth into graft) and osteoinduction (producing signals to induce proliferation of stem cells and their differentiation to bone cells) (Tseng,

Lee et al. 2008). However, autografts have many drawbacks as well, namely a lack of large amounts of bone available for harvesting (the predominant source is iliac crest bone from the pelvis), donor site morbidity as high as 10-30%, the potential for injury to nerves and blood vessels during harvesting, and possible infection or hematoma formation (Younger and Chapman 1989). One alternative graft option used in place of autografts is processed allograft bone taken from cadavers. While these graft materials do not require harvesting a patient's own bone and are available in larger quantities than autografts, they have many drawbacks including a lack of live osteogenic cells, possibility of disease transmission, lack of porosity thus limiting vascular invasion, and limited remodeling and integration with host bone leading to a 25-35% failure rate due to nonunion and fracture, generally occurring within the first year or two after delivery (Berrey, Lord et al. 1990).

Bone Tissue Engineering

Due to the numerous problems inherent in current treatments for large bone defects there is a clear need for improved therapies. Bone tissue engineers aim to fill this need by trying to create a graft substitute possessing the benefits of both autograft and allograft without their drawbacks (Guldberg, Oest et al. 2004). Langer and Vacanti described tissue engineering as the "interdisciplinary field that applies the principles of engineering and the life sciences toward the development of biological substitutes that restore, maintain, or improve tissue function**"** (Langer and Vacanti 1993). The general approach to creating a tissue-engineered graft substitute is to create a construct consisting of some combination of osteoconductive scaffold / matrix / substrate material, osteogenic cells, and / or osteoinductive bioactive factors. The scaffold serves as a template for

repair as well as a delivery vehicle for cells and / or bioactive factors. The bioactive factor generally provides cues to increase differentiation of osteoprogenitors and enhance mineralization. Bioactive factors are generally in the form of an osteoinductive growth factor or gene or other stimulatory molecule. Cells are solely responsible as the endpoint effectors of bone repair because they produce the new bone matrix. Bone tissue engineering therapies either rely on osteogenic responses from existing host cells at defect sites or feature a cell delivery component.

Bone Defect Models

To evaluate potential new tissue engineering therapies for healing large bone defects, *in vitro* studies can give initial proof of concept results but *in vivo* models must ultimately be established since they better resemble the complicated biological environments that would occur in patients. *In vivo* models should be challenging so that the effects of different therapies can be discriminated. Choices for *in vivo* bone defect models include calvarial or mandibular bone defects as well as radial, ulnar, tibial, or femoral long bone defects. Calvarial defects are often repaired after implantation of only porous scaffolds and thus are not a challenging model, likely due to the presence of many osteoprogenitor cells in the surrounding periosteum and an extensive vascular supply source in the dura mater (Guldberg, Oest et al. 2004). Mandibular defects also frequently heal spontaneously, with control saline treatment leading to defect closures of 29% in one study (Srouji, Rachmiel et al. 2005), also likely due to extensive local periosteal osteoprogenitor supplies.

Truly challenging models of large bone defects are critically-sized, meaning that bone will not spontaneously regrow across the defect if it is left empty, even for extended

periods of time (Hollinger and Kleinschmidt 1990). Large defects in the long bones appear to be a better representation of challenging defects than those created in flat bones, as defects can be made increasingly challenging by increasing the percentage of the long bone diaphysis that is osteotomized. While femoral defects require some type of internal or external fixation device to provide defect-site stability, defects created in the ulna, radius, or tibia each feature a load-sharing bone (radius, ulna, or fibula) which may remove the need for added fixation. However, the presence of the adjacent bone presents a periosteal surface that may host a large number of osteoprogenitors and a developed vascular network, and load-sharing bones allow for osteogenic stimulation of defects through mechanical loading (Tuominen, Jamsa et al. 2001).

Femoral segmental bone defects likely represent the most accurate model of challenging large bone defects. These bone defects are isolated from the vascular and osteoprogenitor supplies of adjacent load-sharing bones (except for the limited amounts present at the bone ends bordering the osteotomized defect), and they require fixation devices which generally shield them from osteogenic mechanical stimuli. Femoral bone defect models have been established in a variety of animals including mice, rats, rabbits, and dogs (Tseng, Lee et al. 2008). Rodent models are an attractive option that have been used extensively for preliminary therapies due to a variety of factors including short times to reach skeletal maturity, limited housing requirements, and low costs. The larger sizes of rats compared to mice allow for more manageable physiological and surgical techniques (Hara, Murakami et al. 2008).

Large bone defect models in the rat femur have been used extensively, although many of them are questionable as a critically-sized defect. Defects of 5 mm lengths or

less have been used in both immunocompetent (Yasko, Lane et al. 1992), (Betz, Betz et al. 2006), (Lee, Shea et al. 1994), (Lin, Barrows et al. 2003) and immunocompromised (Jager, Degistirici et al. 2007) rats, but spontaneous healing has occurred in many of them (Yasko, Lane et al. 1992), (Betz, Betz et al. 2006), (Lin, Barrows et al. 2003). Therefore a truly critically-sized rat femoral defect should be larger than 5 mm, and a length of 8 mm has been used previously (Oest, Dupont et al. 2007), (Rai, Oest et al. 2007), (Lieberman, Le et al. 1998).

We have previously established an 8 mm critically-sized rat femoral defect model in immunocompetent Sasco Sprague Dawley rats for evaluating acellular therapies delivered on either poly(L-lactide-co-D,L-Lactide) (PLDL) (Oest, Dupont et al. 2007) or poly(ε-caprolactone) / tricalcium-phosphate (PCL/TCP) (Rai, Oest et al. 2007) porous polymer scaffolds. The fixation device used in the model (Figure 3.1) consists of a modular design in which the polysulfone bridging plate is attached to a stainless steel plate located on each end of the osteotomized defect rather than to the femur itself. This design allows for removal of the defect-bridging polysulfone plate to be removed without agitation of the defect site prior to mechanical testing to evaluate restoration of bone function. This mode of fixation is advantageous over that traditionally used in rat femoral defects, which consists of a simple polyethylene plate that is directly affixed to native bone ends by pins or Kirschner wires. The direct connection between plate and native bone / implanted therapeutic device can block cellular and vascular access to that portion of the device and also lead to ectopic bone formation along the plate (Kadiyala, Young et al. 1997). Additionally, plates must generally be removed by pulling out

fixation pins or by sawing out the middle of the plate prior to mechanical testing, which can lead to destruction of any mineral network formed by the therapeutic construct.

Our current goal of investigating cell-mediated repair of large bone defects in rats using xenogeneic human cells calls for use of an immunocompromised athymic nude rat model since these animals, which lack T-cells, are much less likely to reject implanted foreign cells than immunocompetent rats. Ideally, the model should allow for quantitative analysis methods assessing functional integration with native bone, including bone formation in the defect, vascular ingrowth, scaffold resorption, restoration of mechanical properties, and tracking of delivered cells.

Scaffold / Matrix / Substrate Options:

Scaffold / matrix / substrate biomaterials serve a variety of purposes in bone tissue engineering applications (Lee and Shin 2007). Some of them include acting as a delivery vehicle for bioactive factors or cells and possibly releasing them at a controlled rate, providing structural support to bone defects, and allowing for infiltration of neovasculature and osteogenic cells. Materials should be ideally be biocompatible, noncytotoxic, and nonimmunogenic, allow for cell infiltration, adhesion and proliferation, be biodegradable so that they do not block formation of developing new bone, and have mechanical properties comparable to adjacent bone for structural integrity (Muschler, Lane et al. 1990). Materials should also ideally be compatible with a variety of fabrication techniques and delivery methods including formation as porous scaffolds, microparticles, hydrogels, or nanofibrous membranes. Further fabrication control is possible for some materials through microscale technologies, which allow material characteristics to be controlled at the micron level, better mimicking the features of the

natural bone environment in order to enhance bone repair (Khademhosseini, Langer et al. 2006).

Some general material choices include natural and synthetic polymers, inorganic materials, and their composites. Natural polymers include collagen, fibrin, alginate, silk, hyaluronic acid, and chitosan (Seeherman and Wozney 2005). Most natural polymers are biocompatible, biodegradable, and are easily solubilized. Disadvantages include immunogenicity, poor mechanical strength, fabrication difficulties, and potential risk of pathogen transmission. Since type I collagen is the most abundant protein in the bone extracellular matrix, many have investigated its potential in bone tissue engineering therapies and it is even in use in human clinical bone defect treatments (InFuse by Medtronic). It can be fabricated into a variety of forms and is biocompatible, but it is mechanically weak and degrades rapidly *in vivo*, although chemical crosslinking can enhance strength and increase degradation times. Fibrin has been crosslinked to form an adhesive gel (Arnander, Westermark et al. 2006), which could be injected into defect sites with or without included cells (Bensaid, Triffitt et al. 2003). Silk has strong mechanical properties and is biocompatible and biodegradable (Kim, Kim et al. 2007). Chitosan, which is a derivative of chitin and linear polysaccharide, allows for a variety of formulations, including sponge, porous scaffold, and nanofiber (Jiang, Abdel-Fattah et al. 2006). One disadvantage of chitosan is that it is not readily degraded in normal physiologic fluids and requires more acidic conditions for resorption.

Synthetic polymers are used frequently in bone tissue engineering applications due to the ability to tailor their properties, such as molecular weight, functional groups, and configurations of polymer chains, depending on desired application (Lutolf and

Hubbell 2005). This tailored structure allows for a much better control of degradation kinetics than in natural polymers (Holland and Mikos 2006). Degradation of synthetic polymers generally occurs through hydrolysis and enzymatic cleavage. Synthetic polymers generally possess more mechanical strength than natural polymers and pose less danger of immunogenicity or disease transmission (Saito, Murakami et al. 2005). Possible disadvantages of synthetic polymers include initiation of an inflammatory response or pH decrease due to release of acidic by-products, slow clearance rates, and limited bioactivity. Some of the most common synthetic polymers are made up of α-hydroxy esters and include poly-lactic acid (PLA), poly-glycolic acid (PGA), or their copolymer PLGA, poly-(ε-caprolactone) (PCL), and poly-ethylene glycol (PEG).

Inorganic materials also provide some options for use in bone tissue engineering therapies. Inorganic materials are generally stiffer than organic polymers, but they are also more brittle, some lack bioactivity or sufficient porosity, and degradation kinetics are generally longer than polymers. Many of them contain elements of the inorganic matrix found in bone. Materials include ceramics such as calcium phosphate cement (CPC), bioactive glasses, hydroxyapatite, and β-tricalcium phosphate, as well as metals such as titanium. CPC is biocompatible and biodegradable as well as osteoconductive, and it can be directly injected into bone defects after which it hardens into a solid form (Ginebra, Traykova et al. 2006). Extended growth factor release from CPC and hydroxyapatite can occur due to high binding affinities of some enzymes and proteins. Titanium has high strength and stiffness and is inert, but it lacks bioactivity.

Composites of organic and inorganic materials can produce improved biomaterial properties. Mechanical properties of stiff but brittle inorganic materials can be improved

by the addition of polymers, which provide toughness and elasticity. Additionally, due to differences in degration kinetics, bioactive factors contained within each composite could be delivered at tailored rates, thereby enhancing therapeutic effects.

Bioactive Factor Options

Bone metabolism and development are affected by a multitude of biochemical factors (Sikavitsas, Temenoff et al. 2001). Supplemental delivery of one or more of these factors in bone tissue engineering therapies, generally in supraphysiological doses, can greatly enhance bone defect repair. As described previously, there are a variety of bioactive factor choices, but in general consistent therapeutic effects have been shown after delivery of growth factors, especially the BMPs (Chen, Zhao et al. 2004).

Urist was one of the first to find that demineralized bone matrix displayed osteoinductive properties, mostly due to the fact that it contains low levels of proteins which were termed BMPs (Urist 1965). These cytokines are members of the TGF-β super family. BMP signaling involves binding of this protein to a transmembrane receptor to initiate Smad-dependent and –independent signaling pathways that activate a cascade of osteogenic transcription factors, in particular Runx2 and Osterix (Bucholz 2002). BMPs act by promoting the migration, proliferation, and differentiation of bone-forming cells and their precursors such as MSCs. In addition to its role in matrix mineralization, BMP2 also plays a role in cartilage and skeletal connective tissue formation (Wozney and Rosen 1998). There are multiple isoforms of BMP, and BMP2, 4, and 7 are generally considered the most osteoinductive. BMPs are sufficiently conserved across species so that human BMP is also effective in lower animals (Yoon and Boden 2002). Extraction of beneficial amounts of BMP from bone is not very

practical since there is only about one or two micrograms in one kilogram of cortical bone, but eventually the ability to produce human BMP was realized through recombinant gene technology (Wozney, Rosen et al. 1988).

Systemic growth factor administration is generally not as effective as local delivery due to a lack of long term growth factor stability because of their short biological half lives, tissue-specific growth factor activity, and potential dose-dependent carcigenicity (Lee and Shin 2007). Local delivery is generally accomplished through growth factor immobilization onto or within scaffolds, matrices, or gels. Immobilization methods include noncovalent (physical entrapment, surface adsorption, affinity binding, or ionic complexation) or covalent bonding (chemical conjugation). While local recombinant protein growth factor delivery is more effective than systemic delivery, protein half lives are still short, so effective therapeutic benefits generally require administration of very high doses of protein, often causing ectopic bone formation and having high costs.

One alternative to delivery of large doses of recombinant BMPs to treat bone defects is to program cells to increase their production of these proteins by gene therapy techniques. Gene therapy is the science of transferring genetic material into organisms for therapeutic purposes by altering cellular function or structure at the molecular level (Wu, Razzano et al. 2003). More than 1000 clinical gene therapy trials (mostly Phase I but at least 20 Phase II) have been approved worldwide, with 2 / 3 of them in the United States (Ulrich-Vinther 2007). Some experimental investigations have demonstrated that gene therapy methods for bone regeneration use lower doses of cell-produced growth factors to yield bone healing equivalent to that achieved by the administration of higher

doses of recombinant growth factors (Kofron and Laurencin 2006). Successful gene therapy involves multiple steps including transduction (entry of desired exogenous DNA first into cells and then into their nuclei), transcription of the DNA into RNA, and finally translation as RNA sequences encode for desired protein expression (Oakes and Lieberman 2000). Multiple delivery vehicles, called vectors, have been investigated for delivery of exogenous DNA. Gene therapy approaches can either be *in vivo*, where vectors are delivered directly to the site of repair to transduce host cells, or in *vitro*, where cells are harvested from a patient or allogeneic source, expanded in culture and transduced by the vector, and then implanted in the patient. *In vivo* methods require one surgical step only, but it is more difficult to guarantee transduction of cells and there is a limited selection of cells to target. *In vitro* methods offer better selection of cells to transduce, but they require two surgeries if host cells are used and are often more costly and labor intensive.

Gene therapy vectors can be divided into two main groups, either nonviral or viral. Nonviral vectors are generally less toxic, less immunogenic, and easier to prepare than viral vectors (Jang, Houchin et al. 2004). However, they are also generally less efficient at transducing cells, with one report estimating that the efficiency of nonviral vectors is 10^{-9} that of viral vectors (Franceschi, Wang et al. 2000). Many nonviral vectors also cause high cell mortality (Song, Chau et al. 2004). One type of nonviral vector is the gene-activated matrix (GAM), which consist of a degradable matrix or scaffold containing entrapped or adsorbed expression plasmid DNA (Fang, Zhu et al. 1996), (Jang, Bengali et al. 2006). Other nonviral vectors act to introduce naked DNA into cells, including lipofection, electroporation, and use of gene guns. Due to the

extremely low transduction efficiencies of nonviral vectors, viral vectors currently pose the most potential for use in successfully treating challenging large bone defects.

Viral vectors such as retrovirus, lentivirus, adenovirus, and adeno-associated virus have been used as gene therapy vectors and all have advantages and disadvantages. The primary concern when choosing a viral vector for bone tissue engineering gene therapies must be safety. In general, bone defects are nonlethal conditions so therapies causing even small increases in morbidity or mortality will not be acceptable to patients or surgeons (Baltzer and Lieberman 2004). This need for safety points towards use of a viral vector where delivered DNA remains episomal and does not integrate into the host genome, becoming chromosomal DNA. Retrovirus has been used to deliver the gene encoding for BMP4 to cells that healed rat segmental defects (Rose, Peng et al. 2003). However, retrovirus integrates chromosomally and can cause insertational mutagenesis leading to unpredictable protein expression, so its safety is questionable. Lentivirus is a subclass of retrovirus and has similar disadvantages. Studies using adenoviral vectors to transduce cells with BMPs have been used in animal bone defect models and shown some successes in generating new bone (Betz, Betz et al. 2006), (Lieberman, Le et al. 1998), (Peterson, Zhang et al. 2005). However, adenovirus can cause an immune response due to it producing additional viral proteins other than those encoded for by addition of the transgene of interest. These issues, along with reports of adverse effects in clinical trials utilizing adenoviral and retroviral vectors (Shalala 2000), suggest that other viral vectors may prove to be a better choice for large bone defect repair.

The adeno-associated virus (AAV) possesses many qualities that make it an attractive viral vector choice, such as the absence of host inflammatory, cytotoxic, or cell-

mediated immune responses and the abilities to transduce a broad range of cells including musculoskeletal cells, infect dividing and non-dividing cells, and deliver long term gene expression cell types that have relatively long lifetimes, such as osteocytes or muscle cells. Disadvantages include a limited packaging size, difficulty in AAV production, and lack of long term expression in some cells (Schwarz 2000). The lack of long term gene expression may actually be an advantage for application in healing large bone defects. Local transient expression (on the order of weeks) of a sufficient level of protein product such as BMP2 to initiate osteogenesis is all that is required (Gamradt and Lieberman 2004) to heal most localized bone defects compared to chronic and systemic bone conditions such as osteoporosis which may require extended gene expression for successful treatment. AAV is a non-enveloped, small (≈ 20 nm), single-stranded DNA (5 kb of nucleotides) subclass of parvovirus that is thermostable and resistant to solvents and changes in pH (Coura Rdos and Nardi 2007). Wild type AAV (wtAAV) contains genetic sequences encoding for the proteins Rep and Cap which are responsible for viral replication and encapsidation, but these sequences (along with the majority of the AAV genome) can be removed and replaced by a transgene sequence of interest to from a biologically active recombinant AAV (rAAV) vector (Schwarz 2000). Nearly 80% of all adults have circulating antibodies against wtAAV, however wtAAV is not known to cause disease in the human population (Fielding, Maurice et al. 1998).

Cell Options

While some bone tissue engineering therapies may rely on local host cells to provide an osteogenic response, treatment of challenging large bone defects is likely to require a cell delivery component because patients such as the elderly, smokers, those

receiving chemotherapy or radiation, and those with severely damaged wound beds may have compromised endogenous availability of osteogenic or osteoprogenitor cells (Bruder 1999). Additionally, patients in which a large volume of bone is removed or lost, especially from the long bones, will lose the stem cell populations located in the marrow space as well in the endosteum and periosteum of that bone volume. There are a wide variety of active cell types present within bones, but for tissue engineering therapies delivery of a specific population of cells may be most beneficial (Kadiyala, Young et al. 1997). A large number of cells may be necessary to significantly aid the healing response in challenging large bone defects, therefore stem cells are an attractive candidate for inclusion in bone tissue engineering therapies because they can not only differentiate into cells of an osteogenic lineage but also extensively proliferate to expand the cell supply (Song and Tuan 2004). Stem cells can be delivered to defect sites through direct injection or by seeding them on scaffolds or matrices prior to implantation. Stem cells can be delivered without any modifications, or they can be pre-differentiated in culture or transgenically modified to express desired proteins through gene therapy techniques as described previously.

Autologous stem cells may be harvested from patients with bone defects, expanded in culture and then implanted back into those patients as part of a tissue engineering therapy. Autologous stem cells are an attractive choice because they will not activate an immune response in patients, but again in many challenging bone defect cases there is a very limited supply of endogenous stem cells. Therefore allogeneic stem cells harvested from other patients could potentially be used for treatment. There is evidence to suggest that stem cells are immune-privileged cells such that allogeneic stem cells may

be immunologically inert enough to successfully engraft within patients (Arinzeh, Peter et al. 2003).

There are a variety of stem cell choices for bone tissue engineering, with potentially therapeutic cell types originating from a variety of tissues and originating from a number of stages of development (Waese, Kandel et al. 2008). Some options include adult mesenchymal stem cells (MSCS) derived from the bone marrow, adipose tissue, or muscle. More developmentally primitive stem cell sources include umbilical cord perivascular stem cells (HUCPVC), amniotic fluid stem cells (AFS Cells), and embryonic stem cells (ESCs).

A heterogeneous population of adult stem cells has been found predominantly in the bone marrow (Patterson, Kumagai et al. 2008) but also in adipose tissue (Zuk, Zhu et al. 2001) and skeletal muscle (Jankowski, Deasy et al. 2002), among other locations. Adipose-derived MSCs may be a particularly attractive stem cell source because of their relative abundance and ease of harvest of adipose tissue compared with bone marrow (Wall, Bernacki et al. 2007). Adult MSCs lack a single defining marker, but they share certain features. MSCs adhere to tissue culture plates and have the ability to differentiate into musculoskeletal tissue phenotypes such as bone, cartilage, fat, and fibrous tissue, although some studies have suggested they have even broader differentiation potential (Patterson, Kumagai et al. 2008). MSCs are capable of approximately 50 population doublings in *in vitro* culture (Derubeis and Cancedda 2004). MSCs are generally obtained through marrow aspiration of the superior iliac crest of the pelvis (Pittenger, Mackay et al. 1999).

In addition to adult stem cell sources, a variety of stem cells with osteogenic differentiation potential can be found associated with the developing embryo and fetus. In a recent study directly comparing human adult and fetal bone marrow-derived MSCs, the fetal MSCs displayed significantly higher *in vivo* mineral formation in rats two months after subcutaneous implantation on PCL-TCP scaffolds (Zhang, Teoh et al. 2009). Human umbilical cord perivascular cells (HUCPVCs) are pericyte-like cells from the umbilical cord vessels. These mesenchymal progenitor cells proliferate extensively without loss of multipotent differentiation potential and can form osteoblasts, adipocytes, chondrocytes, myoblasts, and fibroblasts (Sarugaser, Lickorish et al. 2005). A small population of multipotent fetal stem cells exists within the amniotic fluid. (Tsai, Lee et al. 2004), (De Coppi, Bartsch et al. 2007). These cells express the membrane receptor c-kit as well as many ESC markers including SSEA4 and Oct4, require no feeder layers for culture, have not formed teratomas *in vivo*, are capable of more than 300 population doublings in culture due to preservation of telomere length, and can differentiate into cells from all three germ layers in vitro, including osteogenic, adipogenic, myogenic, neurogenic, endothelial, and hepatic phenotypes (Delo, De Coppi et al. 2006). Use of AFS Cells also circumvents ethical controversy associated with use of ESCs. The embryonic stem cell (ESC) can differentiate into cells from all three germ layers, divide and renew itself for very long periods due to extended telomerase expression, and easily be grown in culture (Hyslop, Armstrong et al. 2005). ESCs also have a proliferation rate far faster than MSCS. However, use of ESCs is ethically controversial as harvesting of ESCs requires destruction of human embryos. Furthermore, these cells can cause

teratomas by proliferating and differentiating uncontrollably, and they require animal-derived feeder layers for *in vitro* growth in culture.

Chapter 3

ESTABLISHMENT OF A CHALLENGING LARGE BONE DEFECT MODEL IN IMMUNOCOMPROMISED RATS FOR EVALUATION OF THE ABILITIES OF HUMAN ADULT AND FETAL STEM CELLS TO ENHANCE DEFECT HEALING

Chapter 3: Introduction

To evaluate potential new therapies for healing large bone defects, *in vitro* studies can give initial proof of concept results but *in vivo* models must ultimately be established since they better resemble the complicated biological environments that would occur in patients. *In vivo* models should be challenging so that the effects of different therapies can be discriminated. Choices for *in vivo* bone defect models include both long bone segmental defects (such as in the femur or tibia) and calvarial defects. However, calvarial defects are often repaired after implantation of only porous scaffolds and thus are not a challenging model (Guldberg, Oest et al. 2004). Bone defect models have been established in a variety of animals including mice, rats, rabbits, and dogs (Tseng, Lee et al. 2008). Rodent models are an attractive option that have been used extensively for preliminary therapies due to a variety of factors including short times to reach skeletal maturity, limited housing requirements, and low costs. The larger sizes of rats compared to mice allow for more manageable physiological and surgical techniques (Hara, Murakami et al. 2008). Truly challenging models of large bone defects are critically-sized, meaning that bone will not spontaneously regrow across the defect if it is left empty (Hollinger and Kleinschmidt 1990). Large bone defect models in the rat femur have been used extensively, although many of them are questionable as a critically-sized

defect. Defects of 5 mm lengths or less have been used in both immunocompetent (Yasko, Lane et al. 1992), (Betz, Betz et al. 2006), (Lee, Shea et al. 1994), (Lin, Barrows et al. 2003) and immunocompromised (Jager, Degistirici et al. 2007) rats, but spontaneous healing has occurred in many of them (Yasko, Lane et al. 1992), (Betz, Betz et al. 2006), (Lin, Barrows et al. 2003). Therefore a truly critically-sized rat femoral defect should be larger than 5 mm, and a length of 8 mm has been used often (Oest, Dupont et al. 2007), (Rai, Oest et al. 2007), (Lieberman, Le et al. 1998). We have previously established an 8 mm critically-sized rat femoral defect model in immunocompetent Sasco Sprague Dawley rats for evaluating acellular therapies delivered on either poly(L-lactide-co-D,L-Lactide) (PLDL) (Oest, Dupont et al. 2007) or poly(ε-caprolactone) / tricalcium-phosphate (PCL/TCP) (Rai, Oest et al. 2007) porous polymer scaffolds.

Our current goal of investigating cell-mediated repair of large bone defects in rats using xenogeneic human cells calls for use of an immunocompromised athymic nude rat model since these animals are less likely to reject implanted foreign cells. Ideally, the model should allow for quantitative analysis methods assessing functional integration with native bone, including bone formation in the defect, vascular ingrowth, scaffold resorption, restoration of mechanical properties, and tracking of delivered cells.

Furthermore, our choice of scaffold should support cell delivery, and ideally include 3D porous architecture for cell attachment / proliferation, allow vascular invasion, be biocompatible and bioresorbable, have suitable surface chemistry and mechanical properties similar to the tissue at the implantation site, meet FDA approval, and have reproducible architecture to clinically relevant size and shape (Dawson and

Oreffo 2008), (Jones, Milthorpe et al. 2004). Porous 3D honeycomb-shaped PCL scaffolds, designed and fabricated by fused deposition modeling techniques, meet nearly all of these needs (i.e. PCL has slightly higher mechanical properties than trabecular bone and is resorbed through hydrolysis (Khan, Yaszemski et al. 2008)) and has shown to be an effective scaffold for multiple bone tissue engineering applications (Hutmacher 2000). PCL has been approved by the FDA for use in the human body as a drug delivery vehicle, suture material, or adhesion barrier.

As mentioned previously, stem cells are a key candidate for tissue engineering therapies such as repair of large bone defects due to their ability to proliferate into large numbers of cells as well as differentiate into musculoskeletal cells such as bone, cartilage, and fat cells. Adult stem cells are present in mature adults and their purpose is to supply progenitors for normal tissue turnover and repair of damaged tissue. Friedenstein was one of the first to identify a cell population with strong osteogenic potential in adult bone marrow (Friedenstein 1976). The cells would adhere to tissue culture dishes, form spindle-shaped cells appearing similar to fibroblasts, and proliferate to form colonies, so they were first called colony forming unit-fibroblasts. The cells were also found to have the ability to differentiate down an osteogenic lineage when given the appropriate osteoinductive stimuli. Since Friedenstein's early work, there has been much research investigating adult stem cells present in bone marrow. Adult stem cell populations have been found and referred to by various terms such as mesenchymal stem cells, bone marrow stromal cells, multipotent adult progenitor cells, connective tissue progenitors, and mesodermal progenitor cells (Derubeis and Cancedda 2004), (Patterson, Kumagai et al. 2008).

Some investigators have proposed that all of these differently named cell subtypes are actually indistinguishable (at least at the point of initial culturing) (Lodie, Blickarz et al. 2002), while others claim that they are in fact distinct (Patterson, Kumagai et al. 2008). It is difficult to prove one viewpoint versus the other due to the fact that the adult stem cells lack a single definitive marker (although most display markers SH-2, 3, and 4 and are negative for hematopoeitic markers CD34 and CD45) and there is no knowledge regarding their exact anatomical distribution *in vivo*. Although their primary location is thought to be in bone marrow stroma, they have also been found in other tissues such as trabecular bone, adipose tissue, synovium, skeletal muscle, lung, teeth, and human umbilical cord (Baksh, Song et al. 2004), (Caplan 2004). Although there are possibly some heterogeneities in these cells, they share the features of being adherent in culture conditions and forming colonies of spindle-shaped cells as well as having the ability to form one or more connective tissue phenotypes including bone, cartilage, fat, and fibrous tissue (Patterson, Kumagai et al. 2008). I will refer to these stem cells as mesenchymal stem cells (MSCs). Other groups have shown that under certain conditions these cells can be led to differentiate into neurons and epithelia in skin, lung, liver, intestine, kidney, and spleen, although there is some controversy surrounding their ability to differentiate into cells from non-mesodermal germ layers (Baksh, Song et al. 2004).

Multiple studies have been performed to investigate the MSC as a therapy for healing bone defects. Bruder performed some early investigations, including use of autologous MSCs to heal large segmental defects in canines when delivered on ceramic carriers (Bruder, Kraus et al. 1998) and use of hMSCs to heal critically-sized defects in athymic nude rats when delivered on ceramic carriers (Bruder, Kurth et al. 1998). There

is also evidence that MSCs may cause less of an immune response than other cells types, or even reduce immune responses in general, when implanted into an allogeneic recipient (Le Blanc and Ringden 2006). Arinzeh showed that allogeneic MSCs delivered within hydroxyapatite / tricalcium phosphate carriers could heal large canine femoral bone defects (Arinzeh, Peter et al. 2003). They found no immune response as assessed by analysis of recipient serum for production of antibodies against allogeneic cells. Additionally, MSCs mismatched for major histocompatibility complex antigens were administered intravenously into baboons receiving allogeneic skin grafts, and animals that received MSCs had longer graft survival compared to animals receiving no MSCs (Bartholomew, Sturgeon et al. 2002). Furthermore, when allogeneic MSCs were added to cultures of T cells that were stimulated by allogeneic peripheral blood lymphocytes, a significant and dose-dependent reduction of T-cell proliferation was evident (Di Nicola, Carlo-Stella et al. 2002). Finally, co-delivery of MSCs in an allogeneic renal transplantation model down-regulated rat immune responses, preserving graft function and prolonging animal survival, although not as well as treatment with the immunosuppressant cyclosporine A (Zhang, Qin et al. 2007). However, the immunomodulatory effects of MSCs are still under debate, as co-delivery of MSCs in a rat allogeneic heart transplant model failed to reduce recipient immune responses (Inoue, Popp et al. 2006). There has also been at least one clinical trial involving harvesting of autologous MSCs from bone marrow aspirates, expanding them in culture, and implanting them into segmental defects (Quarto, Mastrogiacomo et al. 2001) .

Although MSCs offer great potential for use in healing large bone defects, they do have some drawbacks. MSC numbers *in vivo* decrease as people age because many of

them differentiate during growth, development, and tissue repair throughout a lifetime (Caplan 2004). Because MSCs are stem cells they can be harvested and expanded *in vitro*, but they reach senescence and lose multilineage differentiation capability after 34-50 population doublings in culture due to telomere shortening (Derubeis and Cancedda 2004). For stem cell-mediated repair of large bone defects in humans, implantation of hundreds of millions of cells might be necessary to achieve a significant therapeutic effect, and achieving that number of MSCs might be difficult. The scarcity of MSCs in large numbers thus prompts the search for alternative sources of multipotent cells for tissue engineering applications (Waese, Kandel et al. 2008).

The embryonic stem cell (ESC) would at first appear to be an optimal alternative to MSCs because it can differentiate into cells from all three germ layers, divide and renew itself for very long periods, and easily be grown in culture. However, harvesting of ESCs requires destruction of human embryos, which is ethically unacceptable to many. Furthermore, these cells can cause teratomas by proliferating and differentiating uncontrollably, and they require feeder layers for *in vitro* growth. Therefore other fetal stem cell sources have been investigated that ideally would exhibit the benefits of the ESC while lacking its limitations. One attractive alternative is the amniotic fluid stem cell.

The process of obtaining amniotic fluid through amniocentesis has been used for years as a generally safe, reliable, and simple screening tool to test the fetus for a variety of developmental and genetic diseases (Caplan, Zwilling et al. 1968). Approximately 10-20 mL of amniotic fluid is harvested during the second trimester of pregnancy, and the fluid contains approximately 10 to 1000 heterogeneous cells per microliter of fluid (Prusa

and Hengstschlager 2002). Researchers have found that subpopulations of multipotent progenitor cells reside within this fluid (Tsai, Lee et al. 2004), (De Coppi, Bartsch et al. 2007). The harvesting protocol to obtain these cells does not interfere with the normal culture process for fetal karyotyping (Tsai, Lee et al. 2004). The multipotent cells, referred to as amniotic fluid stem cells (AFS Cells), make up approximately one percent of the heterogeneous cell population and can be isolated by positive selection for cells expressing the membrane receptor c-kit, which binds to the ligand stem cell factor (De Coppi, Bartsch et al. 2007). These cells express many but not all of the markers of ESCs, require no feeder layers for culture, have not formed teratomas *in vivo*, are capable of more than 300 population doublings in culture due to preservation of telomere length through continued telomerase activity, and can differentiate into cells from all three germ layers *in vitro*, including osteogenic, adipogenic, myogenic, neurogenic, endothelial, and hepatic phenotypes (De Coppi, Bartsch et al. 2007). Use of AFS cells also circumvents ethical controversy associated with use of ESCs. They have been shown to have superior differentiation capacity to become hepatocytes than hMSCs in direct comparison (Zheng, Gao et al. 2008). Of particular importance to bone repair, when cultured in osteogenic media containing dexamethasone, β-glycerol phosphate, and ascorbic acid 2-phosphate hAFS Cells precipitated calcium and expressed alkaline phosphatase, core binding factor A1, and osteocalcin, indicating differentiation into cells of an osteogenic lineage. hAFS Cells have been shown to readily produce robust mineralized matrix within 3D porous polymer scaffolds both *in vitro* and ectopically *in vivo* (Peister, Porter et al. 2008), (Peister, Deutsch et al. 2009). Based on this encouraging initial data, hAFS Cells could be a superior stem cell than hMSCs for application to healing large bone defects. A person's

hAFS Cells could be harvested during amniocentesis, isolated in culture, and cryopreserved for their future use. Additionally, if hAFS Cells are immune-privileged cells, as MSCs possibly are, they could theoretically be obtained from any donor.

The purpose of this Aim was to first establish a critically-sized large bone defect model in immunocompromised nude rats, and then to use that model as a test bed for comparing the therapeutic potentials of human fetal amniotic fluid-derived and adult bone marrow-derived stem cells as effective bone tissue engineering treatment modalities. We confirmed critical defect size, even after treatment with porous polymer scaffolds, establishing the validity of the model as a representation of challenging large bone defects. We found that while hAFS Cell-seeded PCL scaffolds displayed significantly higher mineral formation than hMSC-seeded PCL scaffolds after 12 weeks in *in vitro* culture in the presence of osteogenic stimuli, there were no significant differences in *in vivo* mineral formation or torsional mechanical properties between segmental defect femurs treated with either scaffolds seeded with stem cells from either source or acellular scaffolds. However, grouping all defects treated with stem cells led to significantly higher *in vivo* defect mineral formation as well as maximum torque compared to treatment of defects with acellular PCL scaffolds. The lack of significant differences between individual stem cell groups could be explained by a lack of sufficient osteogenic stimuli, which could push stem cells to differentiate down an osteogenic lineage and enhance defect mineral formation. Another possible explanation could be that implanted stem cells do not survive long enough to reveal any differences between stem cell sources as were observed in the 3D *in vitro* study only after 12 weeks culture.

Chapter 3: Materials and Methods

Scaffold Preparation: Poly(ε-caprolactone) (PCL) cylindrical scaffolds, 9 mm height, 5 mm diameter, and 85% porosity were punched from PCL sheets (Osteopore International, Singapore) using dermal biopsy punches. The scaffolds feature a honeycomb array of layers of interconnected struts oriented in a repeated lay-down pattern of 0 / 60 / 120º. Scaffolds were sterilized by ethanol evaporation and then soaked in a 50 μg / mL solution of the collagen-mimetic peptide GFOGER overnight at 4° C. The peptide, GGYGGGPC$(GPP)_5$GFOGER$(GPP)_5$GPC, was synthesized by the Emory University Microchemical Facility (Atlanta, GA) as described previously (Reyes and Garcia 2003). This peptide contains the GFOGER motif, where O refers to hydroxyproline. The purified peptide was lyophilized as a trifluoroacetic acid (TFA) salt. The peptide was reconstituted at a concentration of 10 mg/mL in a 0.1% TFA solution containing 0.01% sodium azide (NaN_3). The stock solution was diluted the working concentration of 50 μg/mL in PBS. GFOGER interacts with the $\alpha_2\beta_1$ integrin on stem cell surfaces and can induce osteoblast differentiation and enhance matrix mineralization (Reyes and Garcia 2004), (Reyes, Petrie et al. 2007). Next, scaffolds were coated with 1.5 mg / mL type I collagen (Vitrogen 100, Cohesion Technologies, Palo Alto, CA, USA) through lyophilization to increase cell adhesion. Note that scaffolds used in the preliminary *in vivo* nude rat segmental defect study establishing critical defect size were coated with type I collagen but not GFOGER.

Cell Culture: hMSCs (passage 3-4) were obtained as a gift from Dr. Darwin Prockop at Tulane University (New Orleans, LA) and were originally isolated from bone marrow aspirates as described previously (Sekiya, Larson et al. 2002). Human AFS Cells

(p 18-19) were obtained as a gift from Dr. Anthony Atala and Dr. Shay Soker at the Wake Forest Institute for Regenerative Medicine (Winston-Salem, NC) and were originally isolated from human amniotic fluid as described previously (De Coppi, Bartsch et al. 2007). Cells were seeded on tissue culture plates and grown to near-confluence in culture media (α-MEM (Minimum Essential Medium), 16.7% fetal bovine serum (Atlanta Biologicals, Lawrenceville, GA), 100 units/ml penicillin / 100 μg/ml streptomycin / 2 mM L-glutamine [PSL] (Invitrogen, Carlsbad, CA)). Cells were washed with phosphate-buffered saline (PBS, Mediatech Inc., Manassas, VA) and then trypsinized, centrifuged, and resuspended. Cells were counted using a haemocytometer.

For the 3D *in vitro* stem cell source comparison study, one million hMSCs or hAFS Cells in 100 μL of culture media were seeded onto PCL scaffolds (n=6 / cell source) described above and scaffolds were incubated at 37º C / 5% CO_2. Each scaffold was located in one well of a 12-well tissue culture plate and was held with its long axis upright by a custom polymer / stainless steel stand. One hour after seeding 4 mL of culture media was added to each well of the 12-well plate, covering each scaffold in its entirety. Standard culture media was supplemented with 1 nM dexamethasone, 6 mM β-glycerol phosphate, 50 μg/ml ascorbic acid 2-phosphate, and 50 ng / mL L-thyroxine after three days, and this osteogenic media was used throughout the rest of the 12-week study. Also after three days of static culture plates were placed on a rocker plate (The Belly Button, Stovall Life Science Inc., Greensboro, NC) to create dynamic culture conditions, which can increase mass transport throughout constructs and possibly lead to fluid shear stresses on cells that can further push stem cells towards osteogenic differentiation. Media was changed every 3-4 days.

For the *in vivo* segmental defect stem cell source comparison study, culture procedures and scaffold coatings were similar to those used in the 3D *in vitro* study mentioned above. However, in the *in vitro* study only one donor was used per cell source, and in this study cells from an additional donor for each cell source were pooled with cells from the first donor to lessen effects of donor variability. Additionally, scaffolds were loaded with either three million hMSCs or hAFS Cells (n = 14 / source) rather than one million cells. Stem cell-seeded scaffolds were cultured statically for 2 days in standard culture media prior to implantation.

Assessment of Cell Viability: Twelve weeks after seeding cells on scaffolds as described above for the *in vitro* study (one million cells / one donor), one scaffold containing cells from each source was removed from culture, washed with PBS, cut in half longitudinally with a scalpel, and then stained with Live / Dead stain (Molecular Probes, Inc.) Scaffolds were incubated in 4 μM calcein-AM and 4 μM ethidium homodimer-1 for 45 minutes at room temperature. The scaffolds were again rinsed with PBS and then images were obtained on a Zeiss LSM 510 confocal microscope (Carl Zeiss, Thornwood, NY). Green fluorescence of calcein-AM was detected by using a 488-nm Argon ion laser and a band pass 505-550 filter. Red fluorescence of ethidium homodimer-1 was detected by using a 543-nm Helium-Neon laser and a long pass 560 filter. Images were obtained at locations around the periphery, top, bottom, and central cut scaffold faces.

DNA Analysis: Three days after seeding cells as described above for the *in vivo* study (three million cells / two donors), scaffolds from each source were removed from culture in order to quantify amount of DNA present (n = 5 / stem cell source). The

approximate mass of DNA in each diploid human cells is 6.6 pg (Otto 2005), and by evaluating total mass of DNA per scaffold we could estimate the actual number of cells loaded. Although collagen lyophilization onto scaffolds does enhance cell attachment, the retention efficiency will always be less than 100%. Scaffolds were washed with PBS and dried overnight in a speed vacuum (DNA SpeedVac 120, Thermo Scientific). Next scaffolds were digested with Proteinase K (Worthington Biochemical, Lakewood, NJ) in a water bath at 55°C with intermittent vigorous vortexing, followed by DNA quantification using a PicoGreen assay (Quant-iT PicoGreen dsDNA Quantification Kit, (Molecular Probes, Eugene, OR) following the manufacturer's protocol. Fluorescence was measured using a fluorescence plate reader (PerkinElmer HTS 7000) at an excitation of 485-nm and emission of 535-nm. All samples were run in triplicate.

Surgical Technique: All surgical techniques were approved by the Georgia Institute of Technology Institutional Animal Care and Use Committee (protocol A08032). Female immunocompromised athymic nude rats (Charles River Labs, Wilmington, MA), age 13 weeks, were anesthetized using isoflurane. Using an antero-lateral approach, bilateral incisions were made over the lengths of each femur. Each limb received a custom modular fixation plate secured directly to the femur using four miniature screws (J.I. Morris Co, Southbridge, MA), as shown in Figure 3.1 below. This novel modular composite design is used to achieve reproducible stable fixation, provide a window for longitudinal *in vivo* monitoring of 3D bone ingrowth, and allow careful removal of the polysulfone bridging plate from the anchoring stainless steel plates prior to torsional biomechanical testing of functional integration (Oest, Dupont et al. 2007), (Rai, Oest et al. 2007). Bilateral full-thickness diaphyseal segmental defects, 8mm-long,

were created using a miniature oscillating saw and flushed with saline to remove any bone chips.

For the preliminary study to establish defect critical size, a collagen-coated PCL scaffold was press fit into one of the defects and the contralateral defect remained empty (n = 2 / group). For the study comparing stem cell sources, hMSC constructs (n = 9), hAFS Cell constructs (n = 9), or acellular PCL / GFOGER / lyophilized collagen I control scaffolds (n = 8), were press fit into defects. Wound sites were closed with interrupted sutures followed by wound clip application. Rats were given subcutaneous injections of 0.03 mg/kg buprenorphine every 8 hours for the first 48 hours post-surgery and 0.01 mg/kg buprenorphine every 8 hours for the following 24 hours for pain relief. Animals resumed normal ambulation and behavior within three days.

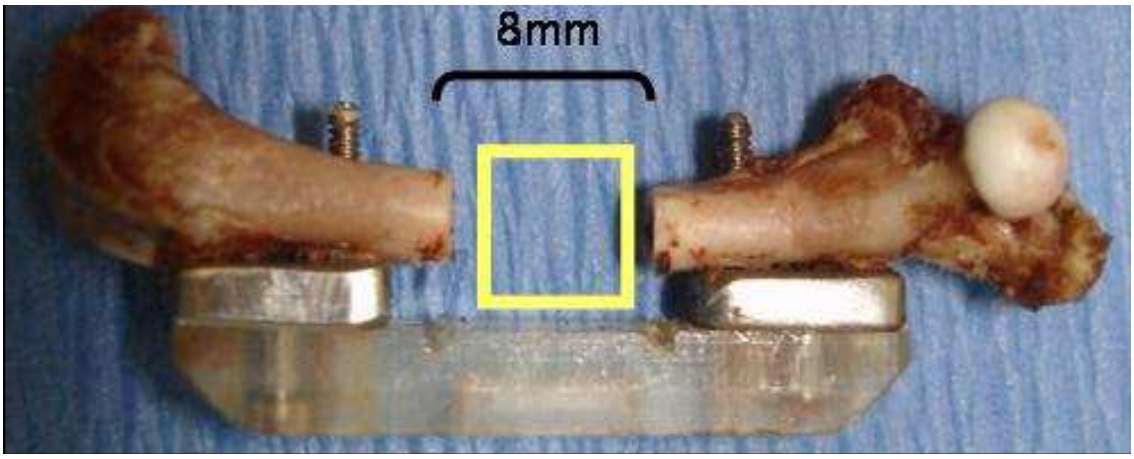

FIGURE 3.1: Critically-sized rat femoral defect, showing modular stainless steel / polysulfone fixation plate

Radiograph Imaging: For both the preliminary and stem cell delivery segmental defect studies, qualitative bone growth into defect sites was assessed by 2D *in vivo* digital

X-rays (Faxitron MX-20 Digital, Faxitron X-ray Corp., Wheeling, IL) taken at 4, 8, and 12 weeks post-surgery after rats were anesthetized with isoflurane.

Microcomputed Tomography (Micro-CT) Imaging: Micro-CT is a fast and non-destructive technique that can be used to characterize and measure the 3D properties of scaffold / tissue composites during bone growth (Jones, Milthorpe et al. 2004). Micro-CT systems use micro-focal spot X-ray images collected from multiple viewing directions to produce 3D reconstructed images of sample material density in attenuating objects such as bone (Guldberg, Ballock et al. 2003), (Guldberg, Lin et al. 2004).

It has previously been shown that cell-seeded scaffolds can be scanned repeatedly to monitor mineral formation as a function of time in culture, and that weekly scanning radiation doses do not significantly affect mineralized matrix formation by rat calvarial cells or rat MSCs (Cartmell, Huynh et al. 2004), (Porter, Lin et al. 2007), (Guldberg, Duvall et al. 2008). For the 3D *in vitro* study comparing stem cell sources, cell / scaffold constructs were sealed in custom sterile containers and scanned by Micro-CT (Viva-CT 40, Scanco Medical, Bassersdorf, Switzerland). Scaffolds were scanned after 3, 6, 9, and 12 weeks in culture. A 38.5 micron voxel resolution, 55-kVP voltage, and 109 μA current were used along with a Gaussian filter (sigma = 1.2, support = 1) to suppress noise, and a density threshold corresponding to 180.52 mg hydroxyapatite / cm^3 was used to discriminate newly formed mineral from polymer scaffolds.

For both *in vivo* studies, quantitative defect site mineral formation was assessed by *in vivo* CT scans at 8 and 12 weeks post-surgery. After application of isoflurane anesthesia, the live rats were positioned in a custom scanning chamber to isolate the defects in the center of the scanning region. A 38.5 micron voxel resolution was used,

and after scanning a constant volume of interest (VOI) approximately 4 1/3 mm long centered in the middle of the defect region was chosen to ensure measurement of new mineral formation and avoid measuring native cortical bone ends. A Gaussian filter was used to suppress noise, and a density threshold corresponding to 272 mg hydroxyapatite / cm^3 was used to discriminate bone from soft tissues and polymer. For the cell delivery study, post mortem *ex vivo* CT scans were performed as well. Rats were sacrificed after 12 weeks and femurs were carefully excised along with surrounding soft tissue, wrapped in PBS-soaked gauze, and frozen at -20ºC until scanning. At the time of post mortem scans, femurs were thawed in PBS, placed in 15 mL microcentrifuge tubes filled with PBS, and then scanned by Micro-CT. A 21 micron voxel resolution was used, and after scanning a constant volume of interest (VOI) approximately 6 1/3 mm long centered in the middle of the defect region was chosen to ensure measurement of new bone formation and avoid measuring native cortical bone ends. A larger VOI was used during post mortem scans because explanted femurs could be aligned concentrically with the center of the bore of the of the CT scanning chamber, whereas during *in vivo* scans full alignment with the CT scanner was not possible due to limitations imposed by the geometry of the live rat within the scanning chamber. A Gaussian filter was used to suppress noise, and a density threshold corresponding to 272 mg hydroxyapatite / cm^3 was used to discriminate bone from soft tissues and polymer. Additionally, explanted naïve femurs from both 25 week old nude rats as well as 25 week old immunocompetent Sasco Sprague Dawley rats (Charles River Labs) (n = 6 / rat type) were wrapped in PBS-soaked gauze and then frozen until Micro-CT imaging using the same settings as the post mortem segmental defect scans described above .

Biomechanical Testing: Femurs from the cell delivery segmental defect study and whole naïve femurs were biomechanically tested to failure in torsion. Immediately following post mortem Micro-CT imaging, defect femurs were carefully cleaned of remaining soft tissue in preparation for torsional testing. Bone ends were potted in custom mounting blocks that contained reservoirs of heated Wood's Metal (Alfa Aesar, Ward Hill, MA), an alloy that melts at low temperatures and quickly solidifies after potting of bone ends. The mounting blocks were then loaded into custom holding brackets attached to an ELF 3200 Electroforce torsion testing system (Bose EnduraTEC Corporation, Minnetonka, MN) fitted with a 2 Nm torsional load cell. Next the polysulfone bridging plate, which had shielded defects from loads and damage, was removed by unscrewing the four screws attaching it to the stainless steel plates, each of which were screwed into to the native femoral bone on either side of the defect site (Figure 3.2). Finally a rotation-controlled torsional load was applied to the femur at a rate of 3 degrees / second and rotation angle, maximum torque, and torsional stiffness were recorded through 90 degrees rotation to avoid analysis of torque generated due to increased stretching of the soft tissues surrounding the defect at higher rotation angles.

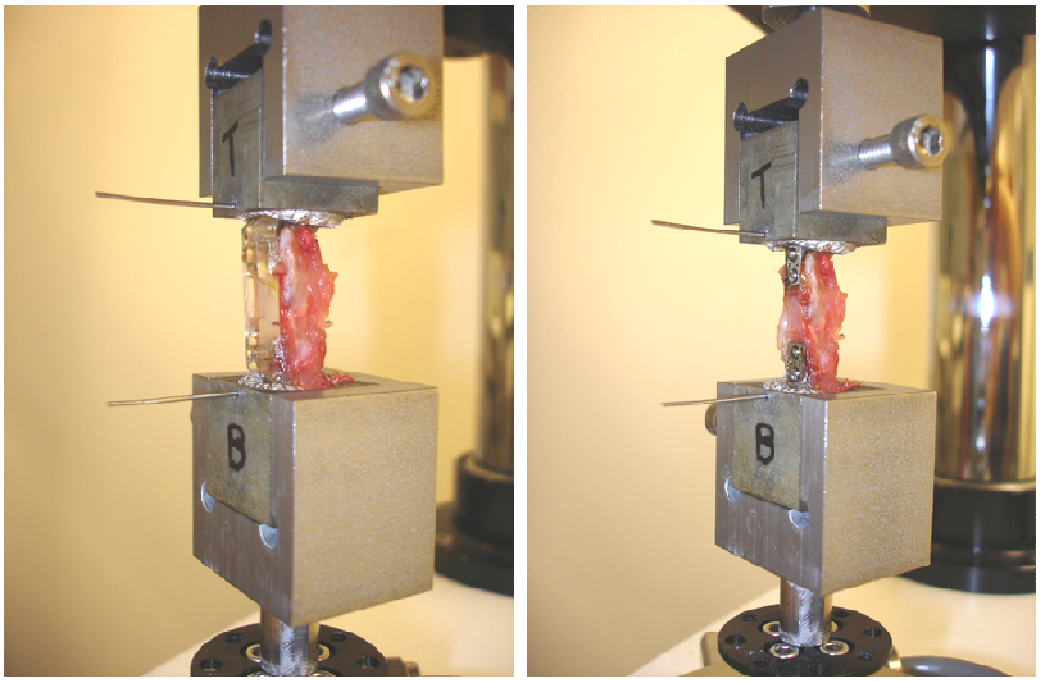

FIGURE 3.2: Segmental defect femur loaded in ELF3200 torsion testing system both before (left) and after (right) removal of polysulfone bridging plate.

Data Analysis: Data were analyzed using GraphPad Prism 5 software (GraphPad Software, Inc., La Jolla, CA). Analyses comparing three or more groups were analyzed using ANOVA with Tukey post hoc analyses for pairwise comparisons. Analyses comparing two groups were analyzed using unpaired t-tests. Whenever required, the raw data was transformed using a natural logarithmic transformation to make the data normal and the variance independent of the mean (Kutner 2005). For the *in vivo* cell delivery segmental defect study, no significant differences existed between hMSC or hAFS Cell treatment, so the two groups were combined into one cellular treatment group. Data are presented as mean ± standard error of mean (SEM). A p-value < 0.05 was considered statistically significant.

Chapter 3: Results

Comparison of Female Age-Matched Immunocompetent Sasco Sprague Dawley and Immunocompromised Nude Rats: The size of female immunocompromised nude rats used during segmental defect studies was significantly lower than that of age-matched immunocompetent Sasco Sprague Dawley rats used previously in the same model, as assessed by comparison of post-segmental defect surgery weights (Figure 3.3A). The geometry of the femurs from both rat strains varied as well, with the proximal ends of nude rat femurs flaring out to a point, creating a teardrop-shaped cross section, compared to the nearly ovular cross sections of Sprague Dawley femurs (Figure 3.3B). Although the femur geometry varied between strains, there were no significant differences in central diaphysis mineral volumes (Figure 3.3C) or maximum torques to failure (Figure 3.3D), however torsional stiffness was significantly lower in nude rats (Figure 3.3E), possibly due to the differences in cross sectional geometry of the femurs or differences in bone material properties between strains.

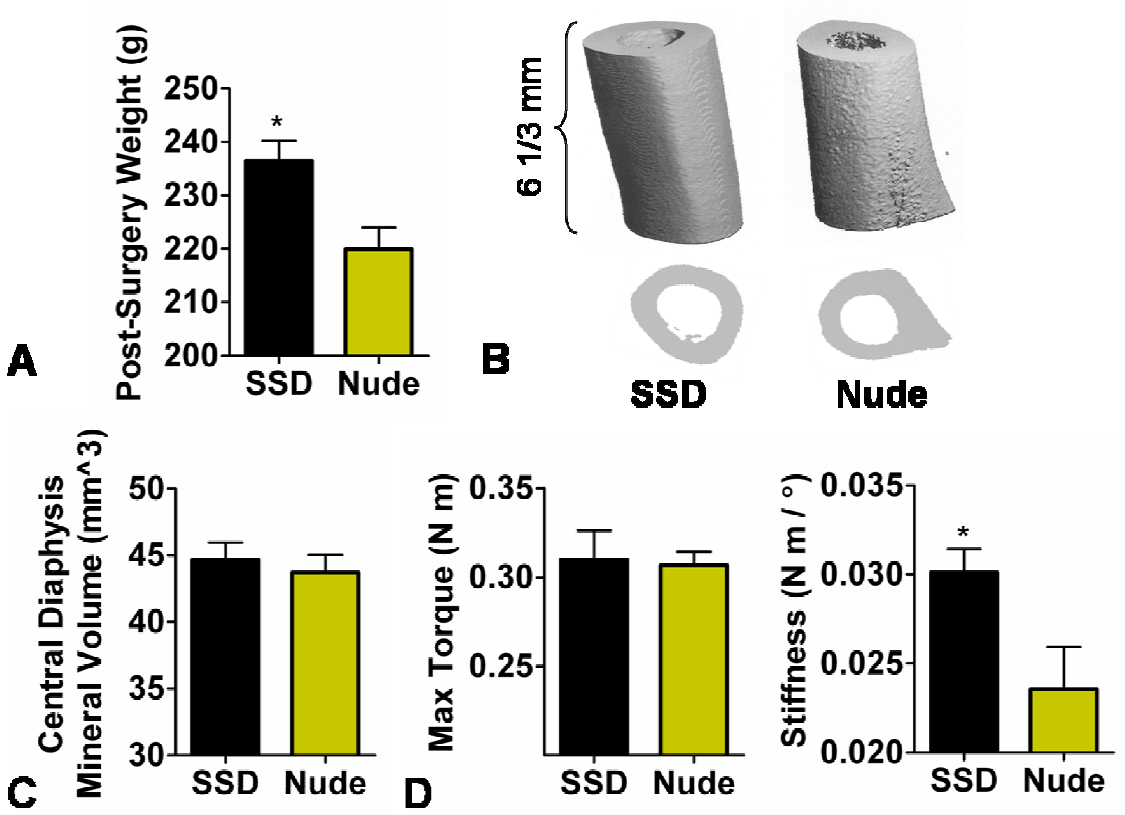

FIGURE 3.3: Comparison of relevant features of immunocompetent Sasco Sprague Dawley rats and immunocompromised nude rats. A) Weight of rats taken after segmental defect surgery. SSD: n = 25, nude: n = 22. Weights for each rat strain were pooled from two different studies to account for variability between litters. B) Comparison of geometries of femurs as assessed by Micro-CT, including transverse cross sections from proximal ends of evaluated diaphyseal VOIs. C) Quantified bone volumes of measured diaphyseal VOIs. D) Comparison of biomechanical properties of whole femurs tested to failure in torsion. C-D: n = 6 / group. * indicates $p < 0.05$.

Confirmation of Critical Size of Segmental Defects in Nude Rats: Negligible bone formation occurred in the empty defects throughout the 12 week period, and even defects that received PCL/Col-I scaffolds did not display bony bridging (Figure 3.4), indicating that the model does represent a critically-sized defect. There was no evidence of impaired health displayed during the study even after repeated handling / anesthesia application during radiograph and Micro-CT imaging.

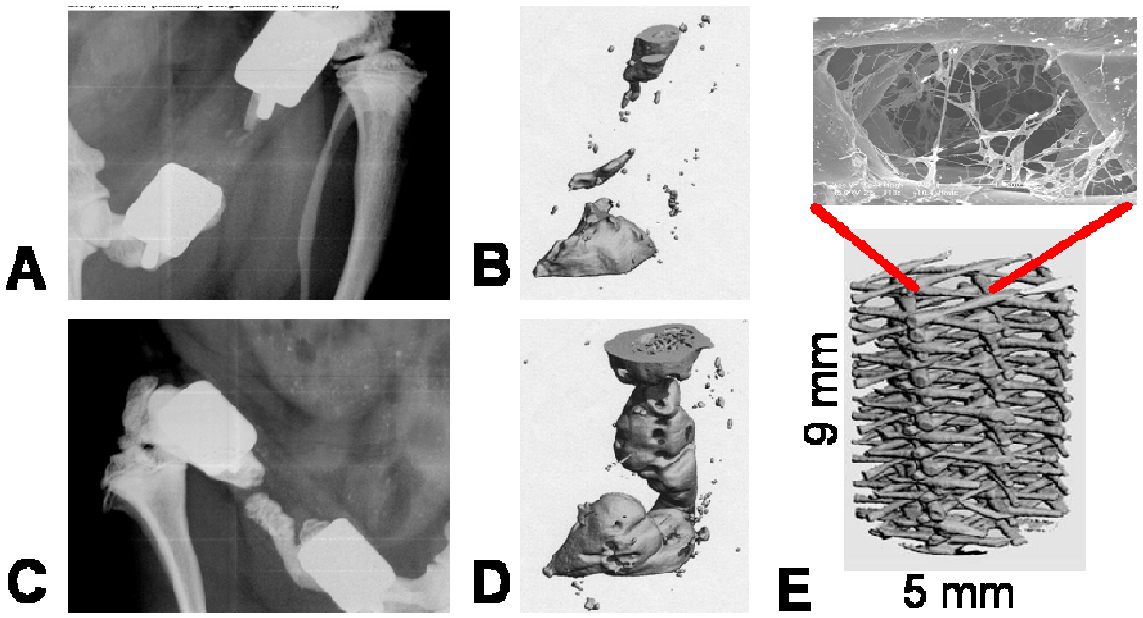

FIGURE 3.4: Week 12 time point 2D radiographic and 3D Micro-CT images of defects receiving either no treatment (A, B) or treatment with PCL scaffold containing lyophilized col I (C, D). Micro-CT images are shown proximal end-down, distal end-up. E) Geometry of PCL scaffold, showing magnified view of collagen lyophilized throughout scaffold pore space.

3D *In Vitro* Comparison of Mineralization Capabilities of Human Fetal and Adult Stem Cell Sources: Mineral volume throughout the scaffolds significantly increased during the course of the study for both cell sources (Figure 3.5 A,B), and at the study endpoint the construct mineral volume was significantly higher within scaffolds that received hAFS Cells compared to those that received hMSCs. For both cell sources, live cells were found along the scaffold periphery, top, bottom, and occupying the central pore spaces of the scaffolds at the 12 weeks post-seeding time point (Figure 3.5A). After 12 weeks *in vitro* culture the vast majority of cells remained viable.

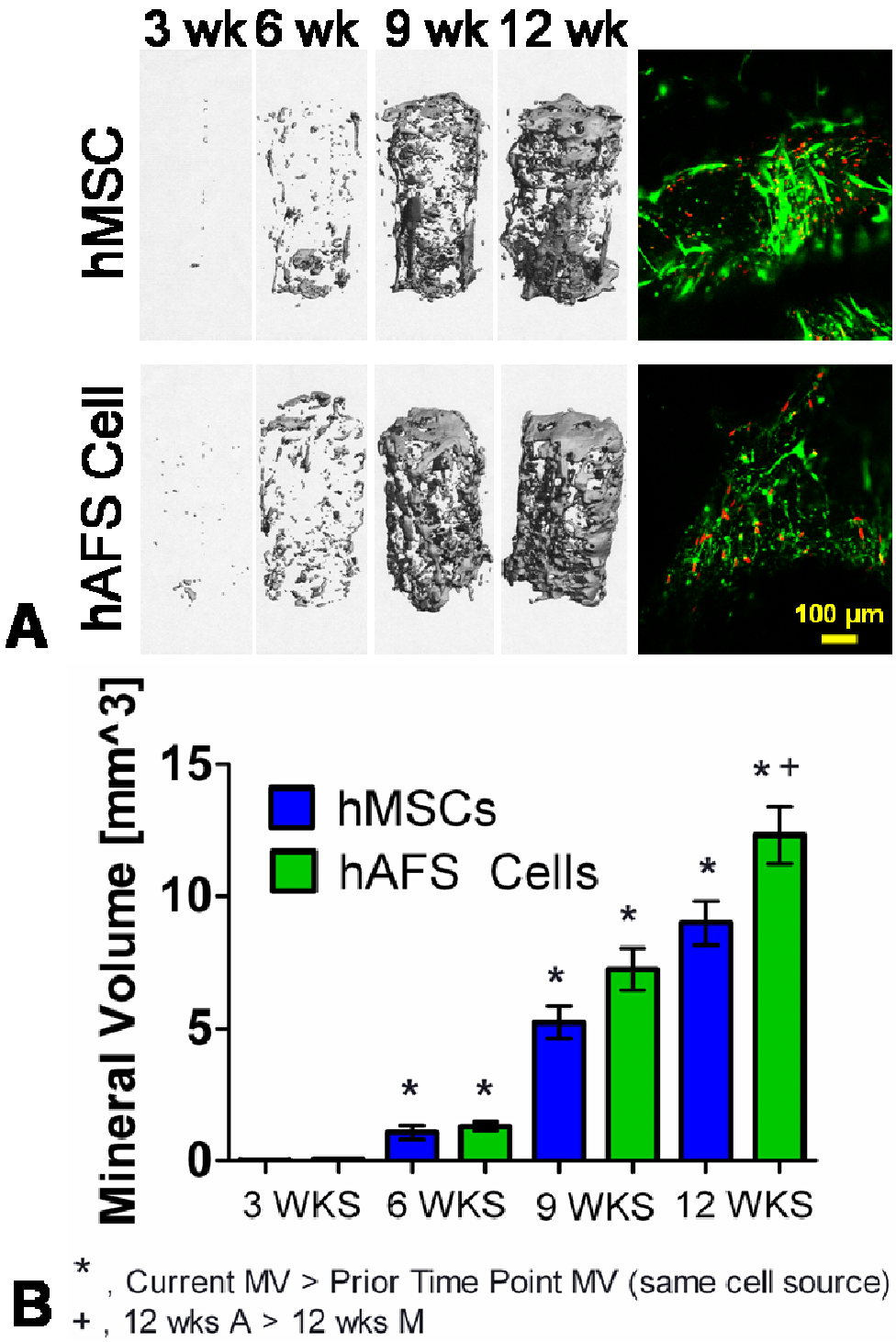

FIGURE 3.5: *In vitro* mineralization of 3D PCL scaffolds seeded with either hMSCs or hAFS Cells. A) Representative mineral formation as assessed by Micro-CT along with Live / Dead images showing viable green cells in the scaffold pore spaces at the 12 week time point. B) Quantitative comparison of bone volume in scaffolds. n = 6 / group. *, + both indicate $p < 0.05$.

***In Vivo* Comparison of Human Fetal and Adult Stem Cell-Mediated Segmental Defect Healing:** After 8 weeks post-surgery, bone bridged 0 / 8 defects that received scaffold only, 4 / 9 defects that received scaffold seeded with hMSCs, and 1 / 9 defects that received scaffold seeded with hAFS Cells, as assessed by double-blind evaluations of 2D radiographs (Figure 3.6). No further bridging occurred by week 12.

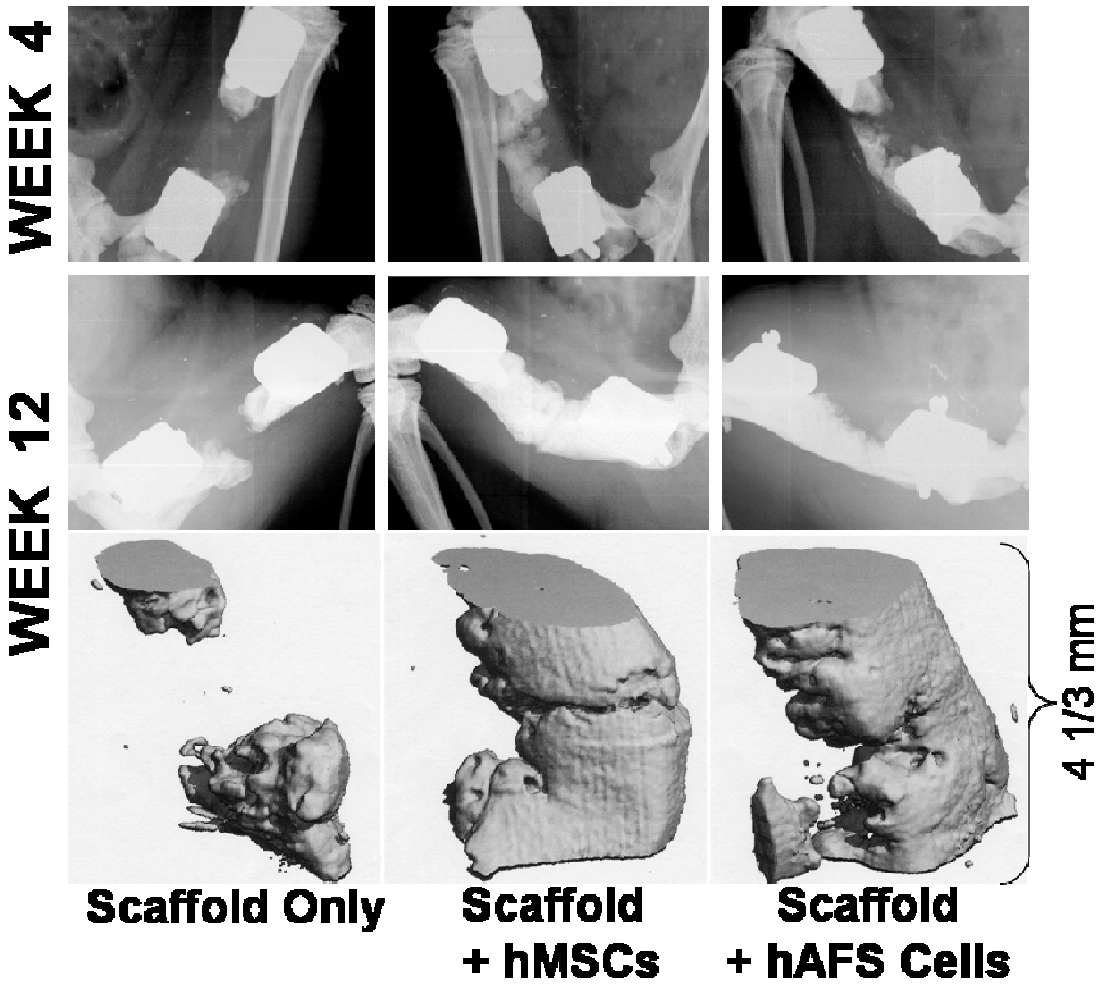

FIGURE 3.6: Radiograph (above) and Micro-CT (below) images of mineral formation in segmental defects treated with PCL scaffolds or PCL scaffolds seeded with three million hMSCs or hAFS Cells. Micro-CT images shown are from *in vivo* scans taken at the 12 week post-surgery time point. Samples chosen represent the maximum mineral formation for each treatment group as assessed by Micro-CT quantification.

Micro-CT quantification of bone volume showed no statistically significant differences between any group (Figure 3.7A), although the average bone volume and standard error for each group from *in vivo* scans at the twelve week time point were as follows: scaffold only – 9.30 ± 2.12 mm^3, scaffold + hMSCs – 29.66 ± 10.31 mm^3, and scaffold + hAFS Cells – 21.76 ± 10.00 mm^3. There were also no significant differences in mechanical properties between any groups (Figure 3.7B). The *in vitro* DNA assay performed prior to implantation showed no significant differences in DNA content per scaffold between the two cell sources, indicating that implanted constructs initially contained similar cell numbers (Figure 3.7C).

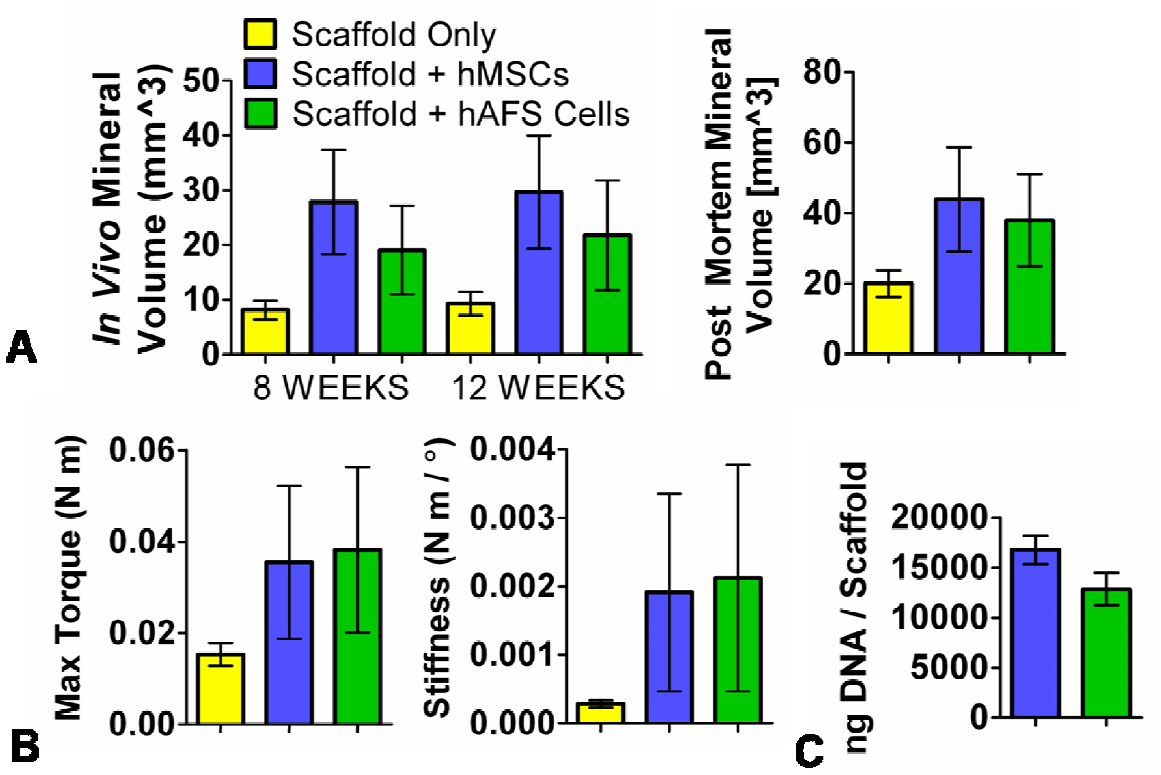

FIGURE 3.7: Quantitative comparison of acellular and cellular segmental defect treatments. A) *In vivo* and post mortem mineral formation within defect sites. B) Biomechanical properties of femurs tested to failure in torsion. C) DNA masses per scaffold. A-B: n = 9 / each cellular group, n = 8 scaffold group. C: n = 5 / group

Although the average values for defect mineral volume and mechanical properties were higher for each stem cell-treated group compared to the acellular scaffold-treated group, significant differences were not found due to high variability. To assess the effects of adding a cellular component for a larger sample size, the two cell treatment groups were combined and compared to treatment with acellular scaffold alone. The combined cellular group displayed significantly higher *in vivo* bone volume as well as maximum torque compared to the acellular group (Figure 3.8 A,B).

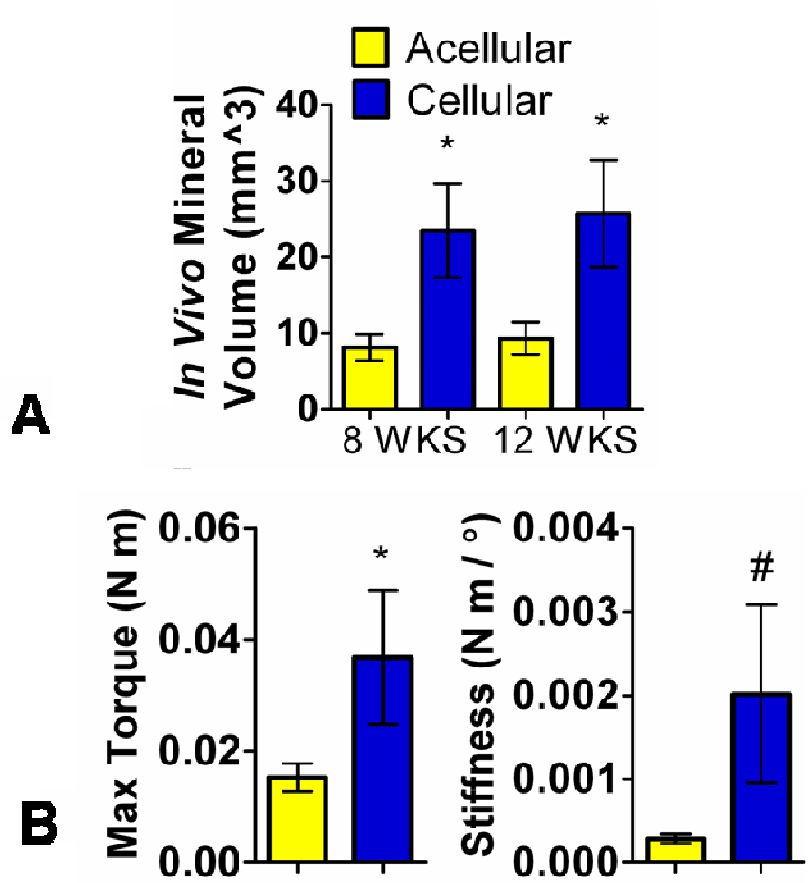

FIGURE 3.8: Quantitative comparison of acellular and pooled stem cell segmental defect treatments. A) *In vivo* mineral formation within defects. B) Biomechanical properties of femurs tested to failure in torsion. Pooled stem cell treatments had significantly higher *in vivo* bone volume and post mortem maximum torque compared to acellular scaffold treatment. n = 18 cellular, n = 8 acellular. * $p < 0.05$; # $p = 0.06$

Chapter 3: Discussion

Cellular activity is a vital component of the large bone defect healing process. In this study, a critically-sized femoral defect model was established in nude rats for evaluating human stem cell-based bone tissue engineering therapies. Delivery of stem cells on a porous polymer scaffold to bone defect sites led to an increase in bone formation and mechanical properties compared to defects receiving scaffold alone. No significant differences in defect bone volume or femoral mechanical properties were observed between adult or fetal stem cell sources. Although stem cell delivery significantly enhanced bone ingrowth and biomechanical properties, consistent bone bridging was not observed, with 4 / 9 hMSC scaffold-treated defects bridging and only 1 / 9 hAFS Cell scaffold-treated defects bridging. Lack of bony unions was likely due to the challenging nature of the 8 mm defect model, which is larger than the standard critical size required for nonunion in untreated controls. Other investigators have used rat femoral defects of 5 mm length or less in both immunocompetent (Lee, Shea et al. 1994), (Lin, Barrows et al. 2003) and immunocompromised (Jager, Degistirici et al. 2007) rats. The 8 mm femoral defect may be especially challenging in 13-week old nude rats compared to other age-matched rat strains such as the immunocompetent Sasco Sprague Dawley rat. We have consistently observed that female nude rats are smaller than age-matched female Sasco Sprague Dawley rats through multiple segmental defect studies, which was quantitatively confirmed by comparison of rat post-surgery weights as shown in Figure 3.3. As rat femur length tends to scale with weight (Hammett 1925), the 8 mm defect may represent a larger percentage of total femur length in the smaller nude rats than in the larger Sasco Sprague Dawley rats.

Another reason for the lack of significant differences in defect repair between individual stem cell treatment groups and the acellular scaffold treatment group may be the presence of a sufficiently large host MSC and osteoprogenitor population to contribute to partial repair of defects in the acellular group. As mentioned, bone tissue engineering therapies including a cellular component may be especially important for treating patients with diminished bone repair capabilities, such as the sick or elderly, due to a lack of endogenous cell supplies. In order to better evaluate the potential of stem cells as a therapeutic agent for those patients, it may be necessary to modify our model by using older nude rats or nude rats with disease conditions, such as nude rats with diabetes induced by the administration of streptozotocin (Kwon, Gao et al. 2008). However, the 13-week-old healthy female nude rat defect model used in these experiments represents a more practical large bone defect model which still serves as a valid and reproducible test bed for comparing xenogeneic human stem cell therapies. Older rats could have varying health problems associated with the aging process and younger rats could have varying responses to disease-initiating treatments, both of which would likely increase the variability between animals and mask the effects of stem cell-based therapies. The current model also allows for a more direct comparison to results from our studies treating 13-week-old healthy female Sasco Sprague Dawley rat defects with acellular therapies than if older or diseased rats were used.

For cell-mediated repair of challenging defects, its may also be necessary to co-delivery programming cues that direct delivered stem cells to differentiate down an osteogenic lineage. Co-delivered osteogenic signals may be particularly important for pluripotent fetal AFS Cells, which are possibly more primitive cells than the more

specialized multipotent adult MSCs. In 3D *in vitro* culture with osteogenic stimuli the hAFS Cells produced significantly more bone than the hMSCs through 12 weeks, possibly indicating that with added cues the hAFS Cells could produce more mineral than the hMSCs *in vivo* as well.

Finally, there is the possibility that delivered human cells may have interacted in a detrimental manner with host cells. Assuming that each human cell contains 6.6 picograms of DNA (Otto 2005), then hMSC scaffolds on average delivered about 2.5 million cells and the hAFS Cell scaffolds delivered about 1.9 million cells, based upon DNA levels measured by DNA assay. Introduction of this number of xenogeneic cells may have elicited some level of immune response from nude rats, limiting their therapeutic effect. While nude rats are T cell-deficient, their immune systems still have other lymphocytes such as natural killer cells and B cells. However, it is unlikely that delivered human stem cells would elicit an immune response, as multiple groups have reported that MSCs may be immune-privileged, as discussed in the chapter introduction. Second, it is possible that delivered human stem cells may have deterred the endogenous cell response, either from host osteoprogenitors or osteogenic cells. During the normal bone repair process host stem cells would occupy the injury site and differentiate into bone forming cells, but in this study the defects are already occupied by delivered cells, possibly limiting the host cellular response.

Chapter 4

EVALUATION OF QUANTUM DOTS AS A HUMAN STEM CELL TRACKING AGENT DURING LARGE BONE DEFECT REPAIR

Chapter 4: Introduction

Delivery of stem cells after bone injury, especially challenging injuries such as fracture nonunions or massive large bone defects, is a potential alternative to the large number of bone grafting operations performed annually (Song and Tuan 2004), (Jaiswal, Haynesworth et al. 1997), (Bucholz 2002). In our model, delivered stem cells should be able to be tracked using *in vivo* and *ex vivo* techniques to assess their location and viability during segmental defect repair. Tracking implanted cells is important for understanding the relative contributions to the regenerated tissues and organs from delivered cells versus host cells (Bucholz 2002), (Shah, Clark et al. 2007). Frangioni and Hajjar have suggested that an ideal agent for tracking stem cells should be biocompatible, safe, nontoxic, not require any genetic modification of the stem cell, permit single-cell detection at any anatomic location, allow quantification of cell number, have minimal or no dilution with cell number, have minimal or no transfer to non-stem cells, permit noninvasive imaging in the living subject over months to years, and require no injection of contrast agent for visualization (Frangioni and Hajjar 2004). Additionally, *in vivo* imaging of specific tissues can be difficult due to non-specific light absorbance and scattering by other tissues leading to their autofluorescence. However, autofluorescence is much lower in the near-infrared wavelengths from 700-1000 nm because the major chromophores in mammals, hemoglobin and water, have local minima in absorption in this range (Lim, Kim et al. 2003), (Smith, Duan et al. 2008).

A fairly new cell tracking modality, the quantum dot, has emerged recently as one option that features many of the desired traits mentioned above. Quantum dots (QDs) are fluorescent nanometer-scale semiconductor crystals composed of group II-VI or II-V elements. They have advantages over other fluorescent markers such as organic dyes and fluorescent proteins, including wide excitation spectrums (excitation by a large range of wavelengths of light), narrow emission spectrums (allowing for multiple populations of different cells to be tracked by loading QDs emitting multiple colors), photostability, and long fluorescence decay lifetimes (Jamieson, Bakhshi et al. 2007). QDs are stable and can undergo repeated cycles of excitation and fluorescence emission for hours with a high level of brightness (10-20 times higher than fluorescent proteins) and limited photobleaching (Alivisatos 1996). Quantum dots used in cell tracking applications are generally composed of a cadmium selenide core and a biologically inert zinc sulfide shell (CdSe/ZnS), and are also often coated with additional materials to aid in cell internalization since raw QDs are generally membrane impermeant (Jaiswal, Goldman et al. 2004). The coatings generally consist of peptides or proteins that increase QD solubility and serve as ligands for integrin binding on cell surfaces prior to QD internalization to endosomes in the cytoplasm. QDs generally do not enter the cell nucleus as their diameters (approximately 20 nm) are much bigger than nuclear pore sizes (5 nm) (Shah, Clark et al. 2007). When QD-loaded cells divide their QD contents are likely asymmetrically divided between daughter cells leading to a loss in concentration per cell. One downside to this particular type of QD is the possible release of toxic cadmium from the core, but the ZnS shell helps to stabilize the core and reduces immunogenicity. Another potential downside is the possibility of QD transfer from

originally loaded cells to neighboring cells, which could defeat the purpose of labeling delivered cells to distinguish them from host cells. However, experiments by Rosen have not shown this to be the case (Rosen, Kelly et al. 2007). *In vitro*, QD-loaded human mesenchymal stem cells (hMSCs) were cocultured with adult cardiac myocytes expressing green fluorescent protein (GFP), and no evidence was found of QDs in GFP-expressing cells. Furthermore, the lysates of QD-loaded hMSCs killed by mechanical disruption were introduced to cardiac myocyte cultures and there was still no evidence of QD uptake by myocytes. *In vivo*, they injected 100,000 QD-loaded hMSCs that were mechanically disrupted to cause cell lysis into the rat ventricle and sacrificed the animals either 1 hour or 1 week later. They did not observe QDs in any cell type in the hearts. However, they did find that QDs were removed from the circulation to organs of the reticuloendothelial system (RES - spleen, liver, lymph nodes), which generally occurs within hours after direct injection of QDs or QD-loaded cells (Ballou, Lagerholm et al. 2004), (Akerman, Chan et al. 2002), (Hoshino, Hanaki et al. 2004), (Fischer, Liu et al. 2006). Another study found that when cells co-labeled with QDs and cell tracker dye were injected intravenously into mice, there were no cells found without both markers five hours later, indicating that no QDs left their original cells to go into other cells and that any cells that died had their QDs cleared from the circulation (Voura, Jaiswal et al. 2004).

The majority of *in vitro* studies using human mesenchymal stem cells loaded with QDs have demonstrated highly efficient internalization into cells and long term fluorescent tracking of QD-loaded cells, with no significant effects on cell viability or proliferation and differentiation capabilities when cells were loaded with low

concentrations of QDs (Shah, Clark et al. 2007), (Seleverstov, Zabirnyk et al. 2006), (Muller-Borer, Collins et al. 2007), (Rosen, Kelly et al. 2007). However, one study reported decreased osteogenic differentiation of QD-loaded hMSCs, showing that they had decreased osteopontin and osteocalcin (markers of osteogenesis) expression compared to QD-free hMSCs, although both groups showed similar alkaline phosphatase expression and there were no effects on proliferation (Hsieh, Wang et al. 2006). One reason for these results might be that they used immortalized hMSCs that may lack certain matrix markers.

In vivo, QD-labeled hMSCs seeded on porcine urinary bladder and delivered to canine hearts showed fluorescence in histological sections taken through 8 weeks of study (Rosen, Kelly et al. 2007). Injection of QDs into tail veins of mice led to accumulation of QDs in RES organs, which displayed fluorescence for at least four months. Neither macroscopic nor microscopic analysis revealed signs of localized necrosis in these organs (Ballou, Lagerholm et al. 2004). Additionally, QD-labeled tumor cells were intravenously injected into mice, and 40 days later there were no apparent detrimental effects on physiology of the host animals, QD-loaded cell survival, or their ability to engraft into native tissue to form tumors (Voura, Jaiswal et al. 2004). Finally, *in vivo* imaging of fluorescence from QD-loaded cells has been observed in mouse capillaries hundreds of microns below the skin after intravenous injection (Larson, Zipfel et al. 2003).

The purpose of this Aim was to label and track human stem cells used in treatment of large segmental bone defects to assess their biodistribution and viability during the bone repair process. Based on the above background, we chose quantum dots

as our cell tracking agent. We first optimized the quantum dot labeling configuration as assessed by *in vitro* fluorescence emission by comparing multiple concentrations and types of quantum dots as well as varying quantum dot incubation times. We also found that low concentration QD-labeling of stem cells does not affect *in vitro* stem cell viability or osteogenic differentiation capacity. However, segmental defect experiments revealed that quantum dot labeling may not be an effective long term *in vivo* stem cell tracking modality, as quantum dots were released from delivered stem cells and internalized by host cells, creating false positive signals. Furthermore, defects treated with scaffolds seeded with QD-loaded hMSCs displayed less robust healing than defects treated by scaffolds seeded with QD-free hMSCs.

Chapter 4: Materials and Methods

Stem Cell Labeling with Quantum Dots: *In Vitro* Preliminary Experiment I: Rat MSCs (rMSCs, p3) were isolated from long bone marrow aspirates as described previously (Hofstetter, Schwarz et al. 2002). 20,000 rMSCs were seeded in each well of 8-well Lab-Tek chambered cover glass plates in 300 μL of culture media (α-MEM, 16.7% FBS, antibiotics), allowed to adhere overnight, and then loaded with either QTracker 800 quantum dots or QDot ITK 800 quantum dots as directed by the manufacturer's protocol (Invitrogen Corporation, Carlsbad, CA). Qtracker QDs have a positive surface charge through an amino-PEGylation surface coating and QDot ITK QDs have a negative surface charge through carboxyl group surface coating. Both types of QD exhibit peak fluorescence emission at a wavelength of 800 nm, which is an attractive feature for *in vivo* imaging because the two major chromophores responsible for animal autofluorescence, hemoglobin and water, display minimal fluorescence emission at these high wavelengths. QDs were loaded at concentrations of 5, 10, or 20 nM, with 10 nM being the manufacturer's standard recommendation. Cells were incubated with QDs for either one hour or overnight (18 hours), washed with PBS, fixed with formalin, and then washed with PBS again prior to imaging. Additionally, some of the wells incubated in 10 nM QDs were stained for five minutes with 5 ng / mL DAPI nuclear stain.

Stem Cell Labeling with Quantum Dots: *In Vitro* Preliminary Experiment II: rMSCs, hMSCs, or hAFS Cells seeded on Lab-Tek 8-well plates were loaded with quantum dots as described above, but at concentrations of 0, 10, 15, and 20 nM, and all were incubated for 18 hours. All wells were fixed and stained with 5 ng / mL DAPI

nuclear stain. Additionally, cells in other 8-well plates were loaded with QDs in the same manner but were not fixed or stained with DAPI; instead they were washed with PBS and then stained with Live / Dead stain (Molecular Probes, Inc.) for 45 minutes to assess cell viability.

Stem Cell Labeling with Quantum Dots: *In Vitro* Effect on Osteogenic Differentiation: To assess quantum dot effects on osteogenic differentiation, 1,000 hMSCs were seeded per well of tissue culture 6-well plates and grown to confluence. 0.5 mL of 5 nM QTracker QDs was then added to half of the wells for 18 hours while the other wells received 0.5 mL of culture media. Next wells were aspirated and 5 mL of culture media supplemented with osteogenic factors (1 nM dexamethasone, 6 mM β-glycerol phosphate, 50 μg/ml ascorbic acid 2-phosphate, and 50 ng / mL L-thyroxine) was added. Plates were cultured dynamically for three weeks in osteogenic media with media changes twice weekly and then a Von Kossa assay was performed to assess mineral formation.

Stem Cell Labeling with Quantum Dots: *In Vivo* I – Preliminary Study: Three million hMSCs or hAFS Cells, each from two different donors, were seeded on 15 cm diameter Tissue culture polystyrene dishes and incubated overnight at 37º C / 5% CO2 in 20 mL culture media (α-MEM, 16.7% FBS, PSL). Cells were then incubated in a 5 nM solution of QTracker 800 quantum dots in 5 mL culture media for 18 hours and then trypsinized and counted using a haemocytometer. Three million QD-labeled hMSCs or QD-labeled hAFS Cells in 100 μL of culture media were seeded onto PCL scaffolds previously coated with GFOGER peptide and lyophilized type I collagen. 4 mL culture media was added after one hour and scaffolds were cultured in 12-well plates as

described in Chapter 3. Cells were allowed to adhere to and spread throughout the scaffolds *in vitro* for 24 hours prior to implanting them in rat femoral defects.

Stem Cell Labeling with Quantum Dots: *In Vivo* II – Live Versus Devitalized Cell Study: Three million hMSCs were seeded on 15 cm diameter Tissue culture polystyrene dishes while three million human embryonic kidney 293 (HEK) cells (p 34, purchased from ATCC (American Type Culture Collection, Manassas, VA)) were seeded on T-150 flasks and incubated overnight in 20 mL media (hMSCs: α-MEM, 16.7% FBS, PSL; HEK cells: DMEM, 10% FBS, PSL). HEK cells were used as a live non-stem cell control because, unlike stem cells, these cells have not been shown to possess an ability to home to injury sites. Cells were then incubated at 37º C / 5% CO2 in a 5 nM solution of QTracker 800 quantum dots in 5 mL culture media for 18 hours and then trypsinized and counted using a haemocytometer. Either three million (hMSCs only) or six million (hMSCs and HEK cells) QD-labeled cells in 100 μL of culture media were seeded onto PCL / GFOGER / Col I scaffolds and cultured as described above prior to implantation. Some QD-labeled hMSC constructs were exposed to devitalizing freeze-thaw cycles after 24 hours culture consisting of three repetitions of freezing at -80ºC for 30 minutes followed by thawing at 37ºC for 30 minutes in a water bath. The cells were devitalized to eliminate the possibility of stem cell migration from the defect site.

Fluorescence Microscopy: Fluorescent images of QD-loaded cells in 8-well Lab-Tek plates as well as in histological cryosection slides from *in vivo* studies were obtained using a Zeiss Axio Observer inverted microscope (Carl Zeiss Inc., Oberkoben, Germany) equipped with a specialized Qdot 800 filter set (Chroma 32021, Chroma Technology, Rockingham, VT).

IVIS Fluorescence Imaging: Macroscopic images of quantum dot fluorescence in 8-well plates were obtained using an IVIS Lumina fluorescent / bioluminescent imaging system (Caliper LifeSciences, Hopkinton, MA) capable of quantifying fluorescence emission levels. Images were taken with 60 second exposure time, small binning, FStop level 2, 745 nm excitation, 800 nm emission, and field of view D (image size 12.5 cm x 12.5 cm) settings.

For *in vivo* fluorescence imaging, in the preliminary *in vivo* study immediately after surgery rats were transported to the IVIS imaging system for *in vivo* fluorescence imaging. The system features an isoflurane gas inlet to keep rats anesthetized during imaging. IVIS imaging was repeated once each week for the duration of the 12-week study, using consistent settings of medium binning, FStop of 1, 13 second excitation time, 710 nm excitation, 800 nm emission, and field of view D. For the live versus devitalized cell *in vivo* study, scans were performed immediately post-surgery and then after 10, 20, 40, 60, and 80 days using the same settings as in the preliminary study. Images were taken of the dorsal view as well as both the left and right sides. Fluorescence count values were measured using a uniform circular region of interest applied at hindlimb defect sites.

Surgical Technique: Femoral segmental defects were created in rat femora as described in Chapter 3. In both of the *in vivo* quantum dot studies, all rats were implanted with scaffolds containing QD-labeled cells in one hindlimb defect and acellular scaffolds only in the contralateral defect. In the preliminary QD study two rats were treated with hMSCs and two rats with hAFS Cells. In the QD study comparing live and devitalized cells, 10 rats were treated with scaffolds containing QD-loaded live

hMSCs (n = 5 three million cells / n = 5 six million cells), 10 rats were treated with scaffolds containing QD-loaded devitalized hMSCs (n = 5 three million cells / n = 5 six million cells), and two rats were treated with six million QD-loaded live HEK cells. One rat treated with QD-loaded hMSCs in the preliminary QD study failed to recover due to misplacement of the internal fixation plate, leading to its euthanization after 4 days.

Radiograph / Micro-CT Imaging and Biomechanical Testing: Rats in the study comparing live and devitalized QD-loaded stem cells were scanned by 2D radiographs at 4, 8, and 12 weeks post-surgery and 3D *in vivo* Micro-CT scans at 8 and 12 weeks post-surgery as described in Chapter 3 (n = 9 live hMSC-loaded animals, n = 9 devitalized hMSC-loaded animals, n = 1 HEK cell-loaded animal). Additionally post mortem Micro-CT scans were performed on the same animals with a higher density threshold corresponding to 385 mg HA/cm^3 to account for denser and more mature bone than in the earlier *in vivo* scans, and because there is not as much extraneous tissue present to absorb photons in explanted femurs compared to *in vivo* limbs. Femurs from the same animals were biomechanically tested in torsion as described previously.

Histological Cryosection Preparation and Imaging: All rats from the preliminary QD study were sacrificed 12 weeks after surgery and had their femurs, kidneys, and organs of the reticuloendothelial system (spleen, liver, lymph nodes) harvested. Femurs were decalcified in Cal-Ex II solution (Fisher Scientific), and then all tissues were fixed in 10% neutral buffered formalin, embedded in OCT cryosectioning media (Tissue-Tek), and then snap frozen in a chilling bath. 50 μm tissue sections were taken using a Microm Cryo-Star HM 560MV cryostat (Thermo Fischer) and attached to Superfrost Plus slides. Glass coverslips were mounted using ProLong Gold antifade

mounting media with DAPI (Invitrogen Corp.) to visualize cell nuclei. In the live versus devitalized cell QD study, one rat each from the live hMSC group, devitalized hMSC group, and HEK group (each originally treated with six million cells per scaffold) was sacrificed 4 weeks after surgery. Animals were chosen that displayed average defect fluorescence intensity per group as assessed by IVIS scan quantification. Femurs were collected, embedded in OCT media, snap frozen, and then sectioned in 20 μm slices. All sections were fixed in 4% formaldehyde in PBS and then permeabilized with acetone. Sections prepared for human nuclei staining were blocked with 5% donkey serum followed by application of a mouse anti-human nuclear antigen monoclonal primary antibody (HuNu, Millipore MAB1281). Sections prepared for rat macrophage staining were blocked with 5% bovine serum albumin followed by application of a mouse anti-rat CD68 primary antibody (AbD Serotec, MCA341R). Next a fluorescent Alexa Fluor® 488 donkey anti-mouse (Invitrogen) secondary antibody was applied to all sections followed by 5 ng / mL DAPI counter-staining. Control sections for each immunolabel excluded primary antibody staining.

***In Vitro* Human Stem Cell Nuclear Labeling:** For 2D *in vitro* human cell nuclear labeling, 100,000 hMSCs were seeded on single-well Lab-Tek chambered cover glass slides and allowed to adhere overnight. Cells were fixed in 10% neutral buffered formalin, permeabilized with acetone, and then blocked in 5% donkey serum followed by application of HuNu monoclonal antibody. Next a fluorescent Alexa Fluor® 488 donkey anti-mouse secondary antibody was applied followed by 5 ng / mL DAPI counter-staining.

Data Analysis: Data were analyzed using GraphPad Prism 5 software. Analyses comparing three or more groups were analyzed using ANOVA with Tukey post hoc analyses for pairwise comparisons. Analyses comparing two groups were analyzed using unpaired t-tests. Whenever required, the raw data was transformed using a natural logarithmic transformation to make the data normal and the variance independent of the mean (Kutner 2005) prior to statistical analysis. If after transformation data still was not normal or variance independent of the mean, data sets were analyzed using the Kruskal-Wallis non-parametric test followed by Dunn's multiple comparison test. For the comparisons of defect site QD fluorescence, repeated measures ANOVA was performed with Bonferroni post tests. For the *in vivo* live versus devitalized stem cell study, no significant differences in defect fluorescence were observed between defects treated with three or six million hMSCs, between defects treated with live or dead stem cells, or between their contralateral acellular control defect sites, so groups were pooled into defects that originally were treated with scaffolds seeded with QD-loaded cells and those treated with acellular scaffolds. HEK cell data are shown but not included in statistical analyses due to small sample size. Data are presented as mean ± standard error of mean (SEM). A p-value < 0.05 was considered significant.

Chapter 4: Results

***In Vitro* Stem Cell Labeling with Quantum Dots:** Fluorescence microscopy images revealed a clear fluorescent signal in all wells containing QD-loaded MSCs (Figure 4.1). While there qualitatively appeared to be minimal differences in fluorescence between QD types and even between different QD concentrations, 18-hour QD incubation increased QD internalization compared to one-hour incubation. QDs were distributed within the cytoplasmic space but not within the nuclei, as shown by the QD "rings".

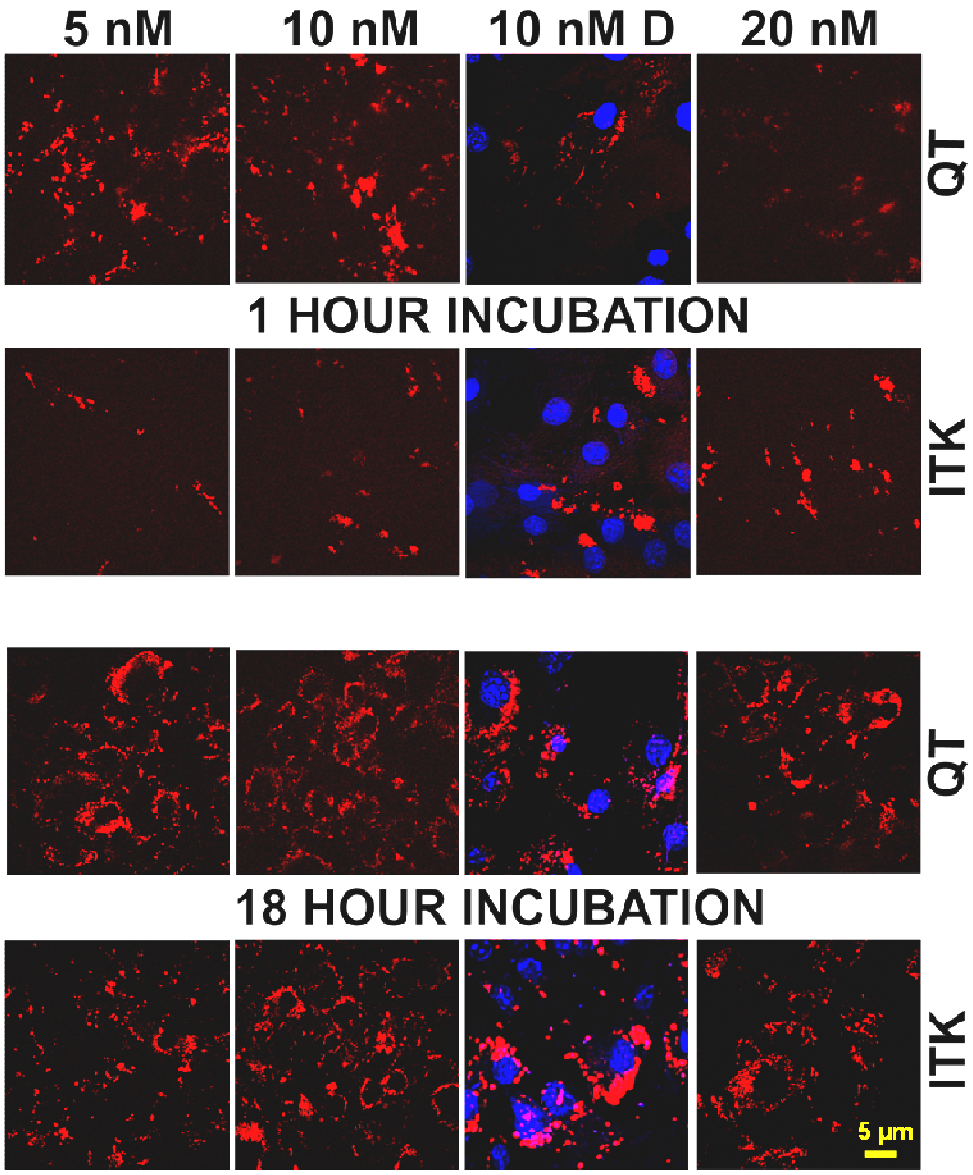

FIGURE 4.1: Fluorescence microscopy images showing quantum dot-labeled rMSCs in 2D culture after incubation with quantum dots for 1 hour or 18 hours. Note presence of red quantum dots in cytoplasmic space surrounding blue nuclei counterstained with DAPI (D). 40X magnification. QT - QTracker 800 QDs, ITK - QDot ITK 800 QDs

When plates were imaged using an IVIS Lumina system, increased fluorescence was confirmed in cells exposed to QDs for 18 hours compared to one hour (Figure 4.2). There was also a qualitative difference in fluorescence between QD types, with the cells

loaded with QTracker QDs (QT) emitting a stronger signal than those loaded with QDot ITK QDs (ITK).

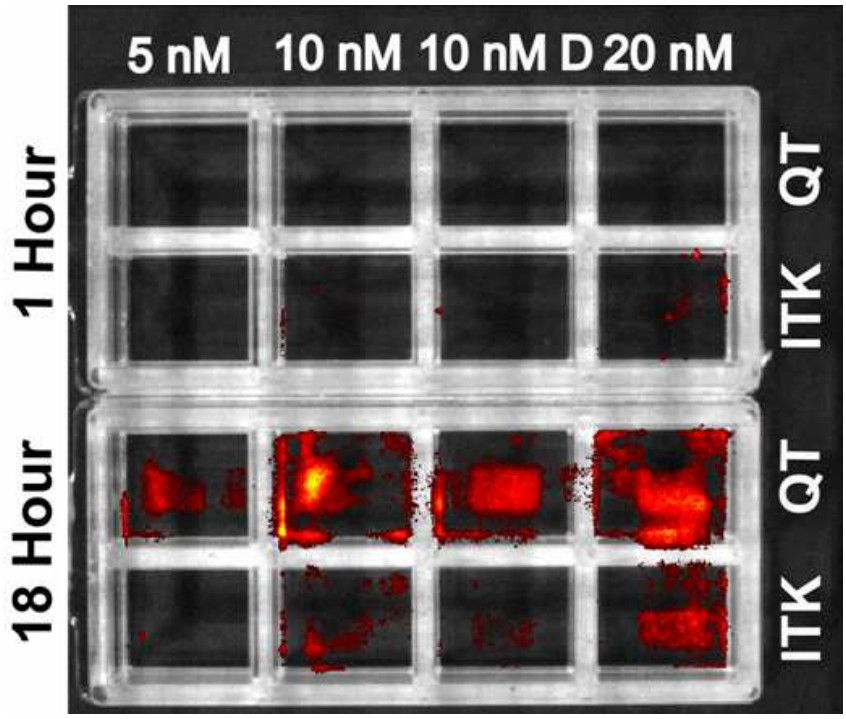

FIGURE 4.2: Comparison of fluorescence emission from quantum dot-loaded rMSCs after either 1 or 18 hour incubation as assessed by IVIS Lumina fluorescent imaging. QT - QTracker 800 QDs, ITK - QDot ITK 800 QDs

Both fluorescence microscopy and IVIS imaging showed a clear fluorescent signal in QD-loaded rat MSCs, hMSCs, and hAFS Cells, indicating QD uptake in multiple stem cell sources and species (Figure 4.3).

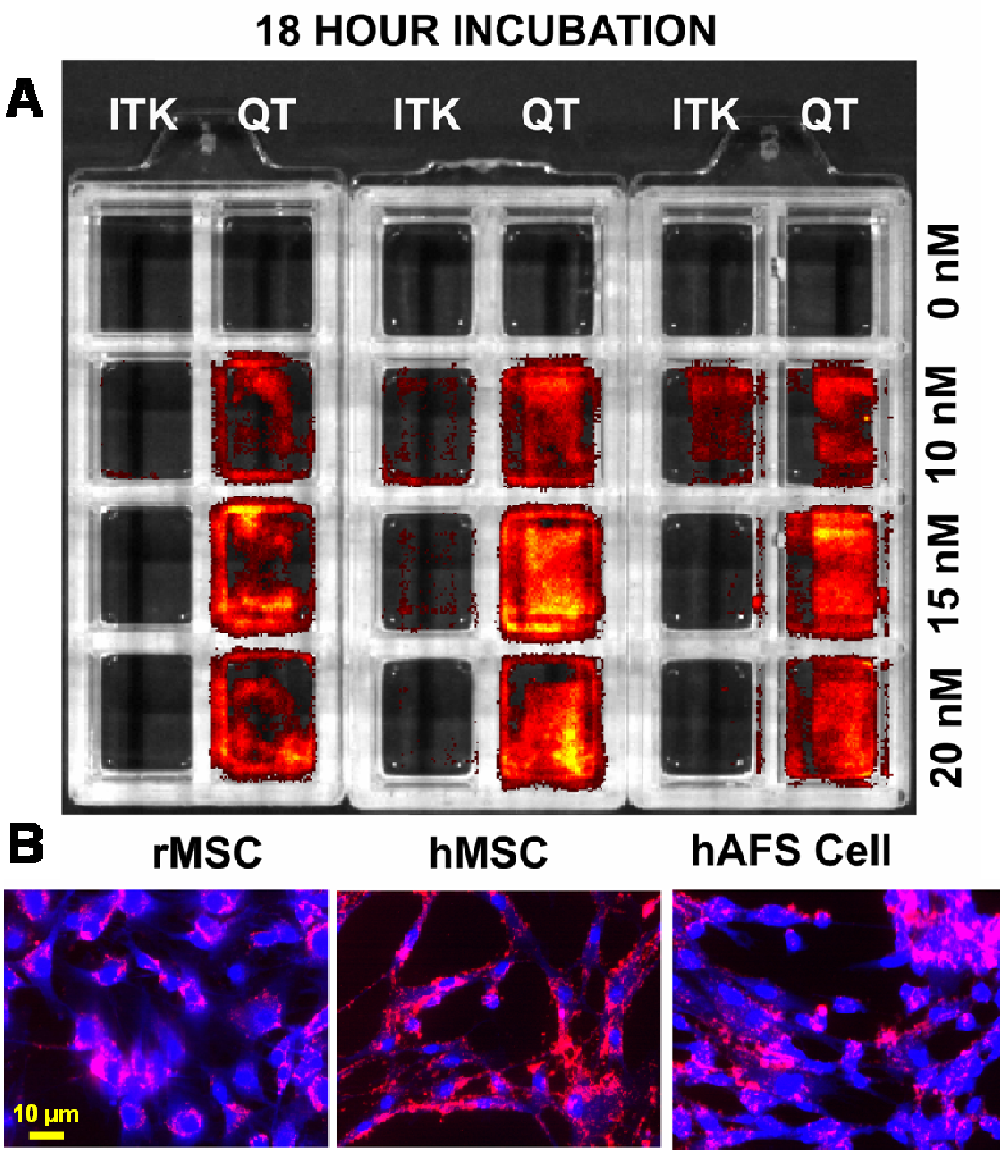

FIGURE 4.3: Comparison of fluorescence emission from rMSCs, hMSCs, and hAFS Cells as assessed by either A) IVIS imaging or B) fluorescence microscopy. Microscopy images shown for 10 nM QD concentration. 20X magnification.

Quantum Dot Effects on 2D *In Vitro* Cell Viability: Live / Dead staining revealed that all QD-loaded stem cells remained viable except for one particular group, the QTracker-loaded rMSCs at the highest QD concentration of 20 nM (Figure 4.4). This finding agrees with the literature that QDs can have cytotoxic effects *in vitro*, but

generally only at higher concentrations. Based on our *in vitro* results, we opted for incubating cells in 5 nM concentration QTracker 800 QDs for 18 hours for our *in vivo* stem cell tracking experiments.

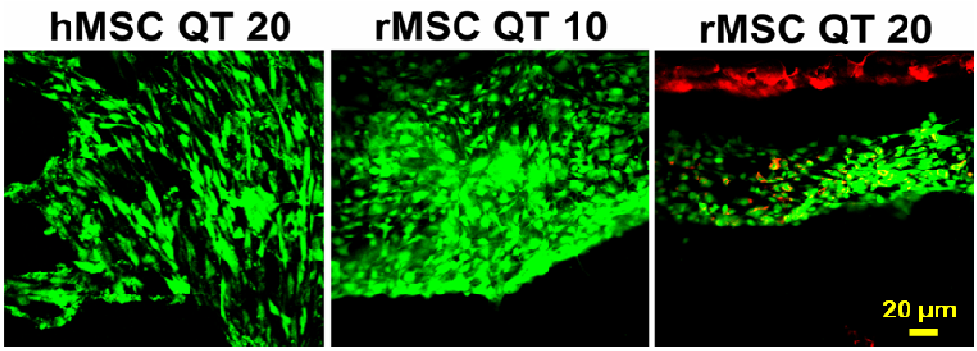

FIGURE 4.4: Fluorescence microscopy images showing presence of live (green) cells and dead (red) cells after Live / Dead stain with calcein / ethidium. Quantum dots only had negative effects on cell viability at the highest concentration of 20 nM in the rMSCs only. 10X magnification.

***In Vivo* Segmental Defect Delivery of QD-Labeled Stem Cells – Preliminary Cell Source Comparison:** Immediately after implantation, IVIS scans revealed a clear fluorescent signal at right hindlimb defect sites that received scaffolds seeded with QD-labeled stem cells from both cell sources (Figure 4.5). Unexpectedly, after one week a signal was detected at not only the right hindlimb defect sites, but also at the left hindlimb control sites which originally received only acellular scaffolds, suggesting possible migration of implanted stem cells. Clear defect site fluorescent signals persisted throughout the duration of the 12-week study.

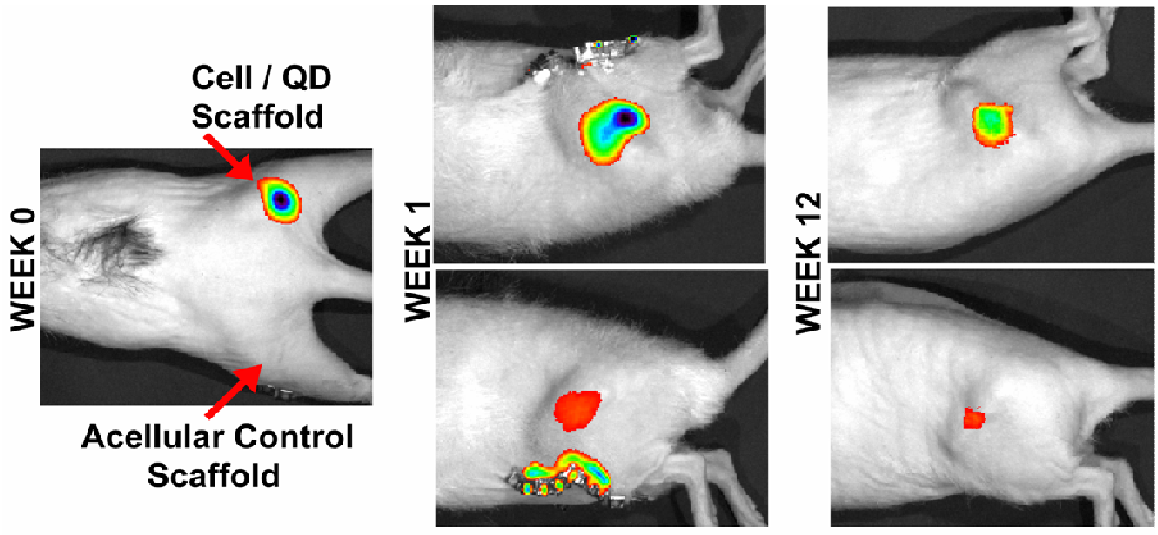

FIGURE 4.5: *In vivo* quantum dot fluorescence – preliminary study. Initial fluorescent signals were observed only at right hindlimb defect sites treated with scaffolds seeded with QD-loaded stem cells, but after one week and for the remainder of the study the signal was present in both right and left hindlimbs in all rats. Results from delivery of a scaffold seeded with QD-labeled hMSCs are shown; similar signals were seen for rats treated with hAFS Cell constructs.

Fluorescent signal intensity at defect sties treated with scaffolds seeded with QD-labeled stem cells decreased rapidly within the first 2 weeks of the study and then decreased slowly during the rest of the study, but remained above background levels (Figure 4.6A). In contrast, fluorescent signal intensity at contralateral defect sites treated with acellular scaffolds increased after one week and then decreased throughout the rest of the study. Significant differences in fluorescence intensity were observed between defects treated with cells and control defects through the first week of the study (Figure 4.6B). Observed fluorescence patterns and intensities were similar for all animals, regardless of stem cell source. There were no observed signs of negative effects from QD exposure on animal morbidity or mortality throughout the study.

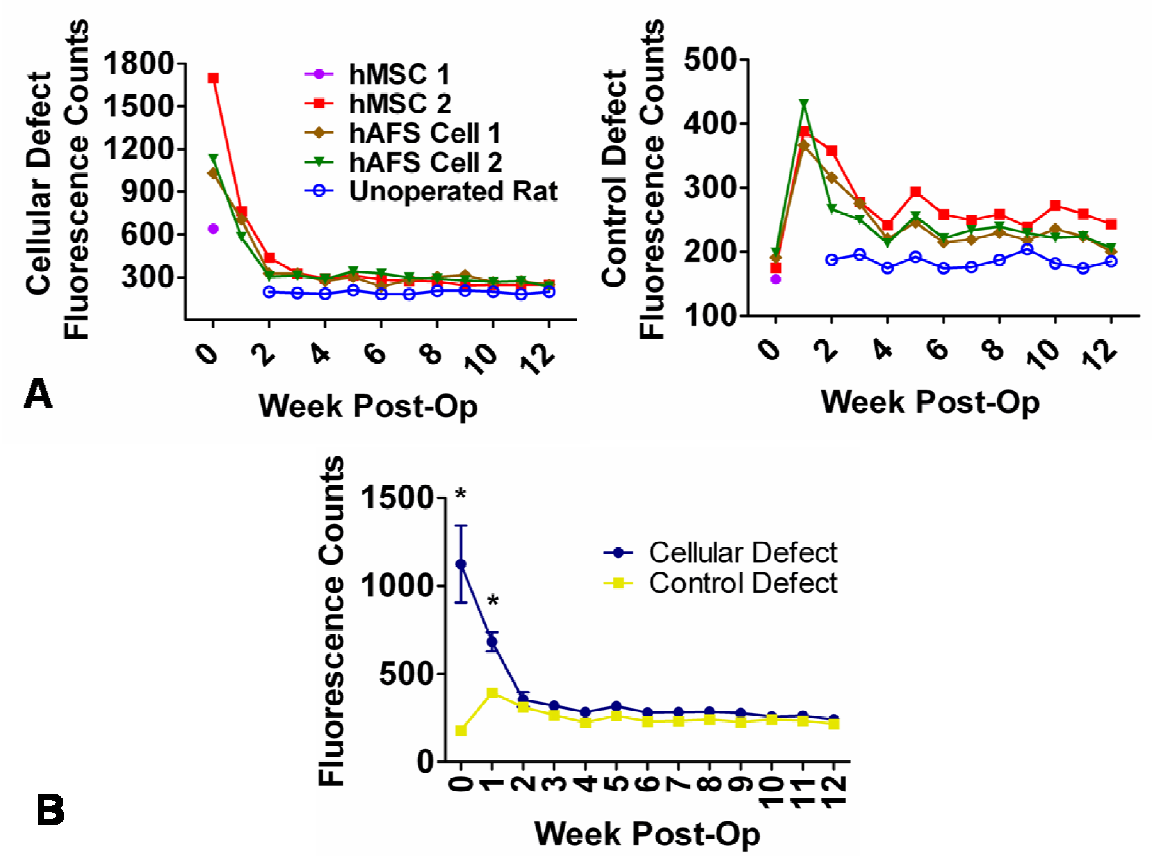

FIGURE 4.6: Defect site fluorescence intensity quantification. A) Comparison of fluorescence emission levels in defect sites originally treated with scaffolds seeded with QD-loaded stem cells and sites originally treated with acellular control scaffolds; note peak in control hindlimb fluorescence after one week. Fluorescence count values remained above background levels observed in an unoperated control rat. B) Comparison of fluorescence emission between grouped cellular and acellular defects. * $p < 0.05$

The presence of fluorescent QDs at defect sites was confirmed in histological cryosections, which revealed QDs amidst DAPI-stained cell nuclei within the PCL scaffold (Figure 4.7A). QD concentration was qualitatively higher in the right hindlimb defect sites originally implanted with QD-loaded cells, and QDs in the defects originally treated with acellular scaffolds were primarily located near the scaffold interface with the bordering fibrous tissue. QDs were also detected in the kidneys as well as the organs of

the reticuloendothelial system (RES) including the liver, spleen, and lymph nodes, although at qualitatively lower concentrations than in either defect site (Figure 4.7B).

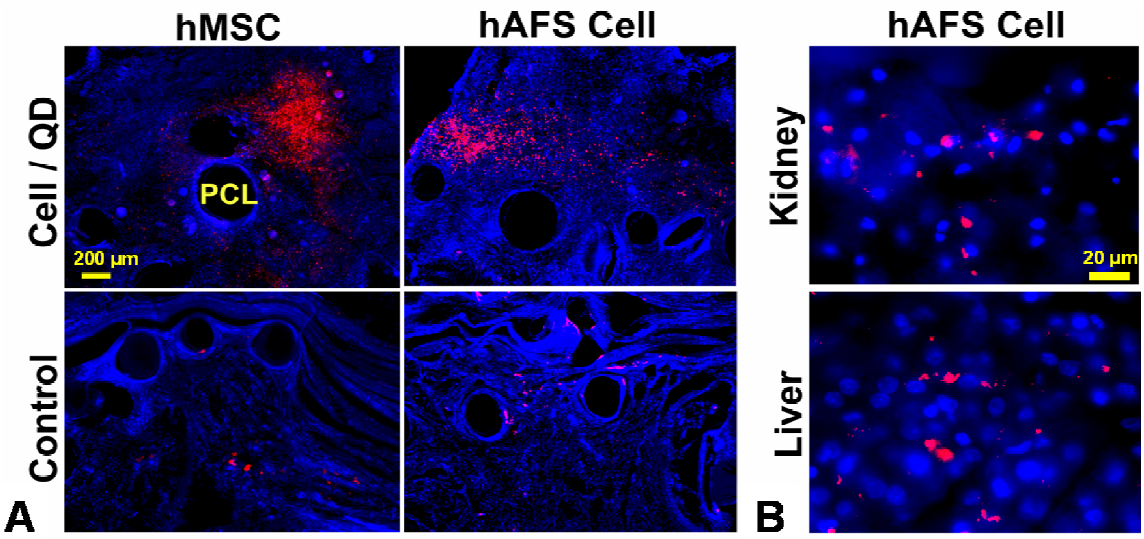

FIGURE 4.7: Quantum dot fluorescence in histological cryosections - preliminary study. A) Quantum dots (red) and DAPI-stained cells (blue) within pore spaces of PCL scaffolds delivered to bone defect sites. 4X magnification. (B) Quantum dots found within liver and kidney. 63X magnification.

***In Vivo* Segmental Defect Delivery of QD-labeled Stem Cells – Analysis of Quantum Dot Fate After Induced Cell Death:** Immediately after surgery a fluorescent signal was detected at defect sites treated with either live or devitalized constructs containing QD-labeled cells but not at the contralateral sites treated with acellular scaffolds. After ten days, all defect sites displayed a clear fluorescent signal, including those treated with acellular scaffolds contralateral to defects treated with QD-containing devitalized hMSCs or human embryonic kidney 293 (HEK) cells (Figure 4.8).

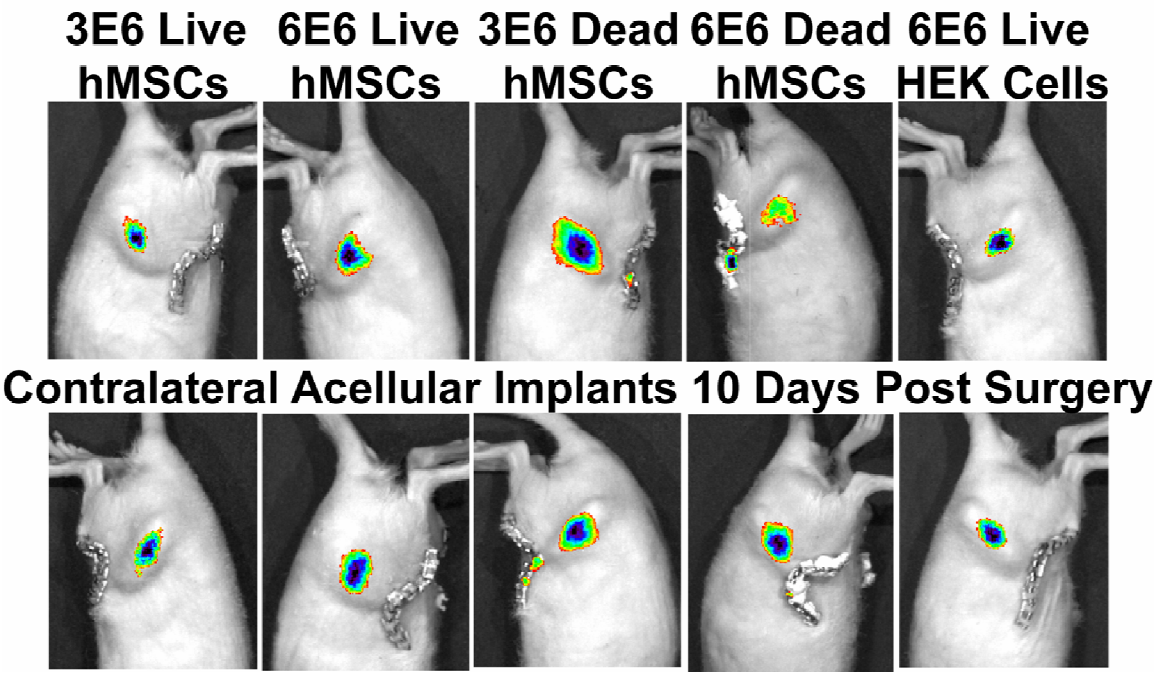

FIGURE 4.8: *In vivo* quantum dot fluorescence – live versus devitalized hMSCs study. Femoral defect site fluorescence 10 days after bone defects were treated by delivery of scaffolds containing either 3 or 6 million QD-loaded live hMSCs, 3 or 6 million QD-loaded devitalized (dead) hMSCs, or 6 million QD-loaded HEK cells, with contralateral defects receiving acellular scaffolds only.

There were no significant differences in defect site fluorescence between live or devitalized cell constructs or between constructs seeded with three or six million cells (Figure 4.9). As a group, defects treated with constructs containing QD-loaded cells displayed a significantly higher fluorescent signal than defects treated with acellular scaffolds only at the day of surgery. By the tenth day after surgery defect fluorescence intensity was similar in all defect sites.

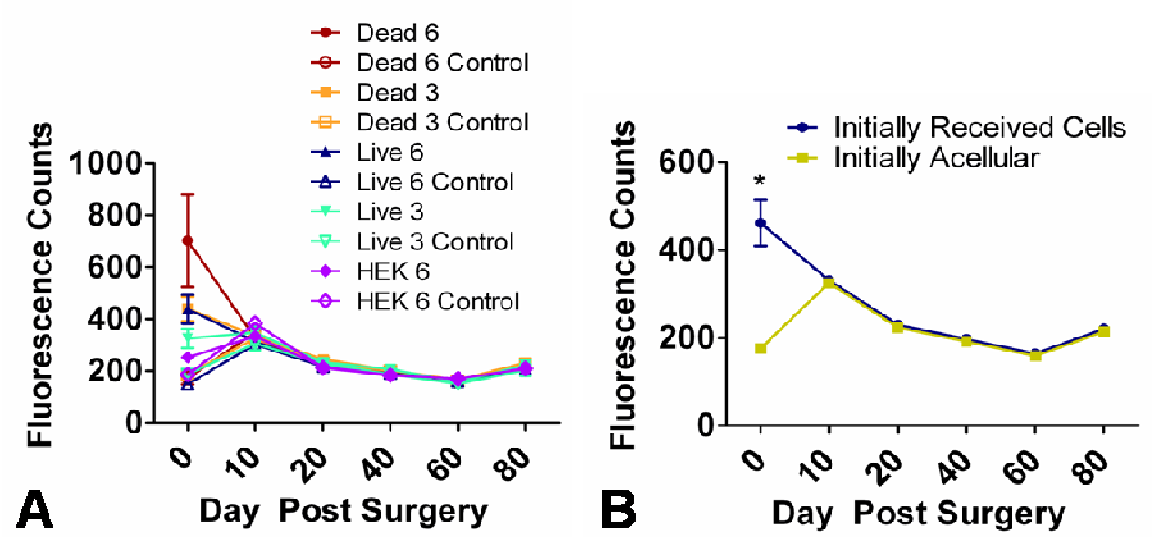

FIGURE 4.9: Quantification of *in vivo* quantum dot fluorescence – live versus devitalized hMSCs study. A) Comparison of fluorescence levels in all individual groups. B) Comparison of fluorescence levels in defects treated with scaffolds seeded with QD-loaded hMSCs and in defects treated with acellular control scaffolds. * $p < 0.05$.

Immunostaining was performed to identify the cell types which were associated with the QDs in rats sacrificed four weeks post-surgery. An antibody specific for human nuclei (HuNu) was first shown to effectively label hMSCs in 2D *in vitro* conditions (Figure 4.10A). Analysis of histological tissue sections taken from defects treated with live hMSCs, devitalized hMSCs, or HEK cells, as well as their contralateral defects, revealed positive HuNu / QD staining in only the live hMSCs and HEK cells implantation sites (Figure 4.10B). However, staining with a rat CD68 macrophage antibody revealed extensive positively stained cells in all groups (Figure 4.10C). At the cell delivery defect site, QDs were found both colocalized with and independent from the stained macrophages in the live hMSC and live HEK constructs but not the devitalized hMSC constructs. Interestingly, the acellular site contralateral to live hMSC constructs also contained QDs colocalized with and independent from the stained macrophages. In

contrast, the acellular sites contralateral to dead hMSC or live HEK constructs only contained QDs associated with macrophages.

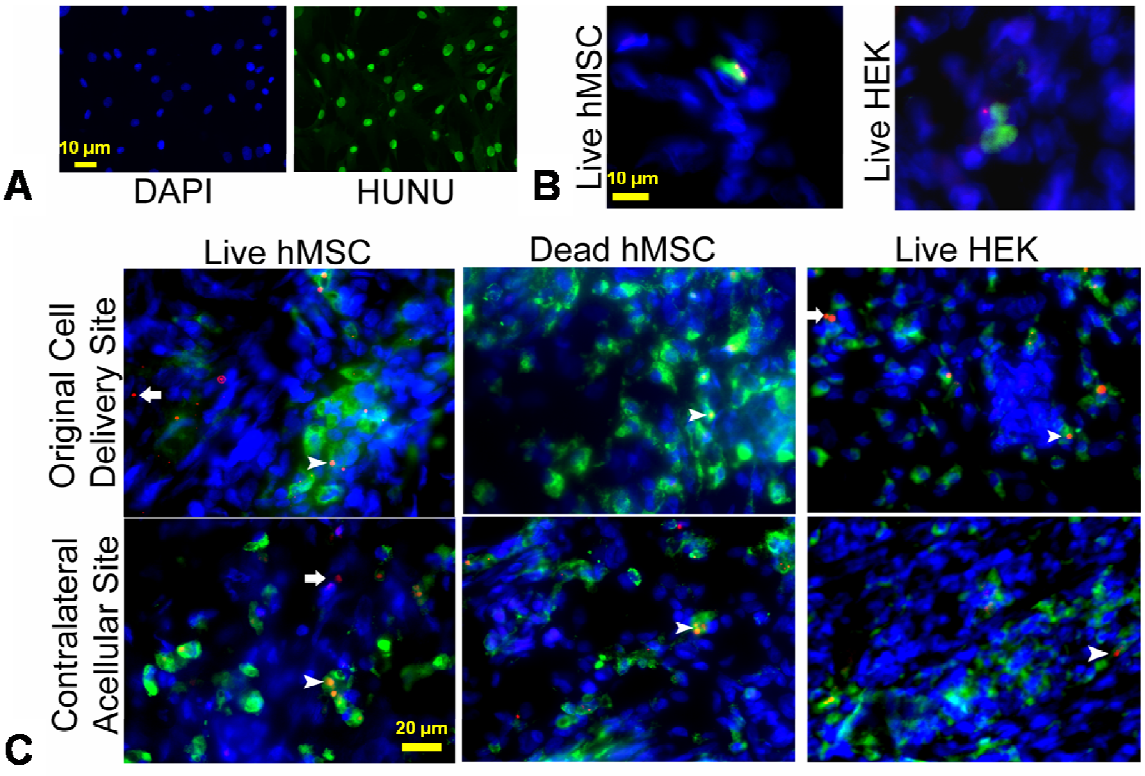

FIGURE 4.10: Immunolabeling to identify cell types associated with quantum dots. A) 2D *in vitro* labeling of hMSCs with DAPI and HuNu human nuclear antibody. 20X magnification. B) Cells labeled with HuNu from defects treated with 6 million live hMSCs or 6 million HEK cells. Green-hMSCs, Blue-DAPI, Red-QDs. 40X magnification. C) Cells labeled with CD68 rat macrophage antibody. Green-macrophages, Blue-DAPI, Red-QDs. Arrowheads point to QDs colocalized with macrophages. Arrows point to QDs separate from macrophages. 40X magnification.

Unlike in the previous study treating segmental defects with QD-free hMSCs, no defects were bridged by 12 weeks post-surgery (Figure 4.11).

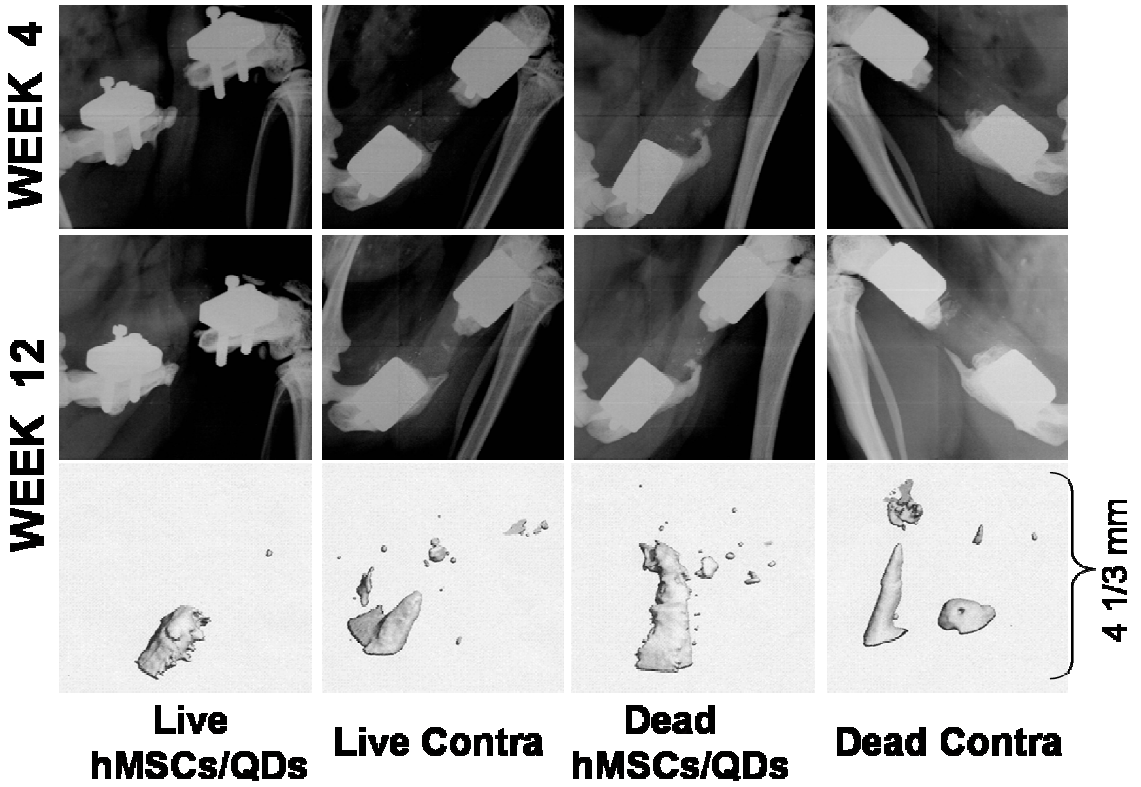

FIGURE 4.11: Qualitative defect site mineral formation after *in vivo* delivery of live or devitalized QD-loaded hMSCs. A) Radiographic (upper) and *in vivo* Micro-CT (lower) images of the representative bone formation per group in defects receiving QD-labeled live hMSC scaffold, acellular scaffold contralateral to live hMSC scaffold, QD-labeled devitalized hMSC scaffold, or acellular scaffold contralateral to devitalized hMSC scaffold.

There were no significant differences in *in vivo* or post mortem defect bone volumes (Figure 4.12A) or maximum torque and torsional stiffness (Figure 4.12B) between groups. The values observed from the QD-free hMSC treated defects used in the first experiment are shown as dashed black lines. There were no observed signs of negative effects from QD exposure on animal morbidity or mortality throughout the study.

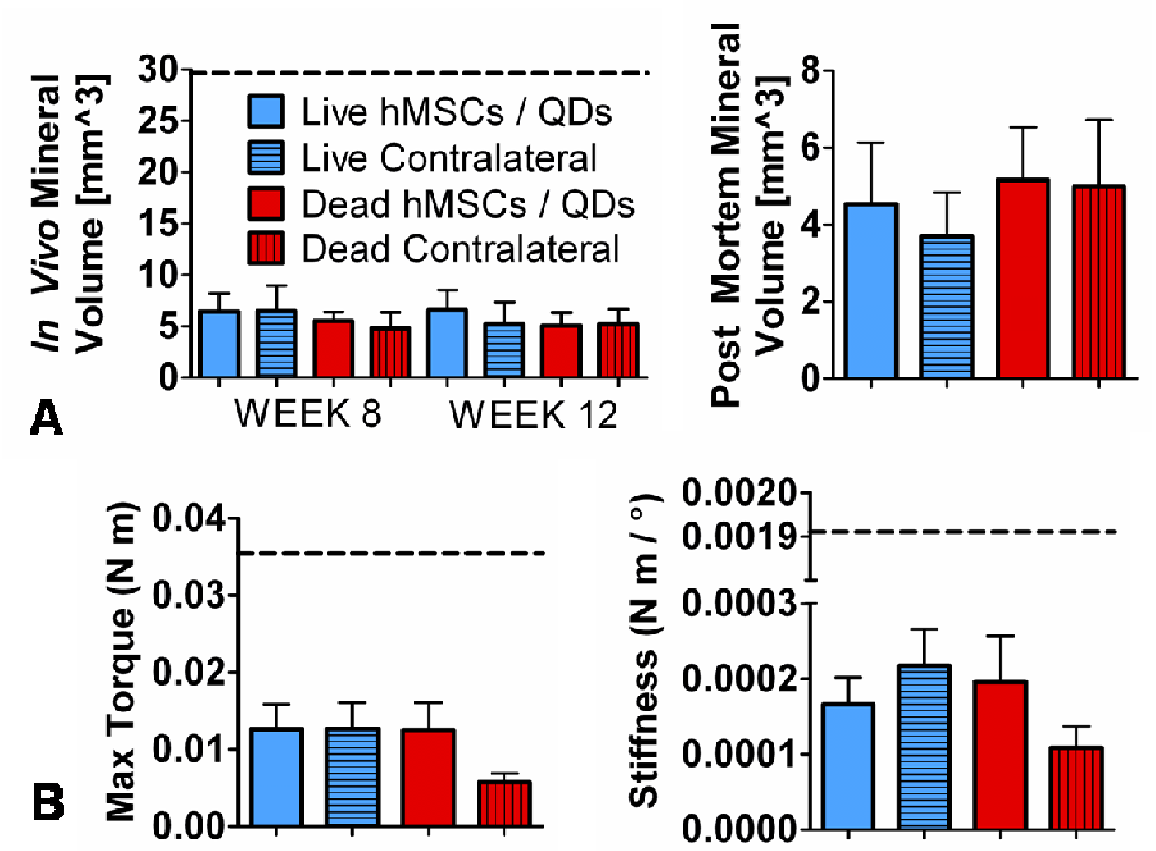

FIGURE 4.12: Quantitative comparison of structure and function results from *in vivo* delivery of scaffolds seeded with live or devitalized QD-loaded hMSCs as well as acellular contralateral control scaffolds. A) *In vivo* and post mortem mineral formation within defect sites. B) Biomechanical properties of femurs tested to failure in torsion. Dashed lines represent average values from defects treated with scaffolds seeded with QD-free hMSCs as displayed in Chapter 3 (data from the week 12 time point are shown in A).

***In Vitro* Quantum Dot Effects on Stem Cell Osteogenic Differentiation**: Finally, although there was a reduced healing response in segmental defects treated with QD-loaded hMSCs compared to defects treated with QD-free hMSCs, quantum dot loading did not reduce *in vitro* hMSC osteogenic differentiation as assessed by qualitatively comparable mineral formation to QD-free hMSCs after Von Kossa assay (Figure 4.13A,B).

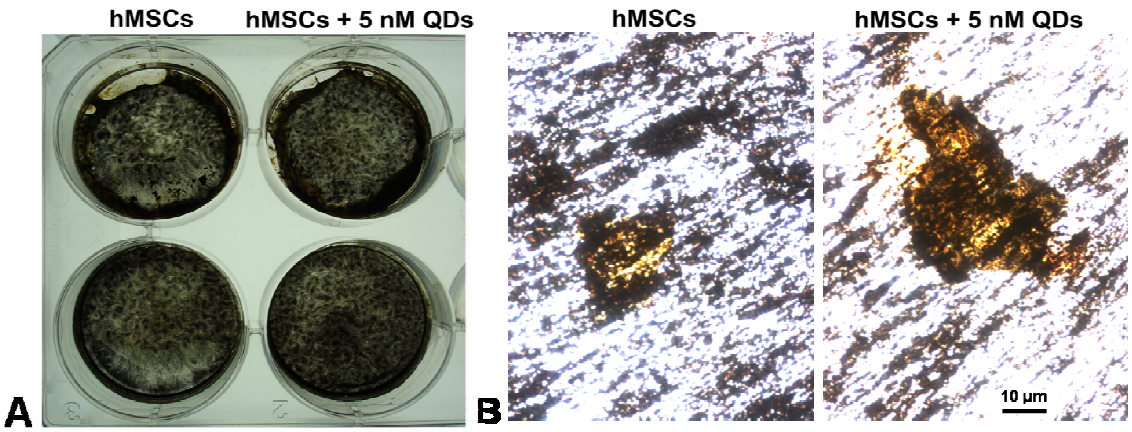

FIGURE 4.13: *In vitro* quantum dot effects on hMSC osteogenic differentiation. A) View of gross mineral formation in wells containing hMSCs with or without QDs. B) View of magnified mineral nodules. 20X magnification.

Chapter 4: Discussion

Stem cell-mediated functional regeneration of segmental bone defects may be limited by short-term cell viability or cell migration from the defect site. This possibility led us to investigate the fate of delivered cells by labeling them with fluorescent quantum dots. In a preliminary study, we observed strong quantum dot fluorescence *in vivo* at the defect site for at least twelve weeks after implantation of scaffolds seeded with QD-loaded stem cells. Interestingly, contralateral defect sites treated with acellular scaffolds began to display clear fluorescent signals one week after implantation, suggesting the possibility that delivered QD-containing stem cells may have homed to the area of tissue damage, which has been reported by multiple groups as an ability of hMSCs (Chamberlain, Fox et al. 2007), (Kumagai, Vasanji et al. 2008), (Karp and Leng Teo 2009), (Laird, von Andrian et al. 2008). The rapid reduction in fluorescent signal strength during the first two weeks of the study could be explained by cell migration from the defect site or by cell death followed by QD clearance and sequestration in the organs of the RES. Later decreases in signal strength could be due to QD redistribution amongst dividing cells, leading to a smaller concentration of QDs per cell. The presence of QDs at defect sites and in RES organs was confirmed by histology. Observing QDs in RES organs substantiated reports that free QDs would not enter neighboring cells but rather enter the circulation and become sequestered in RES organs (Rosen, Kelly et al. 2007), (Voura, Jaiswal et al. 2004), (Ballou, Lagerholm et al. 2004).

In order to confirm that QDs were in fact associated with the delivered stem cells in both original implantation and initially acellular contralateral sites, a second study was performed in which scaffolds were implanted that contained either live or devitalized

QD-loaded hMSCs or QD-loaded non-stem HEK cells. The observation of contralateral fluorescence in all defect sites after 10 days suggested that, at least in the devitalized group, QDs were no longer associated with hMSCs because dead cells would have no ability to migrate. Immunostaining revealed that while a small population of QDs was still associated with hMSCs in the live cell and HEK cell groups, no human cells were detected in contralateral limbs and the majority of QDs in all groups were associated with host macrophage cells. This finding agrees with a recent report that QTracker 565 QDs injected into mice accumulated in murine CD68+ macrophages in atherosclerotic legions (Buono, Anzinger et al. 2009). The mechanism through which QDs delivered at one local injury became associated with macrophages in a separate local injury site remains unclear. Additionally, while 5 nM concentration QD-labeling caused no observed negative effects on cell viability or osteogenic differentiation capacity *in vitro*, QD-loaded live hMSCs failed to enhance bone formation or bridge any defects. This is in contrast to the previous study without QDs in which there was a significant effect of stem cell implantation on bone ingrowth and biomechanical properties and bridging was observed in 4/9 animals receiving hMSCs. The reduction in bridging could be caused by either a reduction in stem cell osteogenic differentiation capacity or in stem cell viability, possibly due to cadmium toxicity and an elevated macrophage infiltration response. The combination of false positive fluorescence signals from QDs taken up by host cells as well as the apparent reduction in *in vivo* healing capacity of constructs loaded with QD-loaded stem cells compared to constructs loaded with QD-free stem cells suggests that an alternate *in vivo* tracking agent is needed to evaluate the distribution and viability of delivered stem cells during the segmental defect healing process.

Chapter 5

ADENO-ASSOCIATED VIRUS (AAV) TRANSDUCTION OF HUMAN STEM CELLS WITH OSTEOGENIC CUES TO ENHANCE BONE FORMATION

Chapter 5: Introduction

While bone tissue engineering therapies delivering stem cells alone can serve as effective treatments, inclusion of added cues that push stem cells towards osteogenic differentiation and stimulate them to produce bone matrix can greatly improve treatment efficacy. Many bone defect therapies have investigated delivery of osteoinductive proteins, and chief amongst them are the bone morphogenetic proteins (BMPs).

Recombinant human BMP2 (rhBMP2) has been used to increase healing of critically-sized defects in rabbit, sheep, dog, and especially rat models (Yasko, Lane et al. 1992), (Lee, Shea et al. 1994), (Oest, Dupont et al. 2007), (Ohura, Hamanishi et al. 1999). The rhBMP2 is usually delivered on carriers such as demineralized bone matrix or collagen sponges. There have also been clinical trials involving rhBMPs, including application of rhBMP7 to large fibular defects (Geesink, Hoefnagels et al. 1999) and tibial nonunions (Friedlaender, Perry et al. 2001), (Govender, Csimma et al. 2002) as well as rhBMP2 application to aid in spinal fusion. Success in these clinical trials led the US Food and Drug Administration to approve application of rhBMP2 on absorbable collagen sponges for single-level interbody fusions of the lumbar spine (InFuse - Medtronic) (Einhorn 2003) and grant a Humanitarian Device Exemption for delivery of rhBMP7 (also called OP-1) on collagen carriers (The OP-1 Device – Stryker) to treat nonunions that have failed to respond to other treatment modalities (Lieberman, Daluiski et al. 2002). However, the extremely high supraphysiological doses of rhBMP2 that have been

required to heal these bone defects can cause problems such as inflammation or ectopic bone formation due to the initial rapid burst release of proteins from the carriers (Cahill, Chi et al. 2009). The high costs of these therapies also prohibit them from being widely used. While BMP-based therapies have largely been shown to be effective for healing bone defects, a better method for BMP production and delivery is needed.

One possible alternative to delivery of large doses of rhBMPs to treat bone defects is to program cells to increase their production of these proteins by gene therapy techniques. Due to its superior safety compared to other viral vectors, AAV likely has the highest potential of all viral vectors for use in treating large bone defects in humans. AAV preclinical *in vivo* studies have been performed in a variety of animal species (predominantly mouse, rat, dog, and primate) providing treatment for a variety of conditions (including hemophilia, cystic fibrosis, Duchenne muscular dystrophy, and rheumatoid arthritis) (Coura Rdos and Nardi 2007). At least two clinical trials have been performed using rAAV, one an *in vivo* approach treating cystic fibrosis and one an *ex vivo* approach treating haemophilia B, but no trials have occurred yet to treat bone and joint diseases, likely due to their less fatal nature (Ulrich-Vinther 2007). In the cystic fibrosis trial more than 100 patients were treated with AAV-CFTR therapy applied by aerosol spray (Moss, Milla et al. 2007). While this study did not lead to any significant improvements in patients, no adverse health effects were reported in response to AAV, and the lack of efficacy could possibly be due to an inefficient aerosolized *in vivo* delivery. In two preclinical studies, direct injection of either AAV-BMP2 or AAV-BMP4 vectors into immunocompetent rat hindlimb muscle led to significant ectopic mineral formation (Chen, Luk et al. 2003), (Luk, Chen et al. 2003), but injection offers

limited control of viral particle distribution, which could limit transduction efficiency or lead to undesirable ectopic bone formation away from bone defect sites. These results call for a better *in vivo* AAV delivery method.

Schwarz and colleagues have recently developed a novel *in vivo* AAV delivery method in a murine allograft model (Ito, Koefoed et al. 2005), (Koefoed, Ito et al. 2005), (Awad, Zhang et al. 2007). Their main research goal was to try to overcome the poor performance of allografts, as described above, through AAV gene therapy. They first used a DNA microarray to find that the main difference in gene expression between allografts and autografts was a lack in expression of vascular endothelial growth factor (VEGF), a stimulator of angiogenesis, and receptor activator of nuclear factor κ-B ligand (RANKL), which is important in fracture callus formation and osteoclastic resorption of bone during remodeling. Next they lyophilized AAV-RANKL and AAV-VEGF particles in a 1% sorbitol solution onto the murine allografts. When these AAV-coated allografts were implanted *in vivo* into large bone defects stabilized with intramedullary pins, the allografts underwent neovascularization and remodeling within 4 weeks, similar to autografts (Ito, Koefoed et al. 2005). They used rAAV-LacZ coated allograft controls to determine the *in vivo* transduction efficiency. LacZ is a reporter gene that encodes for β-Galactosidase (β-Gal), and locating cells producing this protein can be achieved through histological staining with X-Gal (Holt and Sadler 1958). Although their transduction efficiency was low (1-5% of the cells directly surrounding the allografts), it was clearly high enough to cause a significant improvement in allograft integration and revitalization. Furthermore, they found that since AAV is thermostable, AAV-coated allografts could be frozen for months with only minor negative effects on transduction ability.

Next they coated allografts with AAV containing the DNA to encode for the constitutively active form of activin receptor-like kinase 5 (CaAlk2), an active BMP receptor, and implanted them into murine segmental defects. They found that AAV-CaAlk2 coated allografts lacked foreign body reactions, had a bone collar formed along the surface of the allografts, had live bone marrow within allografts, and experienced osteoclastic resorption of allografts (Koefoed, Ito et al. 2005). However, they also found that the nonporous cortical surface of allograft bone prohibits uniform distribution of the rAAV / 1% sorbitol / PBS solution coating prior to freeze-drying.

They then found that demineralization of the allograft surfaces, which created voids within the cortical bone, increased surface adsorption of rAAV-Luciferase coatings and led to longer gene expression of luciferase compared to undemineralized allografts as assessed by continued display of *in vivo* bioluminescence (Yazici, Yanoso et al. 2008). Peak gene expression was delayed to one week post-surgery, which coincides with the end of the inflammatory phase of long bone injury response and the initiation of the reparative phase of bone healing. If an osteogenic gene were delivered in this manner and had similar expression kinetics, it might provide a significant improvement in bone development compared to delivery of recombinant proteins, which have very fast release kinetics that would likely occur during the initial inflammatory response phase of bone healing when there are many complicating and confounding signals present. In one recent study, lyophilization of AAV-BMP2 onto hydroxyapatite scaffolds led to significant ectopic bone formation four weeks after implantation into muscle pouches in the backs of rats (Nasu, Ito et al. 2009). The results of these studies lead us to hypothesize that using a similar AAV-BMP2 gene lyophilization procedure to coat

porous polymer scaffolds prior to stem cell seeding could produce an effective therapy for healing critically-sized large bone defects in our rat model.

Chapter 5: Materials and Methods

Scaffold Preparation / AAV Coating - PLDL Scaffolds: 85% porous polymer poly(L-Lactide co-D,L-Lactide 70:30) (PLDL) cylindrical scaffolds, 8 mm length and 4 mm diameter, were fabricated as previously described (Lin, Barrows et al. 2003), (Oest, Dupont et al. 2007). Briefly, scaffolds were created by coating 100-micron removable stainless steel fibers with a 70% / 30% mixture of liquid PLDL and the porogen azodicarbonamide to create longitudinally oriented macroporosity, while decomposition of the porogen with the addition of heat produced random microporosity. Scaffolds were then sterilized by gamma-irradiation (2.5 Mrad). Finally scaffolds were coated with $5*10^{10}$ rAAV-LacZ particles (Gene Core Facility, University of North Carolina, Chapell Hill, NC) in 100 μL of 1% sorbitol / PBS solution through lyophilization by collaborators at the University of Rochester. All rAAVs used in the experiments described in this Aim were serotype 2 and were under the transcriptional control of the cytomegalovirus (CMV) promoter.

Scaffold Preparation / AAV Coating - PCL Scaffolds: 85% porous PCL cylindrical scaffolds, 8 mm length and 5 mm diameter, were fabricated as described in Chapter 3. All scaffolds were coated with GFOGER and lyophilized type I collagen. Scaffolds were then placed in the wells of custom molds and coated with either 10^{10} scAAV2.5-BMP2 or AAV-Luciferase (AAV-Luc, Gene Core Facility, University of North Carolina, Chapell Hill, NC) particles in 100 μL of 1% sorbitol / PBS solution by lyophilization by collaborators at the University of Rochester. The adeno-associated virus used in this study to deliver the BMP2 transgene was a modified form of the traditional AAV virion that was developed at the University of Rochester. Traditional

AAV has inefficient transgene expression due to the need for duplication of the single-stranded DNA genome prior to transgene expression; however the modified scAAV features self-complimentary DNA strands, increasing the efficiency of transgene expression in MSCs (Kim, Lee et al. 2007).

Cell Culture / AAV Transduction – 2D *In Vitro* scAAV2.5-BMP2 / AAV-Luc: 20,000 hMSCs (p4) or hAFS Cells (p19) were seeded in wells of 24-well plates and allowed to adhere for 24 hours. One mL standard culture media described previously was then added to one group of cells, culture media supplemented with the osteogenic supplements 10 mM β-glycerol phosphate and 50 μg / ml ascorbic acid 2-phosphate was added to the second group, culture media / osteogenic supplements and AAV-Luc viral particles were added to the third group, and culture media / osteogenic supplements and scAAV2.5-BMP2 viral particles were added to the fourth group (n = 5 per group). For viral transduction, $0.5*10^9$ scAAV2.5-BMP2 or control AAV-Luc particles were added per well in 10 μL media and gently agitated for AAV distribution, producing an initial estimated multiplicity of infection (MOI – ratio of number of viral particles to number of cells) of $2.5*10^4$. After 10 minutes 1 mL of media was added per well and plates were cultured at 37°C / 5% CO_2 in an incubator. Media supernates were collected and media changed at day 2, 6, 9, 13, and 16. Supernate BMP2 levels were assessed using an ELISA assay (BMP2-Immunoassay Kit, Quantikine, Cat. #DBP200, R&D Systems). Cell lysates were collected at day 16 and used to determine DNA content through a PicoGreen DNA Assay. The same lysates were used in an alkaline phosphatase activity assay to assess osteogenic differentiation. In this assay, the release of *p*-nitrophenol from *p*-nitrophenyl phosphate by the ALP enzyme is measured (Martin, Dean et al. 1996). The

ALP substrate working solution was made by mixing equal parts of 20 mM p-nitrophenyl phosphate, 1.5 M 2-Amino-2-Methyl-1-Propanol (pH 10.25) and 10 mM $MgCl_2$. The experimental samples were mixed with the freshly made substrate working solution, and incubated for 1 hour at 37° C. The reaction was stopped by adding 1N NaOH, and the absorbance was measured at 405 nm on a plate reader (PowerWave XS, Biotek, VT). All samples were run in triplicate and compared to p-nitrophenol standards.

Cell Culture / AAV Transduction – 2D *In Vitro* AAV-LacZ: hMSC's (p4) were cultured on 6-well plates at a density of 2,000 cells/cm^2 (total cells = 19,200 / well) in culture media. After 24 hours either $5*10^8$ (1X dose) or 10^9 (2X dose) rAAV-LacZ viral particles in 100 µL of PBS were added to the cells in either 3 mL culture media (High transduction volume) or in 500 µL culture media followed by addition of 2.5 mL media after 3 hours (Low transduction volume) (n = 3 per dose per transduction volume). After 3 or 6 days cells were fixed in 0.2% glutaraldehyde and stained with X-Gal for 10 hours followed by counterstaining with nuclear fast red for 60 seconds. X-Gal positive cells were counted and then total cell numbers were calculated by 5 ng / mL DAPI staining followed by cell nuclei counting using fluorescence microscopy images and the image analysis software ImageJ. hMSCs were also cultured in wells of an additional 6-well plate, and after 24 hours cells were fixed in 0.2% glutaraldehyde and stained with 5 ng / mL DAPI, followed by cell nuclei counting in order to quantify average initial number of cells present at the time of transduction (n = 3) for accurate MOI assessment.

Cell Culture / AAV Transduction – 3D *In Vitro* scAAV2.5-BMP2 / AAV-Luc: One million hMSCs or hAFS Cells in 100 µL culture media were seeded on PCL scaffolds previously coated with 10^{10} lyophilized AAV particles for an initial MOI of 10^4.

After seventy-five minutes incubation, 5 mL of culture media supplemented with osteogenic supplements (10 mM β-glycerol phosphate and 50 μg / ml ascorbic acid 2-phosphate) was added to each well of the 12-well plates in which the scaffolds were held, and scaffolds were cultured dynamically on rocker plates for 12 weeks. Media supernates were collected and media changed every three days for eleven weeks. n = 5 per cell type per AAV gene. Supernate BMP2 levels were assess using an ELISA assay (BMP2-Immunoassay Kit, Quantikine, Cat. # DBP200, R&D Systems).

Cell Culture / AAV Transduction – 3D Scaffold Stem Cell Pre-Seeding For *In Vivo* scAAV2.5-BMP2 / AAV-Luc Study: Three million hMSCs were seeded on PCL scaffolds previously coated with 10^{10} lyophilized scAAV2.5-BMP2 or AAV-Luc particles for an initial MOI of $0.333*10^{4}$. Cells were seeded on scaffolds in 100 μL culture media and after 75 minutes 4 mL of culture media was added to each well of the 12-well plates in which the scaffolds were held. Scaffolds were then cultured for two days prior to *in vivo* implantation.

Assessment Of *In Vitro* Cell Viability / DNA Analysis: Cell viability of stem cells seeded on 3D scaffolds was assessed at the end of the twelve week study by Live / Dead staining of one scaffold per AAV coating per cell source followed by fluorescence microscopy imaging as described in Chapter 3. Scaffolds chosen for viability assessment displayed the average mineral volume per group at the 12-week scan time point. The remaining four scaffolds per group were used to quantify DNA levels following the same methods described in Chapter 3. Cell lysates from 24-well plates in the 2D AAV-Luc / AAV-BMP2 study were collected and DNA was extracted into PBS solution by freeze-

thaw cycles and repeated vortexing of sample tubes. DNA levels were measured by PicoGreen assay (n = 5 / group)

Surgical Technique – Segmental Defect Treatment With scAAV2.5-BMP2 Or AAV-Luc Coated PCL Scaffolds, With Or Without Pre-Seeded hMSCs: All surgical techniques were approved the Georgia Institute of Technology Institute Animal Care and Use Committee (protocol A08066). Critically-sized femoral defects were created in 13-week old female Nude rats as described previously in Chapter 3. Defects were treated with one of four constructs: PCL scaffold coated with scAAV2.5-BMP2 or AAV-Luc (*in vivo* gene therapy – a variety of local host cells could be transduced), or PCL scaffold coated with scAAV2.5-BMP2 or AAV-Luc pre-seeded with three million hMSCs (*in vitro* gene therapy – specifically selected cells are transduced, here hMSCs). Sample size was n = 10 per group.

Surgical Technique – Segmental Defect Treatment With AAV-LacZ-Coated PLDL Scaffolds To Assess Short-Term *In Vivo* Transduction: Critically-sized femoral defects were created in 13-week old female Sasco Sprague Dawley rats as described previously in Chapter 3. Defects were treated with either PLDL scaffold or PLDL scaffold previously coated with AAV-LacZ viral particles (n = 3 / group). Animals were sacrificed after two weeks.

Preparation of Histological Cryosections From *In Vivo* rAAV-LacZ Study: Femurs were harvested, fixed in 0.2% glutaraldehyde, washed with PBS, embedded in OCT medium, and frozen at -80º C. Femur / scaffold tissue cryosections five microns thick were obtained using a cryostat, as described above, and mounted on SuperFrost Plus glass slides. Tissue sections were fixed again in 0.2% glutaraldehyde and then

stained with X-Gal and nuclear fast red and coverslipped. Brightfield microscopy was used to obtain images showing both the PLDL scaffold and the soft tissue surrounding it.

Radiograph / Micro-CT Imaging And Biomechanical Testing: 2D radiographs of segmental defect sites were obtained 4, 8, and 12 weeks post-surgery in the *in vivo* study comparing scAAV2.5-BMP2 and AAV-Luc treatments following procedures described in Chapter 3. I*n vitro* mineral formation on 3D scaffolds was measured by Micro-CT scans 3, 6, 9, and 12 weeks after stem cell seeding following procedures described in Chapter 3. Mineral formation in segmental defects was measured by Micro-CT scans performed *in vivo* at 4, 8, and 12 weeks post-surgery as well as in post mortem scans following procedures described in Chapter 3. Post mortem scans were performed using a density threshold corresponding to 385 mg HA/cm^3. Biomechanical torsional tests were performed on explanted femurs taken from rats sacrificed 12 weeks post-surgery as described in Chapter 3. Sample sizes for Micro-CT scans and torsional testing were n = 10 for scAAV2.5-BMP2 scaffold and scAAV2.5-BMP2 scaffold + pre-seeded hMSCs groups, n = 8 for the AAV-Luc scaffold + pre-seeded hMSCs group, and n = 6 for the AAV-Luc scaffold group due to loss of two samples in which the polysulfone plate became detached from the stainless steel plates between weeks 8 and 12.

Data Analysis: Data were analyzed using GraphPad Prism 5 software. Analyses comparing three or more groups were analyzed using ANOVA with Tukey post hoc analyses for pairwise comparisons. Analyses comparing two groups were analyzed using unpaired t-tests. Whenever required, the raw data was transformed using a natural logarithmic transformation to make the data normal and the variance independent of the mean (Kutner 2005) prior to statistical analysis. If after transformation data comparing

three or more groups still was not normal or variance independent of the mean, data sets were analyzed using the Kruskal-Wallis non-parametric test followed by Dunn's multiple comparison test. For the comparisons of *in vitro* BMP2 release over time, repeated measures ANOVA was performed with Bonferroni post tests. For the *in vivo* segmental defect study comparing treatment with scAAV2.5-BMP2 scaffold with or without hMSCs and AAV-Luc scaffold with or without hMSCs, no significant differences were found between the two BMP2 groups or two Luc groups so they were each combined to increase sample size. For the same study, no significant differences were found in week 4 or 12 *in vivo* mineral formation, max torque, or stiffness between the two hMSC-seeded scaffold groups and the two acellular scaffold groups so they were combined to increase sample size. If after natural logarithmic transformation the grouped data variance was still not independent of the mean, Welch's correction for unequal variances was used in the unpaired t-test. Also for the same *in vivo* segmental defect study, no significant differences in biomechanical properties were found between scAAV2.5-BMP2 scaffold-treated defects that were either bridged or unbridged (as assessed by 2D radiograph evaluation), so the single group was split into the two bridged and unbridged groups for comparison of functional restoration with nude rat whole bones. Data are presented as mean ± standard error of mean (SEM). A p-value < 0.05 was considered significant.

Chapter 5: Results

Segmental Defect Site Delivery Of rAAV-LacZ Coated Scaffolds To Assess Transduction Efficiency *In Vivo*: Clear β-galactosidase expression was found in all of the defects receiving rAAV-LacZ coated scaffolds (Figure 5.1).

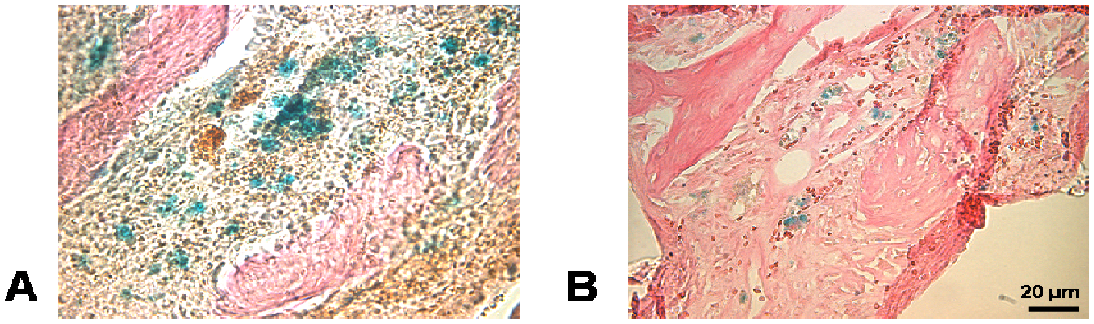

FIGURE 5.1: Histological cryosections showing blue β-galactosidase expression from both A) transduced cells that have infiltrated the PLDL scaffold and B) transduced cells in the fibrous tissue immediately surrounding the implanted rAAV-LacZ coated scaffolds. 10X magnification.

No β-galactosidase expression was found in control defects treated with uncoated PLDL. Transduced cells were found within the scaffolds (though primarily at the periphery) indicating scaffold cellular infiltration (Figure 5.1A). Transduced cells were also found in the soft tissue surrounding the scaffolds (Figure 5.1B). Transduction efficiency, as assessed by qualitative evaluation of β-galactosidase expression in and around the scaffolds, was comparable with that found in the studies by the Schwarz group (Ito, Koefoed et al. 2005).

Evidence Of 2D *In Vitro* scAAV2.5-BMP2 hMSC Transduction And Resulting Increase In Osteogenic Differentiation: Media samples taken from wells containing hMSCs transduced with scAAV2.5-BMP2 displayed significantly higher

BMP2 concentrations than media samples from wells containing hMSCs or hAFS Cells transduced with AAV-Luciferase throughout the duration of the 16-day study (Figure 5.2A). By day six, media from scAAV2.5-BMP2-transduced hMSCs displayed peak BMP2 concentration which was also significantly higher than scAAV2.5-BMP2-transduced hAFS Cells, and this continued throughout the rest of the study. scAAV2.5-BMP2-transduction of hAFS Cells failed to cause an increase in BMP2 concentration in media samples during the 16-day experiment.

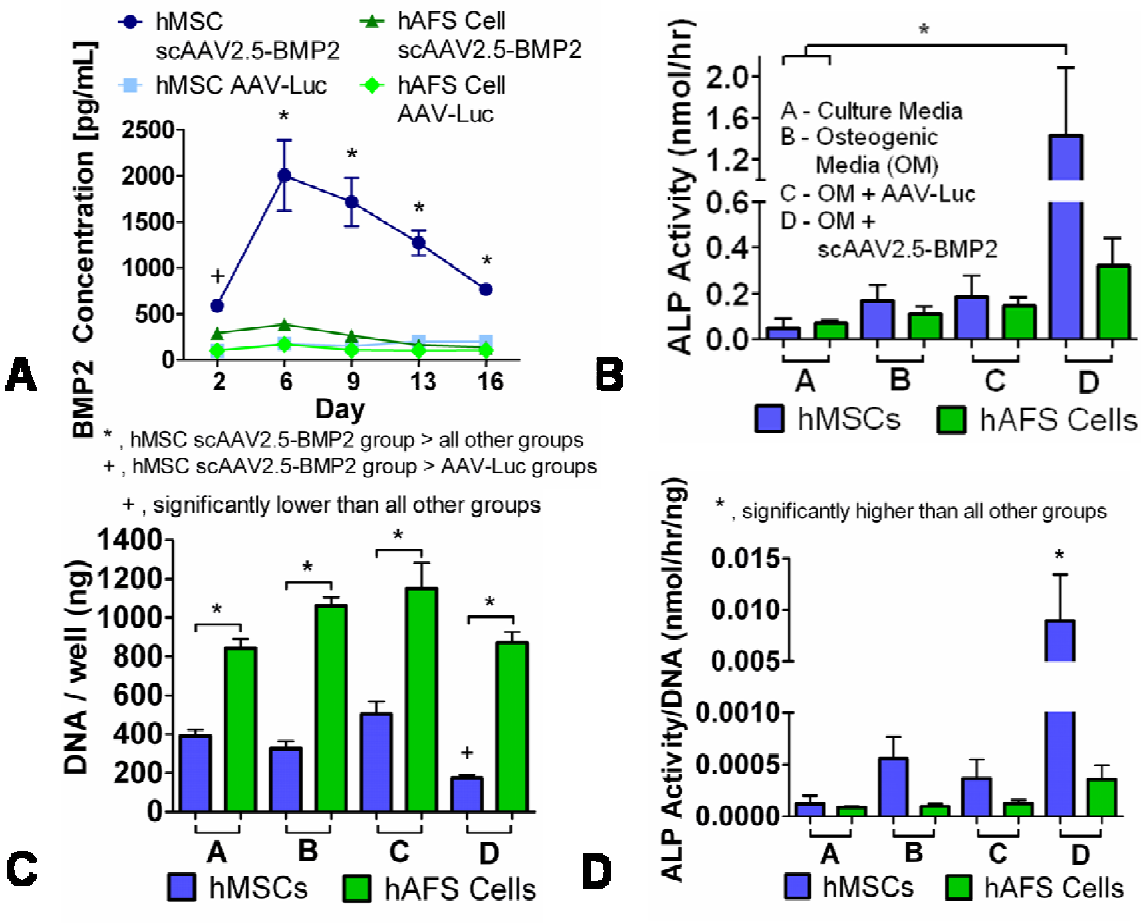

FIGURE 5.2: 2D *in vitro* evidence of scAAV2.5-BMP2 transduction of hMSCs resulting in an increase in osteogenic differentiation. A) BMP2 concentrations in harvested media samples from wells containing stem cells in osteogenic media after Day 0 transduction with scAAV2.5-BMP2 or AAV-Luc. B) ALP activity measured in cell lysates collected 16 days after groups C and D were transduced by AAV-Luc or scAAV2.5-BMP2, respectively. C) DNA levels measured from cell lysates. D) ALP activity normalized by DNA level per well. *, + both indicate $p < 0.05$.

After 16 days, alkaline phosphatase expression in cell lysates was measured to assess osteogenic differentiation of stem cells. An endpoint of 16 days was chosen based upon preliminary studies performed by collaborators at the University of Rochester showing a peak in transient alkaline phosphatase expression from scAAV2.5-BMP2 transduced cells at that time point. ALP activity in hMSCs transduced with scAAV2.5-

BMP2 was significantly higher than in hMSCs and hAFS Cells cultured in non-osteogenic media (Figure 5.2B), but when ALP levels were normalized by DNA content, scAAV2.5-BMP2 transduced hMSC levels were significantly higher than all other groups (5.2D). scAAV2.5-BMP2 transduction of hAFS Cells failed to cause an increase in ALP activity in cell lysates during the 16-day experiment. Cells cultured in osteogenic media in the absence of scAAV2.5-BMP2 failed to experience any significant increases in ALP activity, most likely due to the lack of dexamethasone, a potent stimulator of stem cell osteogenic differentiation, in the media. hAFS Cell DNA levels were significantly higher than hMSC DNA levels in all media condition groups, suggesting increased cell proliferation of hAFS Cells compared to hMSCs (Figure 5.2C). Of particular importance was a significantly reduced DNA content in scAAV2.5-BMP2 transduced hMSCs compared to all other groups, suggesting reduced stem cell proliferation due to increased osteogenic differentiation.

Evidence Of 3D *In Vitro* scAAV2.5-BMP2 hMSC and hAFS Cell Transduction and Resulting Increase in hMSC Osteogenic Differentiation: BMP2 concentrations in media samples from wells containing hMSCs seeded on scAAV2.5-BMP2 coated scaffolds displayed an expression pattern similar to that in the 2D experiment, with a peak one week after transduction (Figure 5.3). Interestingly, BMP2 concentrations from wells containing hAFS Cells seeded on scAAV2.5-BMP2 coated scaffolds significantly increased above levels in all other groups but not until 7 weeks after transduction, and the BMP2 peak was nearly twice as high (7788.74 versus 4811.82 pg/mL) and lasted for three times as long (Day 44-65 versus Day 4-11) in hAFS Cells compared to hMSCs.

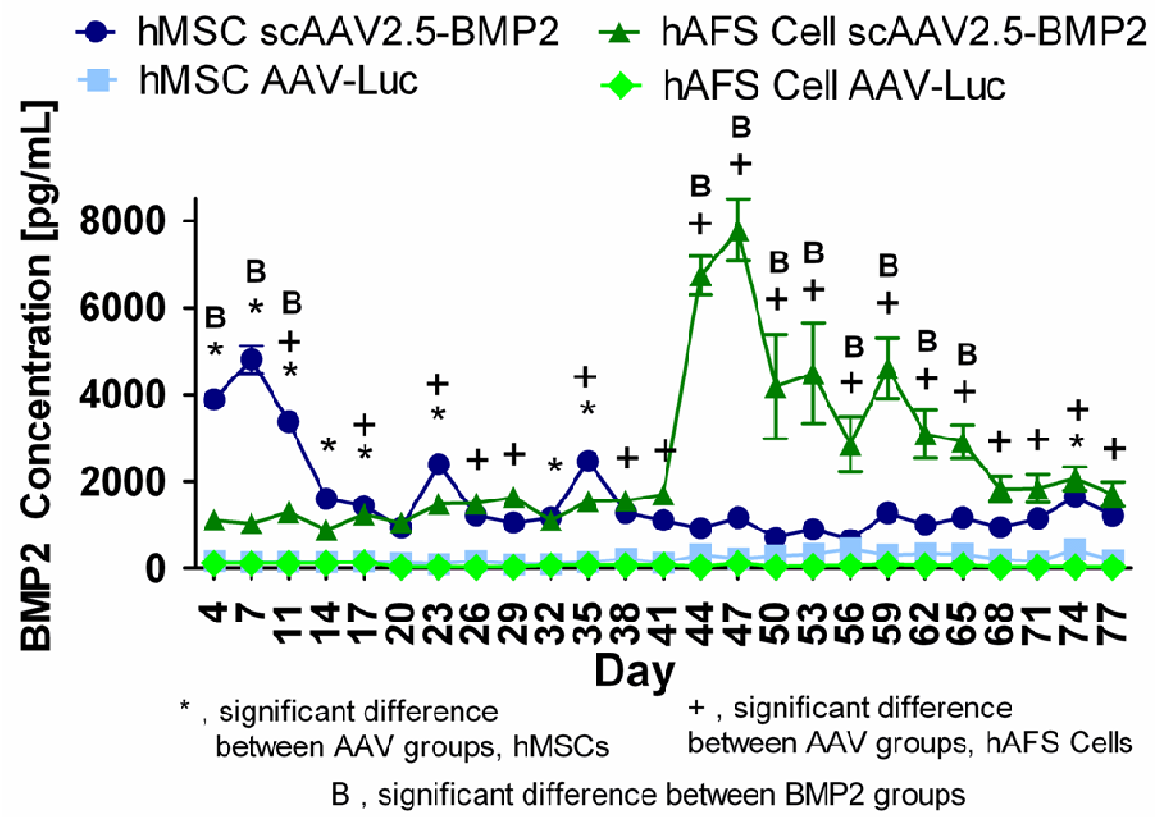

FIGURE 5.3: 3D *in vitro* evidence of scAAV2.5-BMP2 transduction of hMSCs and hAFS Cells. The figure shows BMP2 concentrations in harvested media samples from wells containing stem cells seeded on PCL scaffolds previously coated by scAAV2.5-BMP2 lyophilization. *, + , B all indicate $p < 0.05$

Mineral formation in hMSC-seeded / scAAV2.5-BMP2 coated scaffolds was significantly higher than in hMSC-seeded / AAV-Luc coated scaffolds and hAFS Cell-seeded / scAAV2.5-BMP2 coated scaffolds beginning at week 6 and continuing through weeks 9 and 12 (Figure 5.4A,B). The lack of significant differences at week 3 suggests a delay in osteogenic differentiation, or at least in resulting mineral formation, behind BMP2 expression which peaked at day 7. While BMP2 expression in hAFS Cell-seeded / scAAV2.5-BMP2 coated scaffolds did significantly increase after seven weeks, no

resulting increase in mineral formation occurred by week 12 of the study. Live stem cells were observed throughout scaffolds from each group at week 12 (Figure 5.4C). Live cells were found along the outer circumferential periphery of the cylindrical scaffolds, along the surface of a longitudinally cut cross section (representing cells at the center of the scaffolds), and on both the top and bottom surfaces of the scaffolds. As in the 2D *in vitro* study, DNA content of scaffolds seeded with hMSCs transduced with scAAV2.5-BMP2 was significantly lower than scaffolds seeded with hMSCs transduced with AAV-Luc (Figure 5.5), again likely due to increased stem cell differentiation resulting in reduced stem cell proliferation.

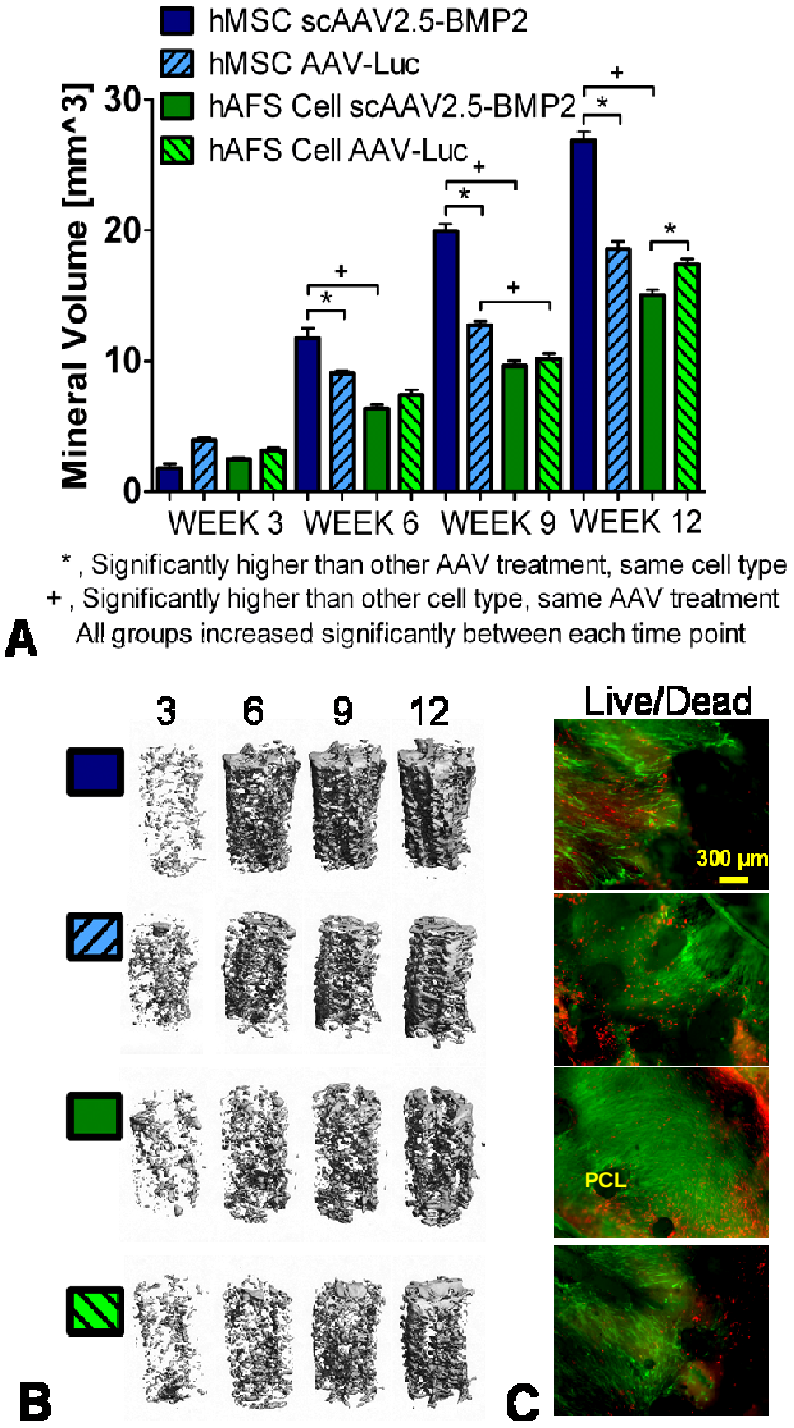

FIGURE 5.4: Evaluation of osteogenic differentiation of stem cells seeded on 3D PCL scaffolds previously coated with lyophilized AAV. A) Quantitative comparison of mineral volumes within PCL scaffolds. *, + both indicate $p < 0.05$. B) Representative Micro-CT images of mineral formation within scaffolds. C) Live / Dead microscopy images of scaffolds showing live green cells along circumferential periphery of scaffolds. A circular PCL strut is labeled. 4X Magnification.

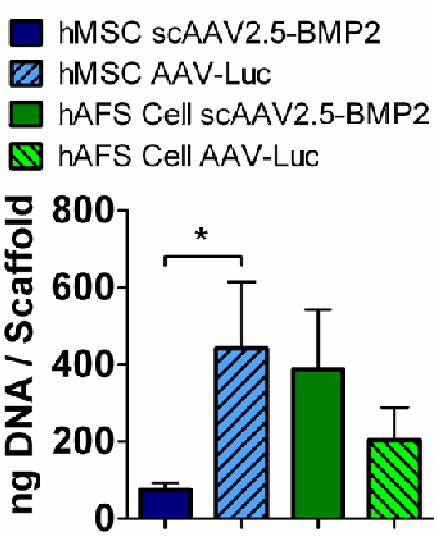

FIGURE 5.5: DNA per scaffold after 12 weeks *in vitro* culture. * $p < 0.05$.

Comparison Of *In Vivo* And *In Vitro* scAAV2.5BMP2 Gene Therapy Approaches For Healing Critically-Sized Nude Rat Femoral Defects: Twelve weeks post-surgery, bony bridging occurred in 5/10 defects treated with scAAV2.5-BMP2 coated scaffolds alone, 3/10 defects treated with scAAV2.5-BMP2 coated scaffolds seeded with hMSCs pre-implantation, 1/6 defects treated with AAV-Luc coated scaffolds alone, and 0/8 defects treated with AAV-Luc coated scaffolds seeded with hMSCs pre-implantation. Note that mineral formation was restricted to the immediate vicinity of the segmental defect site, suggesting that BMP2 delivery via scAAV2.5-BMP2-coated polymer scaffolds avoided the ectopic bone formation that can be associated with bolus delivery of large doses of recombinant BMP2. Representative defect mineral formation in each group is shown in Figure 5.6, both in radiograph images from weeks 4 and 12 and in corresponding week 12 Micro-CT images.

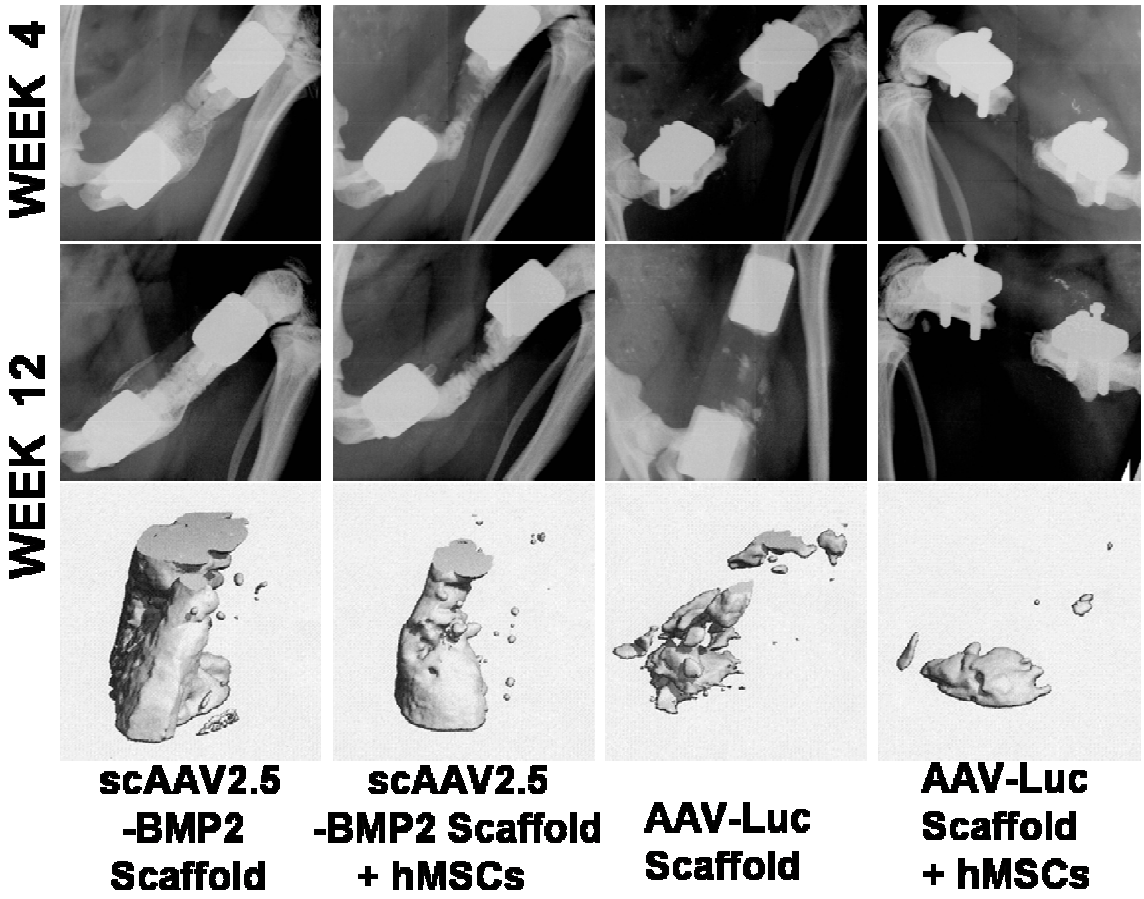

FIGURE 5.6: Qualitative defect site mineral formation after *in vivo* delivery of AAV-coated PCL scaffolds with or without pre-seeding of hMSCs. A) Radiographic (upper) and *in vivo* Micro-CT (lower) images from defects which had the representative mineral formation per group.

Quantitative comparison of Micro-CT-measured mineral volumes revealed significantly higher mineral formation in the scAAV2.5-BMP2 coated scaffold treatment group compared to the AAV-Luc coated scaffold treatment and the hMSC pre-seeded AAV-Luc scaffold treatment groups at week 8 *in vivo* as well as in post mortem scans (Figure 5.7A,B). A significant difference in mineral volume existed between the scAAV2.5-BMP2 scaffold treatment group and the hMSC pre-seeded AAV-Luc scaffold group at week 12. Biomechanical torsional testing revealed significantly higher

maximum torque and torsional stiffness in the scAAV2.5-BMP2 scaffold treatment group compared to the hMSC pre-seeded AAV-Luc scaffold treatment group (Figure 5.7C).

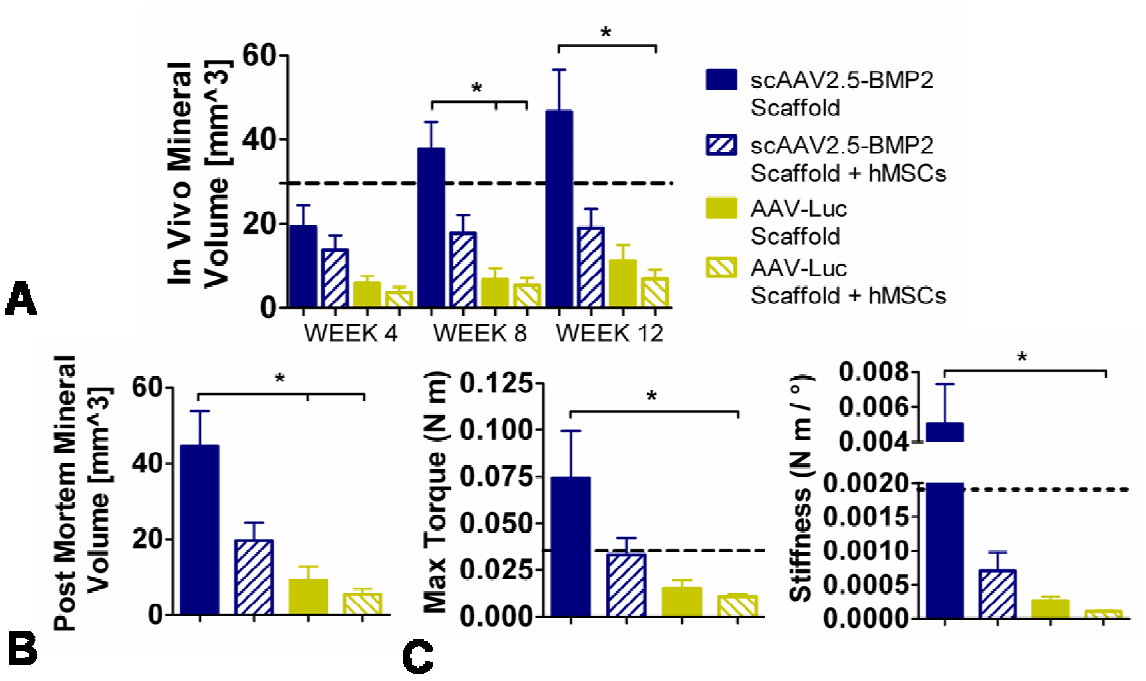

FIGURE 5.7: Quantitative comparison of structure and function results from *in vivo* delivery of AAV-coated scaffolds with or without pre-seeding of hMSCs. A) *In vivo* mineral formation within defect sites. B) Post mortem mineral formation within defect sites C) Biomechanical properties of femurs tested to failure in torsion. Dashed lines represent average values from defects treated with non-AAV scaffolds seeded with hMSCs as reported in Chapter 3 (*in vivo* mineral formation from the week 12 time point are shown). * $p < 0.05$.

Comparison of grouped scAAV2.5-BMP2 therapies with grouped AAV-Luc therapies showed significant differences in both *in vivo* and post mortem mineral volumes (Figure 5.8A) as well as maximum torque and torsional stiffness (Figure 5.8B).

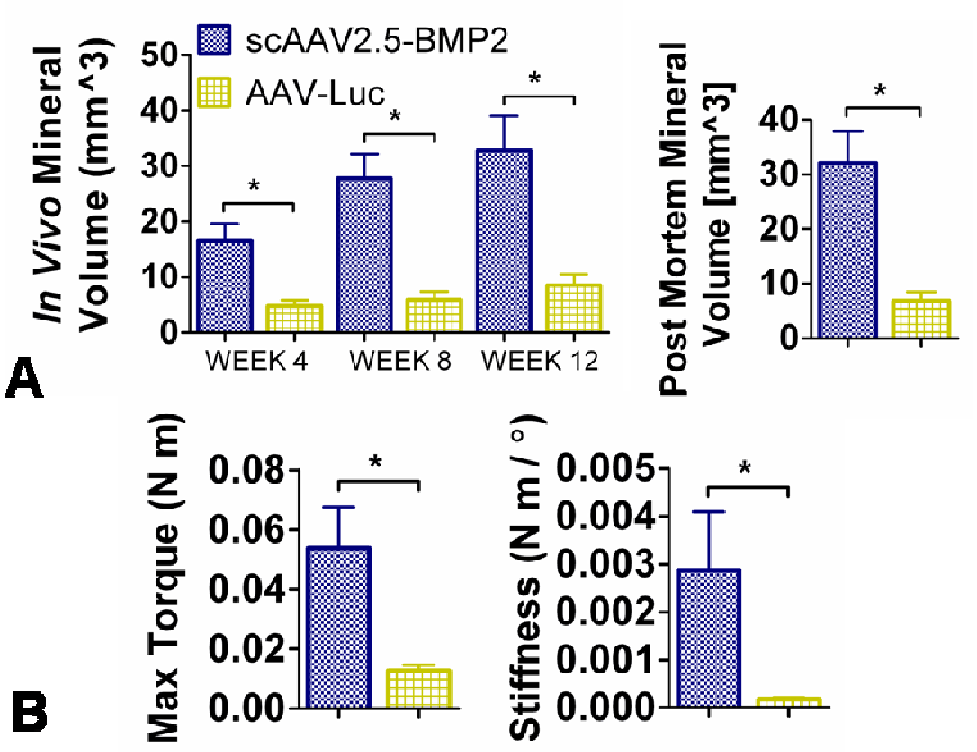

FIGURE 5.8: Quantitative comparison of structure and function results from *in vivo* delivery of scAAV2.5-BMP2 treatments or AAV-Luc treatments. A) *In vivo* and post mortem mineral formation within defect sites. B) Biomechanical properties of femurs tested to failure in torsion. * $p < 0.05$.

Defects treated with scAAV2.5-BMP2 scaffolds were divided into bridged and unbridged groups and biomechanical properties were compared with age-matched whole nude rat femurs as a measure of functional restoration of native bone properties (Figure 5.9). Maximum torque values in bridged scAAV2.5-BMP2 treated defects were 41% of the values in whole nude femurs (0.126 N-m versus 0.307 N-m). Torsional stiffness values in bridged scAAV2.5-BMP2 treated defects were 44% of the values in whole nude femurs (0.010 N-m/° versus 0.023 N-m/°) and were not significantly different from whole nude femurs.

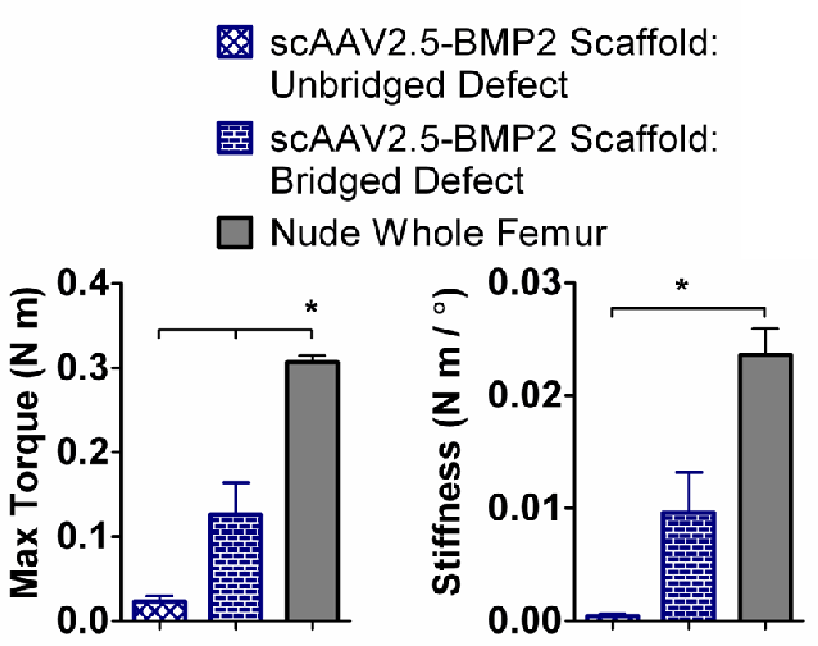

FIGURE 5.9: Quantitative comparison of biomechanical properties of age-matched nude rat whole femurs with unbridged and bridged segmental defect femurs treated by implantation of scAAV2.5-BMP2 coated PCL scaffolds. * $p < 0.05$.

Comparison of grouped hMSC-seeded scaffold therapies with grouped acellular scaffold therapies showed significantly higher week 12 *in vivo* mineral formation (Figure 5.10A) and torsional stiffness (Figure 5.10B) in the acellular therapy group compared to the hMSC therapy group.

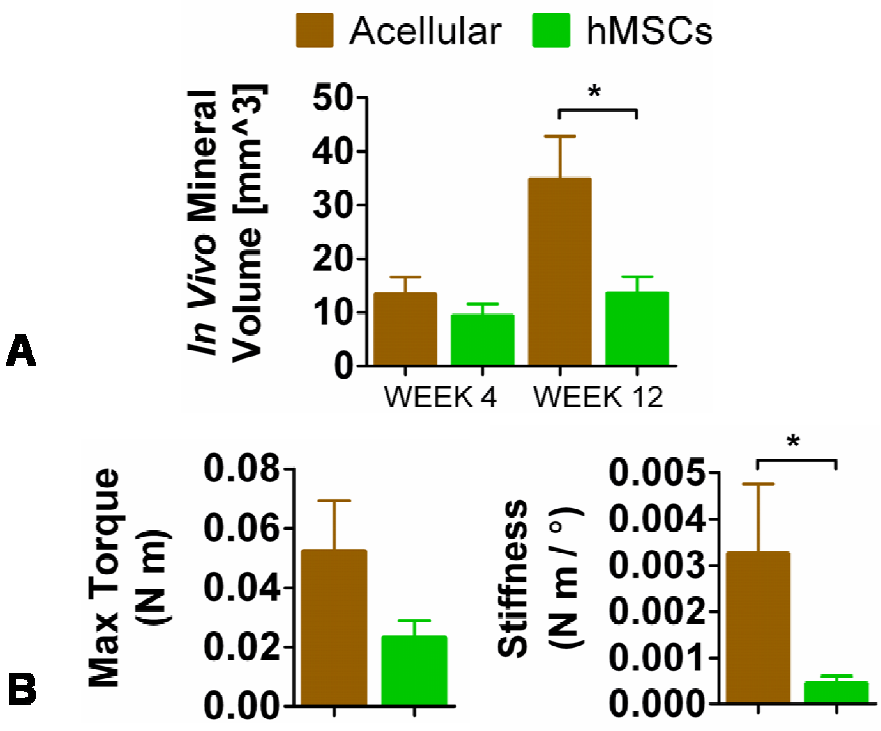

FIGURE 5.10: Quantitative comparison of structure and function results from *in vivo* delivery of hMSC-seeded scaffolds or acellular scaffolds. A) *In vivo* mineral formation within defect sites. B) Biomechanical properties of femurs tested to failure in torsion. * $p < 0.05$.

Assessment Of 2D *In Vitro* AAV-LacZ Transduction Efficiency: The presence of blue β-galactosidase-expressing cells in all wells at both days three and six post-transduction (Figure 5.11A,B) signified successful transduction of hMSCs by AAV-LacZ. Transduction efficiency was determined as the ratio of blue cells over total cells, which were counted in fluorescence microscopy images after DAPI nuclear stain using the software program ImageJ (Figure 5.11C).

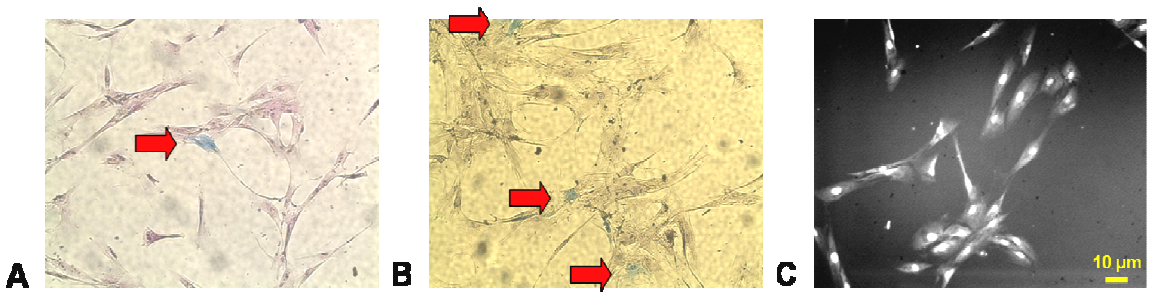

FIGURE 5.11: 2D *in vitro* transduction of hMSCs by AAV-LacZ. A),B) hMSC β-galactosidase expression marked by blue cells three or six days, respectively, after viral transduction. Red arrows point to transduced cells. C) DAPI-stained cell nuclei used to estimate total cell number. 20X Magnification.

Transduction efficiency increased with viral dose and with lowering the media volume containing the viral particles, likely do to better colocalization of the viral particles with the hMSCs (Figure 5.12). Transduction efficiency also increased from day 3 to day 6, likely due to a peak or jump in AAV transgene expression, as seen in the BMP2 expression of scAAV2.5-BMP2 transduced hMSCs after 6-7 days in both 2D and 3D *in vitro* experiments. The only significant differences in transduction efficiency were observed between the low transduction media volume / 2X AAV dose group at day 6 and the high transduction media volume / 1X AAV dose group at both days 3 and 6, likely due to the very small samples sizes. The average initial number of cells calculated in wells 24 hours after seeding was 24,321 per well, giving initial transduction multiplicity of infections of approximately $2*10^4$ and $4*10^4$.

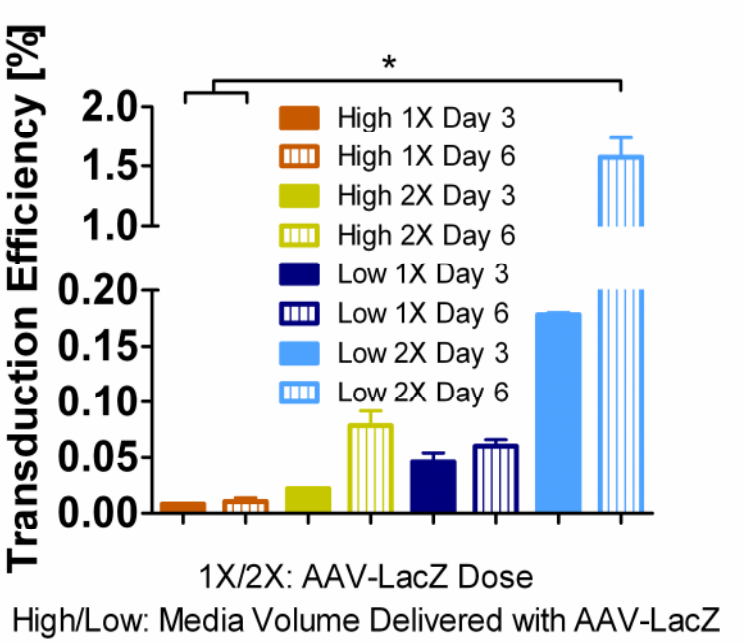

FIGURE 5.12: Effects of viral dose and transduction media volume on AAV-LacZ transduction efficiency.

Chapter 5: Discussion

This study presents evidence that synthetic polymer scaffolds can be functionalized for orthotopic bone repair applications through lyophilization of scAAV encoding the gene for human BMP2. The *in vitro* BMP2 release kinetics showed that transduced marrow-derived stem cells exhibited peak BMP2 release after one week in both 2D and 3D culture, while amniotic-fluid derived cells exhibited a delay of nearly two months before achieving significant BMP2 expression in 3D culture. The hMSC peak release profile is advantageous for bone healing because it approximately coincides with the end of the inflammatory phase of long bone injury response and the initiation of the reparative phase of healing (Yazici, Yanoso et al. 2008). In comparison, bolus delivery of recombinant proteins displays fast release kinetics that would likely occur during the initial inflammatory response phase of bone healing when there are many confounding signals present. Furthermore, the extended BMP2 expression continued through at least five weeks for both stem cell types, which could lead to further mineral formation with time. The BMP2 expressed by transduced hMSCs led to increases in both 2D and 3D osteogenic outcomes, as assessed by increased ALP levels per DNA and increased mineral volumes per scaffold, respectively. The increased osteogenic differentiation also likely resulted in reduced cell numbers as determined by DNA analysis, as fewer stem cells would be available to proliferate and renew the stem cell population. No increases in mineral volumes were found in scAAV2.5-BMP2-transduced hAFS Cell constructs after twelve weeks. The fetus-derived hAFS Cells may be more developmentally primitive than the adult-derived hMSCs, and transduction efficiency differences between the two cell types, such as due to differences in AAV

receptor numbers or activities, may have been responsible for the osbserved differences in BMP2 secretion kinetics between the two sources.

In vivo results revealed that AAV coating of PCL porous polymer scaffolds by lyophilization can serve as a successful vehicle for delivering genes to large bone defects. The preliminary study showed that direct AAV-LacZ scaffold delivery led to *in vivo* transduction of host cells surrounding the defect site within two weeks of implantation. For the second segmental defect study comparing *in vivo* and *in vitro* gene therapy transduction methods, PCL scaffolds rather than PLDL scaffolds were used because various studies in our lab have found that the larger pore sizes of PCL scaffolds accommodate *in vitro* seeding and *in vivo* infiltration of cells better than PLDL scaffolds, which have smaller pore sizes (Oest, Dupont et al. 2007). This study showed that direct delivery of scAAV2.5-BMP2 coated scaffolds to the defect site (*in vivo* gene therapy) led to more defect bridging than delivery of scAAV2.5-BMP2 coated scaffolds pre-seeded with hMSCs before implantation (*in vitro* gene therapy). This may be due to a variety of factors such as the amount of time that cells are directly exposed to the scAAV2.5-BMP2 vector, variability in scAAV2.5-BMP2 transduction and BMP2 expression in different cell types, possible loss of BMP2 expressed by hMSCs in culture prior to implantation, or loss of AAV particles from scaffolds into the surrounding media in culture prior to implantation. Segmental defects treated by *in vivo* delivery of scAAV2.5-BMP2- coated scaffolds displayed significantly higher *in vivo* week 8, *in vivo* week 12, and post mortem mineral volumes as well as maximum torque and torsional stiffness compared to defects treated with AAV-Luc-coated scaffolds pre-seeded with hMSCs. Defects treated with scAAV2.5-BMP2-coated scaffolds also displayed significantly higher *in vivo* week 8 and

post mortem mineral volumes compared to defects treated with AAV-Luc-coated scaffolds, although there were not significant differences in *in vivo* week 12 mineral volumes or biomechanical properties, likely due in part to the smaller sample size of the group (n = 6) compared to AAV-Luc-coated scaffold pre-seeded with hMSCs (n = 8).

When *in vivo* and *in vitro* gene therapy methods were combined, defect treatment by scAAV2.5-BMP2 led to significantly higher *in vivo* and post mortem mineral formation at all time points as well as enhanced biomechanical properties compared to defects treated by AAV-Luc. Because the maximum torque and torsional stiffness values of a structure depend heavily on material continuity throughout the specimen gauge length, defects treated with scAAV2.5-BMP2 scaffolds were divided into bridged and unbridged groups. When isolated, the bridged defects displayed torsional stiffness values that were not significantly different from whole femurs, suggesting partial restoration of femoral biomechanical function.

The results of the *in vivo* study refuted our initial hypothesis that treating defects with scaffolds providing stem cells and osteogenic signals would enhance bone repair over treating defects with scaffolds providing only osteogenic signals. As a whole, defects treated with stem cells displayed significantly lower *in vivo* mineral formation at the study endpoint as well as significantly lower torsional stiffness than defects treated with acellular scaffolds, suggesting that *in vivo* gene therapy was superior to *in vitro* gene therapy. The lack of stem cell-mediated repair may be due to a variety of factors including limited AAV transduction and / or resulting BMP2 production in hMSCs compared to host defect cells and the possible presence of a sufficiently large enough host stem cell supply to limit the contribution of the added hMSCs to the bone repair

process. Furthermore, stem cells transduced with AAV prior to implantation may have experienced an increased immune response upon delivery as active natural killer cells may have responded to the virus. Tranduction of host cells by AAV delivered on scaffolds may have occurred at a later time point when the initial inflammation stage of bone repair was subsiding and a more hospitable immune environment was present. Another unexpected result was the extremely limited repair response in defects treated with AAV-Luc scaffolds pre-seeded with three million hMSCs. While the constructs did not include the osteogenic cues that the scAAV2.5-BMP2 coated scaffolds provided, they still theoretically delivered three million viable hMSCs to the defect sites, which previously led to bridging in 4 / 9 defects when delivered on PCL / GFOGER / Col I scaffolds. This suggests that the presence of the AAV-Luc may have actually detracted from the stem-cell mediated defect repair process, although the mechanism of action remains unclear.

Increasing viral particle dose contributed to increases in transduction efficiency as shown in Figure 5.12. Coating scaffolds with a higher number of viral particles would likely increase the number of cells transduced and lead to increased BMP2 production. Increased BMP2 expression could lead to more robust mineral formation, more bridged defects, and full restoration of femoral biomechanical function. In summary, the results presented are the first to suggest the potential for an off-the-shelf, donor bone graft-free therapy in which pre-sized thermostable porous polymer scaffolds lyophilized with scAAV2.5-BMP2 could be frozen at length until needed for clinical implantation in large bone defect sites.

Chapter 6

SUMMARY AND FUTURE DIRECTIONS

Overall Summary

Bone tissue engineering therapies present an attractive treatment alternative to the current clinical standards of treatment with bone grafts. These therapies generally feature a combination of structural scaffold, biochemical cues, and / or osteogenic or osteoprogenitor cells. Therapies that include cell delivery may be especially attractive for treatment of large bone defects in patients such as the sick or elderly that have reduced supplies of endogenous cells to contribute to the bone repair process. Stem cells have great potential for cellular therapy, as they possess the abilities to proliferate into vast cell numbers needed for repair of large defects as well as differentiate into osteogenic or osteoprogenitor cells. These cells may directly participate in the bone healing response by forming new mineral themselves and they may also secrete biochemical cues to recruit endogenous cells to participate in forming new bone. The optimal stem cell source for bone tissue engineering therapies has not been established, and few studies to date have quantitatively compared stem cell sources in the same reproducible model of large bone defects.

The goal of this thesis was to establish a large bone defect model suitable for evaluation of human stem cell-based tissue engineering therapies and to then quantitatively analyze the abilities of human adult-derived and fetal-derived stem cells to heal defects, both in the absence and presence of osteogenic cues. Human stem cell-based therapies were evaluated in three ways. First, we validated the abilities of fetal amniotic fluid stem cells and adult mesenchymal stem cells to form mineralized tissue *in*

vitro on 3D porous polymer scaffolds and then quantitatively compared segmental defect healing after treatment with hMSC-seeded, hAFS Cell-seeded, or acellular scaffolds (Specific Aim I - Chapter 3). This aim directly addressed the need for direct comparison of various stem cell sources within the same reproducible model of large bone defect repair. This challenging bone defect model could serve as a test bed for future evaluation of stem cell-based bone defect repair therapies. Second, we labeled human stem cells with an *in vivo* tracking agent, the fluorescent quantum dot, in an effort to track stem cell biodistribution and viability during the bone repair process. Our results suggest that while post mortem immunohistochemical techniques could be used to identify delivered cells remaining at the defect site, quantum dots are ineffective as an *in vivo* cell tracking agent for tissue engineering therapies due to false positive signals as well as detrimental effects on cell-mediated bone healing (Specific Aim II - Chapter 4). This aim refuted the claimed abilities of a reportedly effective stem cell tracking agent and suggested the continued need for a better method for determining stem cell distribution after delivery *in vivo*. Third, we evaluated a novel gene therapy approach for delivering osteogenic cues to defects by coating scaffolds with a viral vector encoding the gene for the osteogenic protein BMP2. We did this by first confirming AAV *in vitro* stem cell transduction and resulting increases in osteogenic differentiation, and then utilizing the scAAV2.5-BMP2-coated scaffolds in both *in vivo* (direct scaffold delivery to defect sites) and *in vitro* (pre-seeding of stem cells on scaffolds prior to implantation) gene therapy approaches for segmental defect repair (Specific Aim III - Chapter 5). This aim presented evidence of a novel delivery system of BMP2 for the repair of large bone defects, which with further

refinement and optimization could present a superior therapy compared to current clinical treatments delivering recombinant BMP2 on collagen carriers.

Aim I: Comparison of Adult and Fetal Stem Cell-Based Bone Tissue Engineering Constructs For the Repair of Large Segmental Bone Defects

In this Aim, we first established a challenging and reproducible model of large bone defects in immunocompromised rats for quantitatively comparing human stem-cell based tissue engineering therapies. Next we evaluated the abilities of stem cells from two sources, both adult marrow-derived stem cells and fetal amniotic fluid-derived stem cells, to form mineral when seeded on 3D porous polymer scaffolds in *in vitro* culture conditions. Finally, we analyzed the *in vivo* segmental defect healing response after treatment with either acellular or stem-cell seeded scaffolds and found that addition of stem cells significantly improves defect repair.

Stem Cell Number:

While defects treated with stem cells experienced improved healing over defects treated with acellular scaffolds alone, bony bridging of defects was limited, especially in defects treated with hAFS Cells. While a cellular dose of three million cells was chosen for the *in vivo* study, improved therapeutic effects might be achieved by delivering a higher number of stem cells. In a skeletal muscle injury model in female Sprague Dawley rats, delivery of 10 million autologous MSCs led to higher restoration of muscle contraction forces than delivery of 2.5 million, 1 million, or 0.1 million MSCs (Winkler, von Roth et al. 2009). However, there is likely a threshold stem cell number beyond which adding stem cells would show no benefit, as there is only a finite amount of space within the pore network of scaffolds for cells and mass transport limitations may only allow for a certain level of nutrients to be delivered to cells, beyond which cell death may occur.

Co- / Pre-Seeding of Hematopoietic Stem Cells or Endothelial Cells:

Stem cell-mediated bone defect healing in this Aim could have been limited if cells were not able to obtain a sufficient enough oxygen or nutrient supply to remain viable. The continued viability of stem cells seeded in the cores of scaffolds may be especially dependent on the presence or rapid formation of a vascular network to deliver nutrients and prevent ischemia-related cell death. Seeding scaffolds with hematopoietic stem cells or endothelial cells prior to or in parallel with seeding hMSCs or hAFS Cells may result in a more vascularized construct that is more conducive to stem cell survival following *in vivo* implantation. In one recent report co-seeding of MSCs and hematopoietic stem cells on calcium phosphate scaffolds prior to subcutaneous implantation resulted in increased construct vascularization compared to MSC-seeded scaffolds alone (Moioli, Clark et al. 2008), while another study reported that co-seeding MSCs and endothelial cells on β-TCP scaffolds prior to implantation in rabbit ulnar bone defects resulted in superior construct vascularization and mineralization compared to implantation of MSC-seeded scaffolds alone (Zhou, Lin et al. 2009).

Stem Cell Pre-Differentiation and / or Scaffold Pre-Mineralization:

Stem cells in this Aim were delivered to defects in an undifferentiated state with the expectation that there would be sufficient *in situ* stimuli to direct stem cells to differentiate down an osteogenic lineage or secrete osteoinductive factors. However, pre-differentiation of stem cells prior to implantation, such as by *in vitro* culture with osteogenic supplements, could increase early *in vivo* mineralization capacity. Additionally, extended *in vitro* culture with osteogenic stimuli could lead to mineral deposition throughout scaffolds prior to implantation, presenting mineral nucleation sites

throughout the construct. Effects of stem cell pre-mineralization were evaluated in a small proof of concept preliminary *in vivo* segmental defect study. Six million hAFS Cells were seeded on a PCL scaffold (6 mm diameter) previously coated with lyophilized type I collagen as previously described. This construct was cultured dynamically for six weeks in osteogenic media to differentiate hAFS Cells and induce mineral formation, and then the construct was scanned by Micro-CT along with a scaffold seeded with six million hAFS Cells two days beforehand. One day later both constructs were implanted into bilateral 8 mm segmental defects created in a 20 week old female nude rat. Twelve weeks later both 2D radiographs and Micro-CT scans revealed that the defect treated with the premineralized construct displayed reduced defect mineral formation compared to the defect treated with the non-predifferentiated / non-premineralized construct (Figure 6.1).

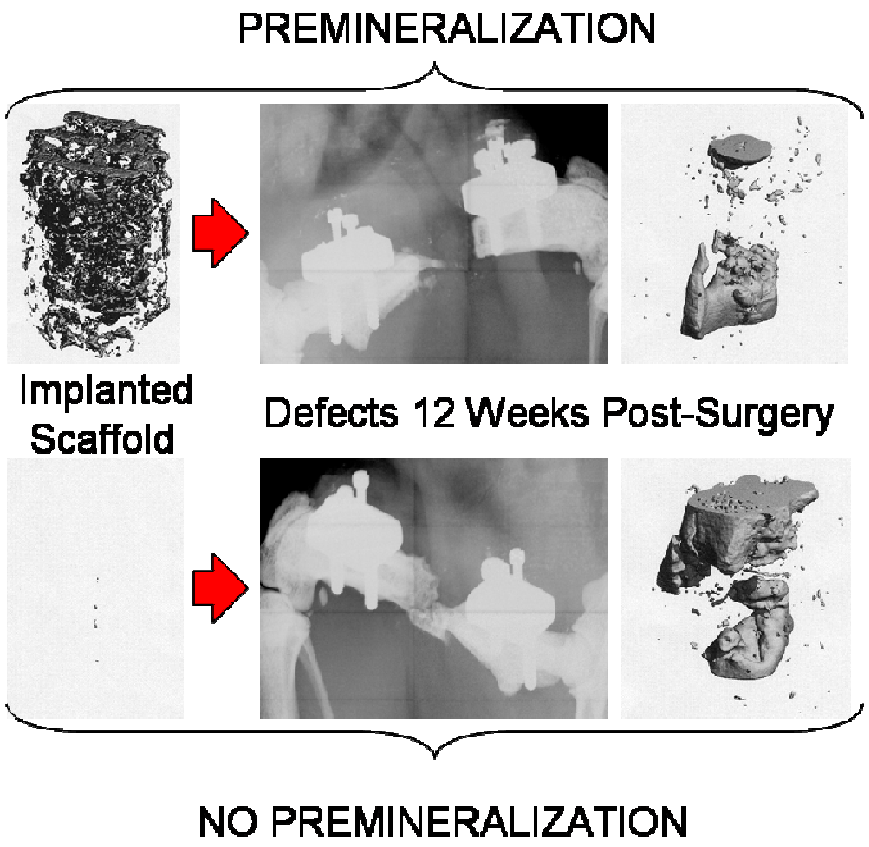

FIGURE 6.1: Effects of stem cell premineralization on segmental defect healing. Micro-CT scans of hAFS Cell-seeded PCL scaffolds one day pre-surgery (left) and resulting segmental defect repair 12 weeks after implantation (right).

Although no definite conclusions can be made with a sample size of only one, this preliminary experiment prompts two interesting speculations. First, the defect treated with the non-premineralized scaffold experienced bony bridging as assessed by evaluation of 2D radiographs at the twelve week time point. Again, delivery of six million hAFS Cells may lead to superior defect repair than delivery of three million hAFS Cells, which only led to bony bridging in 1/9 segmental defects (Specific Aim I / Figure 3.6). Second, the premineralized defect displayed poor defect healing, which may be due to a reduction in stem cells present at the time of implantation. As described in Specific Aim III, stem cell-seeded constructs that displayed the highest mineral volumes

were found to contain the lowest amounts of DNA, suggesting lower numbers of cells (Figure 5.4, Figure 5.5) compared to groups displaying less mineral. As stem cells seeded on the scaffolds differentiate into osteogenic cells or osteogenic precursors, the number of proliferating stem cells is likely reduced. The increased scaffold mineral volume at the time of implantation may be less important to defect healing than the initial number of stem cells present. Furthermore, cells contained within pre-mineralized tissue may be more isolated from biochemical cues at the defect site, and mineral may form a barrier between cells and the ingrowing vascular supply, impeding mass transport and affecting cell viability within the scaffold. The results of this pilot study are in agreement with a previous report that culture of MSCs in osteogenic media for 16 days prior to implantation into a critically-sized rat cranial defect (pre-mineralization) decreased the healing response compared to treatment with undifferentiated MSCs. However, short-term culture in osteogenic media for 4 days prior to implantation (pre-differentiation) led to an improved healing reponse compared to undifferentiated MSCs (Castano-Izquierdo, Alvarez-Barreto et al. 2007). In another *in vitro* study, pre-mineralization of titanium scaffolds prior to seeding hMSCs led to increases in osteogenic differentiation compared to hMSCs seeded on plain titanium scaffolds, as assessed by calcium content (Pham, Kasper et al. 2008).

Stem Cell Delivery Vehicle:

The experiments performed in this study showed that PCL scaffolds coated with GFOGER and lyophilized type I collagen could serve as an efficient structural network for stem cell attachment followed by mineral formation. While PCL degrades *in vivo* through hydrolysis, histological evaluation of femoral defect sections performed 12

weeks post-surgery clearly showed the presence of PCL scaffold remaining at the defect site (Figure 4.7A). While scaffolds serve as an initial structural framework on which new mineral can form, they could also impede further bone formation by occupying space within the defect. Some reports have estimated the time for complete resorption of PCL scaffolds to be approximately 24 months and possibly longer depending on specific geometries and *in vivo* environments (Meyer and Wiesmann 2006). Use of a porous polymer scaffold with faster degradation kinetics could ensure that new bone formation is not impeded by remaining scaffold material, as could cellular delivery in a fibrin or alginate gel or delivery of cells seeded on a 2D cylindrical mesh tube.

Stem Cell Delivery Timing:

As mentioned previously, the initial phase of the healing response to long bone injuries is an inflammatory phase during which there are a variety of confounding signals present that may be detrimental to differentiation of delivered stem cells (Yazici, Yanoso et al. 2008). If stem cell delivery were delayed until the initiation of the reparative phase of bone healing which begins approximately one week after initial injury, then the cells might be implanted into a more hospitable environment which could facilitate differentiation and enhance bone repair (Meijer, de Bruijn et al. 2007). A similar delayed ESC-derived cardiomyocyte delivery has been advocated for repair of heart tissue after infarction (Laflamme and Murry 2005). Delayed delivery could be accomplished by first creating empty defects, closing the wound sites, and then reopening them a week or two later to deliver stem cell-seeded scaffolds. A biocompatible cylindrical plug or spacer could be inserted into the defect space to preserve an open volume for later scaffold insertion.

Immunosuppression:

As mentioned in Chapter 3, nude rats lack T cells but still possess other lymphocytes such as natural killer cells and B cells. While there were no gross signs of an immune response caused by implantation of xenogeneic hMSCs or hAFS Cells, it is still possible that they elicited some form of immune response detrimental to stem cell survival and osteogenic differentiation. In a recent study hAFS Cells were rejected after application in rat myocardium in both immunocompetent and in immunocompromised rats (Chiavegato, Bollini et al. 2007). Therefore the addition of an immunosuppressant such as anti-asialo GM1 antibody, which specifically blocks natural killer cell activity (Kasai, Yoneda et al. 1981), could possibly enhance human stem cell viability and cell-mediated bone defect repair.

Mechanical Loading:

Defects in this study were predominantly shielded from mechanical loads by stiff polysulfone bridging plates. Because increased strains from mechanical loading can enhance cell-mediated bone modeling, use of a bridging plate with some level of compliance could stimulate delivered cells to increase defect repair. We have recently modified our bridging plate design to allow for controlled *in vivo* axial loading of defect sites, however the design has currently only been used in combination with acellular treatments (Boerckel, Dupont et al. 2009).

Aim II: Tracking Delivered Human Stem Cells During The Segmental Defect Healing Process

In this Aim, we sought to label stem cells with an *in vivo* tracking agent in order to track their biodistribution and viability during the segmental defect repair process. We chose quantum dots as our *in vivo* tracking agent based upon favorable reports in the literature and successful short-term *in vitro* experiments suggesting a strong potential for *in vivo* fluorescence imaging detection as well as a lack of observed detrimental effects on cell viability and function. However, application in segmental defect studies revealed the quantum dot as a poor choice for long term *in vivo* cell tracking during large bone defect repair due to false positive signals caused by QD transfer to host cells as well as a detrimental effect on the bone healing process. A small population of delivered human cells was identified at the defect site through post mortem histological immunostaining performed four weeks after cell delivery.

In Vivo Cell Tracking Agent:

As mentioned above, quantum dots failed to satisfactorily track labeled stem cells throughout the defect repair process, suggesting the need for an alternative *in vivo* cell tracking agent. One possible option that has been described is the genetic modification of MSCs with the genes for both luciferase (Luc) and green fluorescent protein (GFP) expression (Blum, Temenoff et al. 2004), (Day, Kawecki et al. 1998), (Hara, Murakami et al. 2008). This dual-labeling option is advantageous because after stem cells are introduced to a gene delivery vector, the population of stem cells that has been successfully labeled with the transgene for GFP could be isolated by fluorescence activated cell sorting (FACS). Next this GFP positive cell population could be used for

in vivo implantation and tracking with the knowledge that delivered cells should also express luciferase, increasing the chances of *in vivo* bioluminescence detection. Furthermore, if the labeled cells died they would cease to express a bioluminescent signal, meaning that a continued bioluminescent signal would indicate presence of viable stem cells without the chance of the false positive signals that discouraged the continued use of quantum dots. Additionally, retrovirally dual-labeled Luc / GFP MSCs have been shown to retain the capacity to osteogenically differentiate and increase *in vivo* bone formation (Olivo, Alblas et al. 2008). This cell tracking option would possess many desirable traits for an *in vivo* cell tracking agent, however, the safety and biocompatibility of such as system would need to be evaluated prior to and during long term *in vivo* use due to the genetic modification of cells and the requirement for injection of luciferin prior to bioluminescence imaging.

Aim III: Adeno-Associated Viral Vector Transduction of Human Stem Cells with Osteogenic Cues To Enhance Bone Formation

In this Aim, we first evaluated the ability of porous polymer scaffolds bioactivited through adeno-associated virus lyophilization to transduce cells at segmental defect sites. Next we confirmed that AAV encoding the osteogenic gene BMP2 could successfully transduce human stem cells *in vitro* eliciting their osteogenic differentiation. Finally we compared segmental defect repair after treatment with AAV-BMP2 coated scaffolds or AAV-BMP2 coated scaffolds pre-seeded with hMSCs. Only the *in vivo* gene therapy approach of direct AAV-BMP2 scaffold delivery led to significantly better defect repair than treatment with control scaffolds.

Viral Particle Dose:

Seeding one million hMSCs on PCL scaffolds coated with 10^{10} scAAV2.5-BMP2 viral particles led to stem cell transduction as measured by secreted BMP2 levels (Figure 5.3) and resulted in increased *in vitro* mineral formation within scaffolds (Figure 5.4). However, seeding three million hMSCs on similar scaffolds failed to significantly increase *in vivo* mineral formation in segmental defects. The lack *in vivo* mineral formation may be due to a multiplicity of infection that was only one third of that used in the *in vitro* study ($0.333 * 10^4$ versus 10^4). As described in Chapter 5, using a higher viral particle dose resulting in a higher MOI contributes to increased transduction efficiency in hMSCs (Figure 5.13). Assuming that scaffolds would not experience a loss in viral particles as coating density increased, then tripling the number of scAAV2.5-BMP2 particles coated onto scaffolds for *in vivo* implantation would produce an equal

MOI to that used in 3D *in vitro* experiments and possibly lead to further *in vivo* mineral production from transduced hMSCs. A viral particle dose response segmental defect experiment where scaffolds were coated with different quantities of AAV prior to seeding hMSCs and implanting into defect sites would help to establish the relationship between AAV MOI and *in vivo* healing capacity. Additionally, a study should be performed to evaluate viral particle retention efficiency with varying scaffold coating densities to reduce the likelihood of loss of viral particles from scaffolds prior to stem cell transduction.

Co-Delivery of Multiple Viral Vectors:

While the BMPs have proven to be some of the most potent osteoinductive proteins, a variety of other proteins play key roles during the bone repair process and their delivery could enhance the defect repair process. BMP2 and TGF-β co-delivery were previously shown to synergistically enhance *in vivo* ectopic mineralized matrix formation in a murine model compared to treatment with either growth factor alone (Simmons, Alsberg et al. 2004). Coating scaffolds with the genes encoding both proteins could lead to a similar enhancement of segmental defect repair.

One particular concern in treating large bone defects with high quantities of stem cells seeded throughout scaffolds is the possible loss of viability. After implantation a key element in maintaining stem cell viability is the development of a vascular network throughout the scaffold to provide cells with oxygen and nutrients crucial to their survival (Meijer, de Bruijn et al. 2007). Rapid formation of a vascular network may be especially important for translational therapies where bone tissue engineering constructs would have to be scaled up for treatment of larger human bones, as stem cells at the center of

constructs could initially be millimeters or even centimeters away from a vascular supply. Delivery of oxygen and nutrients to cells by diffusion alone would be insufficient, creating a rapid loss in viability of delivered cells. To facilitate vascular network development, delivered stem cells could be transduced by AAV encoding not only osteogenic BMP2 but also an angiogenic protein such as vascular endothelial growth factor (VEGF). A similar approach was previously reported in which rat subcutaneous implantation of PLG scaffolds co-delivering the recombinant proteins VEGF and PDGF led to significantly higher scaffold vascular invasion than scaffolds delivering either protein alone (Richardson, Peters et al. 2001).

***In Vivo* Segmental Defect Study Duration:**

The *in vivo* segmental defect studies described in this study did not exceed twelve weeks in duration. Our previous segmental defect studies in Sasco Sprague Dawley rats (Oest, Dupont et al. 2007), (Rai, Oest et al. 2007) have shown that the majority of *in vivo* mineral formation occurs within the first eight weeks of the study, and changes between eight and twelve weeks are minimal. This trend was observed in the segmental defect study described in Chapter 1 delivering adult or fetal stem cells seeded on porous polymer scaffolds (27.86 mm^3 week 8 versus 29.66 mm^3 week 12, hMSCS / 19.06 mm^3 week 8 versus 21.76 mm^3 week 12, hAFS Cells) (Figure 3.7A). When treating defects with scAAV2.5-BMP2 coated scaffolds, with or without pre-seeded hMSCs, there is the possibility that extending the study duration to sixteen or twenty weeks would lead to increases in *in vivo* bone volume. AAV-delivered genes may be expressed by transduced cells throughout their entire lifetimes. Extending study duration may be especially important if defects were treated with scAAV2.5-BMP2 transduced hAFS Cells due to

their observed BMP2 release kinetics (Figure 5.3), which displayed significantly higher BMP2 levels than AAV-Luc transduced cells throughout nearly the entire 12-week study, and especially high levels during a peak lasting between weeks seven and ten post-transduction. This extended-duration osteoinductive protein release could lead to increases in *in vivo* mineral formation for weeks after that, suggesting the need for a longer study length.

MSC Implantation Into Immunocompetent Sasco Sprague Dawley Rats:

As described in Chapter 3, 13-week old female nude rats used in these studies are generally smaller than age-matched female Sasco Sprague Dawley rats (Figure 3.3) that we have used previously in acellular segmental defect therapies. In addition to differences in size, there could also be differences in the ways that the two rat strains respond to biochemical factors (Kacew, Ruben et al. 1995). As described previously, both MSCs and AAV may be non-immunogenic, so they could theoretically still be used to effectively treat defects in immunocompetent SSD rats. However, allogeneic rat MSCs may need to be used rather than xenogeneic human MSCs to avoid cell rejection. Successful treatment of defects in SSD rats with allogeneic MSC / AAV treatments would support use of allogeneic human MSCs and AAV to treat bone defects in humans, possibly without the need for immunosuppression.

Conclusions

Challenging large bone defects and nonunions pose a clinical problem that currently lacks an adequate therapeutic solution. Bone tissue engineers aim to provide that solution, and tissue engineering therapies that include a cellular component are likely necessary for effective treatment of severe defects in patients lacking sufficient endogenous cell populations. While autologous stem cell therapies can enhance the large bone defect healing response, allogeneic stem cell delivery may be necessary for treating those patients with limited autologous supplies or in cases where there is not sufficient time to harvest, expand, and reimplant autologous cells. However, there have currently been few preclinical studies that quantitatively compared therapies using different stem cell sources in the same large bone defect model. Maximizing therapeutic effects by selecting a preferred stem cell source and delivery method in preclinical studies will facilitate translation of stem cell therapies to clinical applications.

The central theme of the work in this thesis consisted of developing a novel challenging model of large bone defects for quantitative comparison of human stem cell-based therapies, and then evaluating the abilities of both adult and fetal stem cell-seeded constructs to enhance defect repair, both with and without added osteogenic stimuli. Our hypothesis that treatment of large bone defects with stem cell-seeded constructs would increase bone repair over treatment with acellular constructs in the absence of added osteogenic stimuli was validated; however, no clear advantage was discerned between defect treatment with adult marrow-derived stem cell versus fetal amniotic fluid-derived stem cell constructs. The lack of individual differences in defect healing between adult hMSC-seeded scaffold treatment, fetal hAFS Cell-seeded scaffold treatment, and

acellular scaffold treatment is possibly due to endogenous host cell contributions to repair, to the high variability in repair outcomes within treatment groups, and to a small therapeutic effect size of the stem cell treatments compared to that of osteogenic protein delivery, which we have observed previously in a similar immunocompetent rat segmental defect model.

Our attempts to non-invasively track delivered stem cells *in vivo* throughout the defect repair process were unsuccessful due to the limitations of our cell tracking agent, thus preventing us from verifying our hypothesis that a portion of delivered cells would remain viable at the defect site throughout the study to contribute to bone repair. Although post mortem analysis with immunohistochemistry indicated that some human stem cells remained at the defect site four weeks after implantation, the vast majority of cells were no longer there, suggesting the need for a better delivery system. However, our studies generated the valuable finding that the fluorescent quantum dot, previously reported to potentially be an excellent *in vivo* cell tracking agent, should not be used for long term cell tracking during bone repair due to its internalization into host cells, thus creating a false positive signal, and its possible detrimental effects on bone repair. This work suggests that continued emphasis on improved cell delivery and tracking methods are required if long term viability and engraftment of delivered cells is to be achieved.

Our hypothesis that delivery of osteogenic cues to defect sites would enhance defect healing was confirmed, as scAAV2.5-BMP2 treatment groups displayed significantly more defect mineral formation and mechanical properties than AAV-Luc treatment groups. Our hypothesis that bone repair would be enhanced by the combined treatment of stem cells and osteogenic cues was denied, with implantation of acellular

scAAV2.5-BMP2 coated scaffolds resulting in increased defect bridging compared to implantation of scAAV2.5-BMP2 coated scaffolds pre-seeded with hMSCs. This finding does not rule out the possibility that scAAV2.5-BMP2 scaffold / hMSC treatments could be effective at treating large bone defects, as increases in viral particle number or stem cell delivery into elderly or sick patients lacking endogenous cell supplies may elicit improved cell-mediated responses. However, this finding does present the first evidence of a novel acellular orthotopic bone tissue engineering therapy with the potential for off-the-shelf clinical application in treating large bone defects or nonunions, as biodegradable porous polymer scaffolds of varying sizes could be coated by thermostable scAAV2.5-BMP2 lyophilization and then frozen until needed.

BIBLIOGRAPHY

Akerman, M. E., W. C. W. Chan, et al. (2002). "Nanocrystal targeting in vivo." Proc Natl Acad Sci U S A **99**: 12617-21.

Alivisatos, A. P. (1996). "Semiconductor clusters, nanocrystals, and quantum dots." Science **271**: 933-937.

Allori, A. C., A. M. Sailon, et al. (2008). "Biological basis of bone formation, remodeling, and repair-part I: biochemical signaling molecules." Tissue Eng Part B Rev **14**(3): 259-73.

Arinzeh, T. L., S. J. Peter, et al. (2003). "Allogeneic mesenchymal stem cells regenerate bone in a critical-sized canine segmental defect." J Bone Joint Surg Am **85-A**(10): 1927-35.

Arnander, C., A. Westermark, et al. (2006). "Three-dimensional technology and bone morphogenetic protein in frontal bone reconstruction." J Craniofac Surg **17**(2): 275-9.

Awad, H. A., X. Zhang, et al. (2007). "Recent advances in gene delivery for structural bone allografts." Tissue Eng **13**(8): 1973-85.

Baksh, D., L. Song, et al. (2004). "Adult mesenchymal stem cells: characterization, differentiation, and application in cell and gene therapy." J Cell Mol Med **8**(3): 301-16.

Ballou, B., B. C. Lagerholm, et al. (2004). "Noninvasive imaging of quantum dots in mice." Bioconjug Chem **15**(1): 79-86.

Baltzer, A. W. and J. R. Lieberman (2004). "Regional gene therapy to enhance bone repair." Gene Ther **11**(4): 344-50.

Baron, R. (1993). Anatomy and ultrastructure of bone. Primer on the metabolic bone diseases and disorders of mineral metabolism. M. Favus. New York, Raven Press**:** 3-9.

Bartholomew, A., C. Sturgeon, et al. (2002). "Mesenchymal stem cells suppress lymphocyte proliferation in vitro and prolong skin graft survival in vivo." Exp Hematol **30**(1): 42-8.

Bensaid, W., J. T. Triffitt, et al. (2003). "A biodegradable fibrin scaffold for mesenchymal stem cell transplantation." Biomaterials **24**(14): 2497-502.

Berrey, B. H., Jr., C. F. Lord, et al. (1990). "Fractures of allografts. Frequency, treatment, and end-results." J Bone Joint Surg Am **72**(6): 825-33.

Betz, O. B., V. M. Betz, et al. (2006). "Direct percutaneous gene delivery to enhance healing of segmental bone defects." J Bone Joint Surg Am **88**(2): 355-65.

Blum, J. S., J. S. Temenoff, et al. (2004). "Development and characterization of enhanced green fluorescent protein and luciferase expressing cell line for non-destructive evaluation of tissue engineering constructs." Biomaterials **25**(27): 5809-19.

Boerckel, J. D., K. M. Dupont, et al. (2009). "In vivo model for evaluating the effects of mechanical stimulation on tissue-engineered bone repair." J Biomech Eng **131**(8): 084502.

Boyle, W. J., W. S. Simonet, et al. (2003). "Osteoclast differentiation and activation." Nature **423**(6937): 337-42.

Bruder, S. P. (1999). "Tissue engineering of bone. Cell based strategies. ." Clin Orthop Relat Res **367S**: S68-83.

Bruder, S. P., K. H. Kraus, et al. (1998). "The effect of implants loaded with autologous mesenchymal stem cells on the healing of canine segmental bone defects." J Bone Joint Surg Am **80**(7): 985-96.

Bruder, S. P., A. A. Kurth, et al. (1998). "Bone regeneration by implantation of purified, culture-expanded human mesenchymal stem cells." J Orthop Res **16**(2): 155-62.

Bucholz, R. W. (2002). "Nonallograft osteoconductive bone graft substitutes." Clin Orthop Relat Res: 44-52.

Buckwalter, J. A., M. J. Glimcher, et al. (1996). "Bone biology. II: Formation, form, modeling, remodeling, and regulation of cell function." Instr Course Lect **45**: 387-99.

Buckwalter, J. A., M. J. Glimcher, et al. (1996). "Bone Biology." J Bone Joint Surg **77A**: 1256-89.

Buono, C., J. J. Anzinger, et al. (2009). "Fluorescent pegylated nanoparticles demonstrate fluid-phase pinocytosis by macrophages in mouse atherosclerotic lesions." J Clin Invest **119**(5): 1373-81.

Cahill, K. S., J. H. Chi, et al. (2009). "Prevalence, complications, and hospital charges associated with use of bone-morphogenetic proteins in spinal fusion procedures." Jama **302**(1): 58-66.

Caplan, A. I. (2004). "Mesenchymal Stem Cells." Handbook of Stem Cells **2**: 299-308.

Caplan, A. I., E. Zwilling, et al. (1968). "3-acetylpyridine: effects in vitro related to teratogenic activity in chicken embryos." Science **160**(831): 1009-10.

Carano, R. A. and E. H. Filvaroff (2003). "Angiogenesis and bone repair." Drug Discov Today **8**(21): 980-9.

Cartmell, S., K. Huynh, et al. (2004). "Quantitative microcomputed tomography analysis of mineralization within three-dimensional scaffolds in vitro." J Biomed Mater Res A **69**(1): 97-104.

Castano-Izquierdo, H., J. Alvarez-Barreto, et al. (2007). "Pre-culture period of mesenchymal stem cells in osteogenic media influences their in vivo bone forming potential." J Biomed Mater Res A **82**(1): 129-38.

Chamberlain, G., J. Fox, et al. (2007). "Concise review: mesenchymal stem cells: their phenotype, differentiation capacity, immunological features, and potential for homing." Stem Cells **25**(11): 2739-49.

Chen, D., M. Zhao, et al. (2004). "Bone morphogenetic proteins." Growth Factors **22**(4): 233-41.

Chen, Y., K. D. Luk, et al. (2003). "Gene therapy for new bone formation using adeno-associated viral bone morphogenetic protein-2 vectors." Gene Ther **10**(16): 1345-53.

Chiavegato, A., S. Bollini, et al. (2007). "Human amniotic fluid-derived stem cells are rejected after transplantation in the myocardium of normal, ischemic, immuno-suppressed or immuno-deficient rat." J Mol Cell Cardiol **42**(4): 746-59.

Coura Rdos, S. and N. B. Nardi (2007). "The state of the art of adeno-associated virus-based vectors in gene therapy." Virol J **4**: 99.

Currey, J. (1984). The mechanical properties of materials and the structure of bone. The mechanical adaptations of bone. Princeton, Princeton University Press**:** 3-37.

Dawson, J. I. and R. O. Oreffo (2008). "Bridging the regeneration gap: stem cells, biomaterials and clinical translation in bone tissue engineering." Arch Biochem Biophys **473**(2): 124-31.

Day, R. N., M. Kawecki, et al. (1998). "Dual-function reporter protein for analysis of gene expression in living cells." Biotechniques **25**(5): 848-50, 852-4, 856.

De Coppi, P., G. Bartsch, Jr., et al. (2007). "Isolation of amniotic stem cell lines with potential for therapy." Nat Biotechnol **25**(1): 100-6.

Dee, R. (1988). Bone Healing. Principles of Orthopaedic Practice. R. Dee, Mango, E., Hurst, E. New York, McGraw-Hill**:** 68-73

Delo, D. M., P. De Coppi, et al. (2006). "Amniotic fluid and placental stem cells." Methods Enzymol **419**: 426-38.

Derubeis, A. R. and R. Cancedda (2004). "Bone marrow stromal cells (BMSCs) in bone engineering: limitations and recent advances." Ann Biomed Eng **32**(1): 160-5.

Di Nicola, M., C. Carlo-Stella, et al. (2002). "Human bone marrow stromal cells suppress T-lymphocyte proliferation induced by cellular or nonspecific mitogenic stimuli." Blood **99**(10): 3838-43.

Einhorn, T. A. (2003). "Clinical applications of recombinant human BMPs: early experience and future development." J Bone Joint Surg Am **85-A Suppl 3**: 82-8.

Fang, J., Y. Y. Zhu, et al. (1996). "Stimulation of new bone formation by direct transfer of osteogenic plasmid genes." Proc Natl Acad Sci U S A **93**(12): 5753-8.

Fielding, A. K., M. Maurice, et al. (1998). "Inverse targeting of retroviral vectors: selective gene transfer in a mixed population of hematopoietic and nonhematopoietic cells." Blood **91**(5): 1802-9.

Fischer, H. C., L. Liu, et al. (2006). "Pharmacokinetics of Nanoscale Quantum Dots: In Vivo Distribution, Sequestration, and Clearance in the Rat." Advanced Functional Materials **16**: 1299-1305.

Franceschi, R. T., D. Wang, et al. (2000). "Gene therapy for bone formation: in vitro and in vivo osteogenic activity of an adenovirus expressing BMP7." J Cell Biochem **78**(3): 476-86.

Frangioni, J. V. and R. J. Hajjar (2004). "In vivo tracking fo stem cells for clinical trials in cardiovascular disease." Circulation **110**: 3378-3383.

Friedenstein, A. J. (1976). "Precursor cells of mechanocytes." Int Rev Cytol **47**: 327-59.

Friedlaender, G. E., C. R. Perry, et al. (2001). "Osteogenic protein-1 (bone morphogenetic protein-7) in the treatment of tibial nonunions." J Bone Joint Surg Am **83-A Suppl 1**(Pt 2): S151-8.

Frost, H. M. (1963). Bone Remodelling Dynamics. Springfield, IL, Charles C. Thomas.

Gamradt, S. C. and J. R. Lieberman (2004). "Genetic modification of stem cells to enhance bone repair." Ann Biomed Eng **32**(1): 136-47.

Geesink, R. G., N. H. Hoefnagels, et al. (1999). "Osteogenic activity of OP-1 bone morphogenetic protein (BMP-7) in a human fibular defect." J Bone Joint Surg Br **81**(4): 710-8.

Ginebra, M. P., T. Traykova, et al. (2006). "Calcium phosphate cements as bone drug delivery systems: a review." J Control Release **113**(2): 102-10.

Govender, S., C. Csimma, et al. (2002). "Recombinant human bone morphogenetic protein-2 for treatment of open tibial fractures: a prospective, controlled,

randomized study of four hundred and fifty patients." J Bone Joint Surg Am **84-A**(12): 2123-34.

Gray, H. (1918). Anatomy of the Human Body. Philadelphia, Lea & Febiger.

Guldberg, R. E., R. T. Ballock, et al. (2003). "Analyzing bone, blood vessels, and biomaterials with microcomputed tomography." IEEE Eng Med Biol Mag **22**(5): 77-83.

Guldberg, R. E., C. L. Duvall, et al. (2008). "3D imaging of tissue integration with porous biomaterials." Biomaterials **29**(28): 3757-61.

Guldberg, R. E., A. S. Lin, et al. (2004). "Microcomputed tomography imaging of skeletal development and growth." Birth Defects Res Part C Embryo Today **72**(3): 250-9.

Guldberg, R. E., M. Oest, et al. (2004). "Functional integration of tissue-engineered bone constructs." J Musculoskelet Neuronal Interact **4**(4): 399-400.

Hammett, F. S. (1925). "A Comparison of Bone Growth in Length with Bone Growth in Weight." J Gen Physiol **9**(1): 63-71.

Hara, M., T. Murakami, et al. (2008). "In vivo bioimaging using photogenic rats: fate of injected bone marrow-derived mesenchymal stromal cells." J Autoimmun **30**(3): 163-71.

Harada, S. and G. A. Rodan (2003). "Control of osteoblast function and regulation of bone mass." Nature **423**(6937): 349-55.

Hofstetter, C. P., E. J. Schwarz, et al. (2002). "Marrow stromal cells form guiding strands in the injured spinal cord and promote recovery." Proc Natl Acad Sci U S A **99**(4): 2199-204.

Holland, T. A. and A. G. Mikos (2006). "Biodegradable polymeric scaffolds. Improvements in bone tissue engineering through controlled drug delivery." Adv Biochem Eng Biotechnol **102**: 161-85.

Hollinger, J. O. and J. C. Kleinschmidt (1990). "The critical size defect as an experimental model to test bone repair materials." J Craniofac Surg **1**(1): 60-8.

Holt, S. J. and P. W. Sadler (1958). "Studies in enzyme cytochemistry. III. Relationships between solubility, molecular association and structure in indigoid dyes." Proc R Soc Lond B Biol Sci **148**(933): 495-505.

Hoshino, A., K. Hanaki, et al. (2004). "Applications of T-lymphoma labeled with fluorescent quantum dots to cell tracing markers in mouse body." Biochem Biophys Res Commun **314**(1): 46-53.

Hsieh, S. C., F. F. Wang, et al. (2006). "The inhibition of osteogenesis with human bone marrow mesenchymal stem cells by CdSe/ZnS quantum dot labels." Biomaterials **27**(8): 1656-64.

Hutmacher, D. W. (2000). "Scaffolds in tissue engineering bone and cartilage." Biomaterials **21**: 1169-1185.

Hyslop, L. A., L. Armstrong, et al. (2005). "Human embryonic stem cells: biology and clinical implications." Expert Rev Mol Med **7**(19): 1-21.

Inoue, S., F. C. Popp, et al. (2006). "Immunomodulatory effects of mesenchymal stem cells in a rat organ transplant model." Transplantation **81**(11): 1589-95.

Ito, H., M. Koefoed, et al. (2005). "Remodeling of cortical bone allografts mediated by adherent rAAV-RANKL and VEGF gene therapy." Nat Med **11**(3): 291-7.

Jager, M., O. Degistirici, et al. (2007). "Bone healing and migration of cord blood-derived stem cells into a critical size femoral defect after xenotransplantation." J Bone Miner Res **22**(8): 1224-33.

Jaiswal, J. K., E. R. Goldman, et al. (2004). "Use of quantum dots for live cell imaging." Nat Methods **1**(1): 73-8.

Jaiswal, N., S. E. Haynesworth, et al. (1997). "Osteogenic differentiation of purified, culture-expanded human mesenchymal stem cells in vitro." J Cell Biochem **64**(2): 295-312.

Jamieson, T., R. Bakhshi, et al. (2007). "Biological applications of quantum dots." Biomaterials **28**(31): 4717-32.

Jang, J. H., Z. Bengali, et al. (2006). "Surface adsorption of DNA to tissue engineering scaffolds for efficient gene delivery." J Biomed Mater Res A **77**(1): 50-8.

Jang, J. H., T. L. Houchin, et al. (2004). "Gene delivery from polymer scaffolds for tissue engineering." Expert Rev Med Devices **1**(1): 127-38.

Jankowski, R. J., B. M. Deasy, et al. (2002). "Muscle-derived stem cells." Gene Ther **9**(10): 642-7.

Jiang, T., W. I. Abdel-Fattah, et al. (2006). "In vitro evaluation of chitosan/poly(lactic acid-glycolic acid) sintered microsphere scaffolds for bone tissue engineering." Biomaterials **27**(28): 4894-903.

Jones, A. C., B. Milthorpe, et al. (2004). "Analysis of 3D bone ingrowth into polymer scaffolds via micro-computed tomography imaging." Biomaterials **25**(20): 4947-54.

Kacew, S., Z. Ruben, et al. (1995). "Strain as a determinant factor in the differential responsiveness of rats to chemicals." Toxicol Pathol **23**(6): 701-14; discussion 714-5.

Kadiyala, S., R. G. Young, et al. (1997). "Culture expanded canine mesenchymal stem cells possess osteochondrogenic potential in vivo and in vitro." Cell Transplant **6**(2): 125-34.

Kalfas, I. H. (2001). "Principles of bone healing." Neurosurg Focus **10**(4): E1.

Karp, J. M. and G. S. Leng Teo (2009). "Mesenchymal stem cell homing: the devil is in the details." Cell Stem Cell **4**(3): 206-16.

Karsenty, G. (2003). "The complexities of skeletal biology." Nature **423**(6937): 316-8.

Kasai, M., T. Yoneda, et al. (1981). "In vivo effect of anti-asialo GM1 antibody on natural killer activity." Nature **291**(5813): 334-5.

Khademhosseini, A., R. Langer, et al. (2006). "Microscale technologies for tissue engineering and biology." Proc Natl Acad Sci U S A **103**(8): 2480-7.

Khan, Y., M. J. Yaszemski, et al. (2008). "Tissue engineering of bone: material and matrix considerations." J Bone Joint Surg Am **90 Suppl 1**: 36-42.

Kim, H. J., U. J. Kim, et al. (2007). "Bone regeneration on macroporous aqueous-derived silk 3-D scaffolds." Macromol Biosci **7**(5): 643-55.

Kim, S. J., W. I. Lee, et al. (2007). "Stable gene expression by self-complementary adeno-associated viruses in human MSCs." Biochem Biophys Res Commun **360**(3): 573-9.

Koefoed, M., H. Ito, et al. (2005). "Biological effects of rAAV-caAlk2 coating on structural allograft healing." Mol Ther **12**(2): 212-8.

Kofron, M. D. and C. T. Laurencin (2006). "Bone tissue engineering by gene delivery." Adv Drug Deliv Rev **58**(4): 555-76.

Kronenberg, H. M. (2003). "Developmental regulation of the growth plate." Nature **423**(6937): 332-6.

Kumagai, K., A. Vasanji, et al. (2008). "Circulating cells with osteogenic potential are physiologically mobilized into the fracture healing site in the parabiotic mice model." J Orthop Res **26**(2): 165-75.

Kutner, M. H., et al. (2005). Applied linear statistical models. New York, NY, McGraw-Hill.

Kwon, D. S., X. Gao, et al. (2008). "Treatment with bone marrow-derived stromal cells accelerates wound healing in diabetic rats." Int Wound J **5**(3): 453-63.

Laflamme, M. A. and C. E. Murry (2005). "Regenerating the heart." Nat Biotechnol **23**(7): 845-56.

Laird, D. J., U. H. von Andrian, et al. (2008). "Stem cell trafficking in tissue development, growth, and disease." Cell **132**(4): 612-30.

Langer, R. and J. P. Vacanti (1993). "Tissue engineering." Science **260**(5110): 920-6.

Larson, D. R., W. R. Zipfel, et al. (2003). "Water-soluble quantum dots for multiphoton fluorescence imaging in vivo." Science **300**(5624): 1434-6.

Le Blanc, K. and O. Ringden (2006). "Mesenchymal stem cells: properties and role in clinical bone marrow transplantation." Curr Opin Immunol **18**(5): 586-91.

Lee, S. C., M. Shea, et al. (1994). "Healing of large segmental defects in rat femurs is aided by RhBMP-2 in PLGA matrix." J Biomed Mater Res **28**(10): 1149-56.

Lee, S. H. and H. Shin (2007). "Matrices and scaffolds for delivery of bioactive molecules in bone and cartilage tissue engineering." Adv Drug Deliv Rev **59**(4-5): 339-59.

Lieberman, J. R., A. Daluiski, et al. (2002). "The role of growth factors in the repair of bone. Biology and clinical applications." J Bone Joint Surg Am **84-A**(6): 1032-44.

Lieberman, J. R., L. Q. Le, et al. (1998). "Regional gene therapy with a BMP-2-producing murine stromal cell line induces heterotopic and orthotopic bone formation in rodents." J Orthop Res **16**(3): 330-9.

Lim, Y. T., S. Kim, et al. (2003). "Selection of quantum dot wavelengths for biomedical assays and imaging." Mol Imaging **2**: 50-64.

Lin, A. S., T. H. Barrows, et al. (2003). "Microarchitectural and mechanical characterization of oriented porous polymer scaffolds." Biomaterials **24**(3): 481-9.

Lodie, T. A., C. E. Blickarz, et al. (2002). "Systematic analysis of reportedly distinct populations of multipotent bone marrow-derived stem cells reveals a lack of distinction." Tissue Eng **8**(5): 739-51.

Luk, K. D., Y. Chen, et al. (2003). "Adeno-associated virus-mediated bone morphogenetic protein-4 gene therapy for in vivo bone formation." Biochem Biophys Res Commun **308**(3): 636-45.

Lutolf, M. P. and J. A. Hubbell (2005). "Synthetic biomaterials as instructive extracellular microenvironments for morphogenesis in tissue engineering." Nat Biotechnol **23**(1): 47-55.

Martin, J. Y., D. D. Dean, et al. (1996). "Proliferation, differentiation, and protein synthesis of human osteoblast-like cells (MG63) cultured on previously used titanium surfaces." Clin Oral Implants Res **7**(1): 27-37.

Meijer, G. J., J. D. de Bruijn, et al. (2007). "Cell-based bone tissue engineering." PLoS Med **4**(2): e9.

Meyer, U. and H. P. Wiesmann (2006). Bone and Cartilage Engineering. Heidelberg, Springer.

Moioli, E. K., P. A. Clark, et al. (2008). "Synergistic actions of hematopoietic and mesenchymal stem/progenitor cells in vascularizing bioengineered tissues." PLoS ONE **3**(12): e3922.

Moss, R. B., C. Milla, et al. (2007). "Repeated Aerosolized AAV-CFTR for Treatment of Cystic Fibrosis: A Randomized Placebo-Controlled Phase 2A Trial." Human Gene Therapy **18**: 726-732.

Muller-Borer, B. J., M. C. Collins, et al. (2007). "Quantum dot labeling of mesenchymal stem cells." J Nanobiotechnology **5**: 9.

Muschler, G. F., J. M. Lane, et al. (1990). The Biology of Spinal Fusion. Spinal Fusion Science and Technique. J. M. Cotler and H. P. Cotler. Berlin, Springer-Verlag**:** 9-21.

Nasu, T., H. Ito, et al. (2009). "Biological activation of bone-related biomaterials by recombinant adeno-associated virus vector." J Orthop Res **27**(9): 1162-8.

Oakes, D. A. and J. R. Lieberman (2000). "Osteoinductive applications of regional gene therapy: ex vivo gene transfer." Clin Orthop Relat Res(379 Suppl): S101-12.

Oest, M. E., K. M. Dupont, et al. (2007). "Quantitative assessment of scaffold and growth factor-mediated repair of critically sized bone defects." J Orthop Res **25**(7): 941-50.

Ohura, K., C. Hamanishi, et al. (1999). "Healing of segmental bone defects in rats induced by a beta-TCP-MCPM cement combined with rhBMP-2." J Biomed Mater Res **44**(2): 168-75.

Olivo, C., J. Alblas, et al. (2008). "In vivo bioluminescence imaging study to monitor ectopic bone formation by luciferase gene marked mesenchymal stem cells." J Orthop Res **26**(7): 901-9.

Otto, W. R. (2005). Fluorimetric DNA Assay of Cell Number. Epidermal Cells, Humana Press. **289**.

Parfitt, A. M. (1984). "The cellular basis of bone remodeling: the quantum concept reexamined in light of recent advances in the cell biology of bone." Calcif Tissue Int **36 Suppl 1**: S37-45.

Patterson, T. E., K. Kumagai, et al. (2008). "Cellular strategies for enhancement of fracture repair." J Bone Joint Surg Am **90 Suppl 1**: 111-9.

Peister, A., E. R. Deutsch, et al. (2009). "Amniotic Fluid Stem Cells Produce Robust Mineral Deposits on Biodegradable Scaffolds." Tissue Eng Part A.

Peister, A., B. D. Porter, et al. (2008). "Osteogenic differentiation of amniotic fluid stem cells." Biomed Mater Eng **18**(4-5): 241-6.

Peterson, B., J. Zhang, et al. (2005). "Healing of critically sized femoral defects, using genetically modified mesenchymal stem cells from human adipose tissue." Tissue Eng **11**(1-2): 120-9.

Pham, Q. P., F. K. Kasper, et al. (2008). "The influence of an in vitro generated bone-like extracellular matrix on osteoblastic gene expression of marrow stromal cells." Biomaterials **29**(18): 2729-39.

Pittenger, M. F., A. M. Mackay, et al. (1999). "Multilineage potential of adult human mesenchymal stem cells." Science **284**(5411): 143-7.

Porter, B. D., A. S. Lin, et al. (2007). "Noninvasive image analysis of 3D construct mineralization in a perfusion bioreactor." Biomaterials **28**(15): 2525-33.

Prusa, A. R. and M. Hengstschlager (2002). "Amniotic fluid cells and human stem cell research: a new connection." Med Sci Monit **8**(11): RA253-7.

Quarto, R., M. Mastrogiacomo, et al. (2001). "Repair of large bone defects with the use of autologous bone marrow stromal cells." N Engl J Med **344**(5): 385-6.

Rai, B., M. E. Oest, et al. (2007). "Combination of platelet-rich plasma with polycaprolactone-tricalcium phosphate scaffolds for segmental bone defect repair." J Biomed Mater Res A **81**(4): 888-99.

Recker, R. R. (1992). Embryology, anatomy, and microstructure of bone. Disorders of Bone and Mineral Metabolism. F. L. Coe, Flavus, M.J. New York, Raven**:** 219-240.

Reyes, C. D. and A. J. Garcia (2003). "Engineering integrin-specific surfaces with a triple-helical collagen-mimetic peptide." J Biomed Mater Res A **65**(4): 511-23.

Reyes, C. D. and A. J. Garcia (2004). "Alpha2beta1 integrin-specific collagen-mimetic surfaces supporting osteoblastic differentiation." J Biomed Mater Res A **69**(4): 591-600.

Reyes, C. D., T. A. Petrie, et al. (2007). "Biomolecular surface coating to enhance orthopaedic tissue healing and integration." Biomaterials **28**(21): 3228-35.

Richardson, T. P., M. C. Peters, et al. (2001). "Polymeric system for dual growth factor delivery." Nat Biotechnol **19**(11): 1029-34.

Robey, P. G. (1989). "The biochemistry of bone." Endocrinal Metab Clin North America **18**: 859-902.

Robling, A. G., A. B. Castillo, et al. (2006). "Biomechanical and molecular regulation of bone remodeling." Annu Rev Biomed Eng **8**: 455-98.

Rose, T., H. Peng, et al. (2003). "The role of cell type in bone healing mediated by ex vivo gene therapy." Langenbecks Arch Surg **388**(5): 347-55.

Rosen, A. B., D. J. Kelly, et al. (2007). "Finding fluorescent needles in the cardiac haystack: tracking human mesenchymal stem cells labeled with quantum dots for quantitative in vivo three-dimensional fluorescence analysis." Stem Cells **25**(8): 2128-38.

Saito, N., N. Murakami, et al. (2005). "Synthetic biodegradable polymers as drug delivery systems for bone morphogenetic proteins." Adv Drug Deliv Rev **57**(7): 1037-48.

Sarugaser, R., D. Lickorish, et al. (2005). "Human umbilical cord perivascular (HUCPV) cells: a source of mesenchymal progenitors." Stem Cells **23**(2): 220-9.

Schwarz, E. M. (2000). "The adeno-associated virus vector for orthopaedic gene therapy." Clin Orthop Relat Res(379 Suppl): S31-9.

Seeherman, H. and J. M. Wozney (2005). "Delivery of bone morphogenetic proteins for orthopedic tissue regeneration." Cytokine Growth Factor Rev **16**(3): 329-45.

Sekiya, I., B. L. Larson, et al. (2002). "Expansion of human adult stem cells from bone marrow stroma: conditions that maximize the yields of early progenitors and evaluate their quality." Stem Cells **20**(6): 530-41.

Seleverstov, O., O. Zabirnyk, et al. (2006). "Quantum dots for human mesenchymal stem cells labeling. A size-dependent autophagy activation." Nano Lett **6**(12): 2826-32.

Shah, B. S., P. A. Clark, et al. (2007). "Labeling of mesenchymal stem cells by bioconjugated quantum dots." Nano Lett **7**(10): 3071-9.

Shalala, D. (2000). "Protecting Research Subjects - What Must Be Done." New England Journal of Medicine **343**(11): 808-810.

Sikavitsas, V. I., J. S. Temenoff, et al. (2001). "Biomaterials and bone mechanotransduction." Biomaterials **22**(19): 2581-93.

Simmons, C. A., E. Alsberg, et al. (2004). "Dual growth factor delivery and controlled scaffold degradation enhance in vivo bone formation by transplanted bone marrow stromal cells." Bone **35**(2): 562-9.

Smith, A. M., H. Duan, et al. (2008). "Bioconjugated quantum dots for in vivo molecular and cellular imaging." Adv Drug Deliv Rev **60**(11): 1226-40.

Song, L., L. Chau, et al. (2004). "Electric field-induced molecular vibration for noninvasive, high-efficiency DNA transfection." Mol Ther **9**(4): 607-16.

Song, L. and R. S. Tuan (2004). "Transdifferentiation potential of human mesenchymal stem cells derived from bone marrow." Faseb J **18**(9): 980-2.

Srouji, S., A. Rachmiel, et al. (2005). "Mandibular defect repair by TGF-beta and IGF-1 released from a biodegradable osteoconductive hydrogel." J Craniomaxillofac Surg **33**(2): 79-84.

Tsai, M. S., J. L. Lee, et al. (2004). "Isolation of human multipotent mesenchymal stem cells from second-trimester amniotic fluid using a novel two-stage culture protocol." Hum Reprod **19**(6): 1450-6.

Tseng, S. S., M. A. Lee, et al. (2008). "Nonunions and the potential of stem cells in fracture-healing." J Bone Joint Surg Am **90 Suppl 1**: 92-8.

Tuominen, T., T. Jamsa, et al. (2001). "Bovine bone implant with bovine bone morphogenetic protein in healing a canine ulnar defect." Int Orthop **25**(1): 5-8.

Ulrich-Vinther, M. (2007). "Gene therapy methods in bone and joint disorders. Evaluation of the adeno-associated virus vector in experimental models of articular cartilage disorders, periprosthetic osteolysis and bone healing." Acta Orthop Suppl **78**(325): 1-64.

Urist, M. R. (1965). "Bone: formation by autoinduction." Science **150**(698): 893-9.

Voura, E. B., J. K. Jaiswal, et al. (2004). "Tracking metastatic tumor cell extravasation with quantum dot nanocrystals and fluorescence emission-scanning microscopy." Nat Med **10**(9): 993-8.

Waese, E. Y., R. R. Kandel, et al. (2008). "Application of stem cells in bone repair." Skeletal Radiol **37**(7): 601-8.

Wall, M. E., S. H. Bernacki, et al. (2007). "Effects of serial passaging on the adipogenic and osteogenic differentiation potential of adipose-derived human mesenchymal stem cells." Tissue Eng **13**(6): 1291-8.

Weiner, S., Wagner, H.D. (1998). "The Material Bone: Structure-Mechanical Function Relations." Annual Review of Materials Science **28**: 271-298.

Werntz, J. R., J. M. Lane, et al. (1996). "Qualitative and quantitative analysis of orthotopic bone regeneration by marrow." J Orthop Res **14**(1): 85-93.

Winkler, T., P. von Roth, et al. (2009). "Dose-response relationship of mesenchymal stem cell transplantation and functional regeneration after severe skeletal muscle injury in rats." Tissue Eng Part A **15**(3): 487-92.

Wozney, J. M. and V. Rosen (1998). "Bone morphogenetic protein and bone morphogenetic protein gene family in bone formation and repair." Clin Orthop Relat Res(346): 26-37.

Wozney, J. M., V. Rosen, et al. (1988). "Novel regulators of bone formation: molecular clones and activities." Science **242**(4885): 1528-34.

Wu, D., P. Razzano, et al. (2003). "Gene therapy and tissue engineering in repair of the musculoskeletal system." J Cell Biochem **88**(3): 467-81.

Yasko, A. W., J. M. Lane, et al. (1992). "The healing of segmental bone defects, induced by recombinant human bone morphogenetic protein (rhBMP-2). A radiographic, histological, and biomechanical study in rats." J Bone Joint Surg Am **74**(5): 659-70.

Yazici, C., L. Yanoso, et al. (2008). "The effect of surface demineralization of cortical bone allograft on the properties of recombinant adeno-associated virus coating." Biomaterials **29**: 3882-3887.

Yoon, S. T. and S. D. Boden (2002). "Osteoinductive molecules in orthopaedics: basic science and preclinical studies." Clin Orthop Relat Res(395): 33-43.

Younger, E. M. and M. W. Chapman (1989). "Morbidity at bone graft donor sites." J Orthop Trauma **3**(3): 192-5.

Zhang, W., C. Qin, et al. (2007). "Mesenchymal stem cells modulate immune responses combined with cyclosporine in a rat renal transplantation model." Transplant Proc **39**(10): 3404-8.

Zhang, Z. Y., S. H. Teoh, et al. (2009). "Superior osteogenic capacity for bone tissue engineering of fetal compared with perinatal and adult mesenchymal stem cells." Stem Cells **27**(1): 126-37.

Zheng, Y. B., Z. L. Gao, et al. (2008). "Characterization and hepatogenic differentiation of mesenchymal stem cells from human amniotic fluid and human bone marrow: A comparative study." Cell Biol Int **32**(11): 1439-48.

Zhou, J., H. Lin, et al. (2009). "The repair of large segmental bone defects in the rabbit with vascularized tissue engineered bone." Biomaterials.

Zuk, P. A., M. Zhu, et al. (2001). "Multilineage cells from human adipose tissue: implications for cell-based therapies." Tissue Eng **7**(2): 211-28.